

A DISCRETE-TO-CONTINUUM MODEL OF WEAKLY INTERACTING INCOMMENSURATE TWO-DIMENSIONAL LATTICES: THE HEXAGONAL CASE

MALENA I. ESPAÑOL*, DMITRY GOLOVATY†, AND J. PATRICK WILBER†

Abstract. In this paper, we extend the discrete-to-continuum procedure we developed in [1] to derive a continuum variational model for a hexagonal twisted bilayer material in which one layer is fixed. We use a discrete energy containing elastic terms and a weak interaction term that could utilize either a Lennard-Jones potential or a Kolmogorov-Crespi potential. To validate our modeling, we perform numerical simulations to compare the predictions of the original discrete model and the proposed continuum model, which also show an agreement with experimental findings for, e.g., twisted bilayer graphene.

Key words. heterostructure, bilayer graphene, domain wall, moiré pattern, discrete-to-continuum modeling

1. Introduction. In this paper, we apply a discrete-to-continuum procedure to develop a model that predicts relaxation in a twisted bilayer of hexagonal atomic lattices. Relaxation of bilayer graphene, other layered two-dimensional materials, and van der Waals heterostructures has attracted significant interest over the last several years [2, 3, 4]. Predicting lattice reconstruction and equilibrium configurations is crucial for understanding some of the fundamental physical phenomena displayed by bilayers and heterostructures [5, 6, 7, 8, 9]. The quasiperiodic relaxed moiré patterns that occur in slightly misaligned or slightly incommensurate lattices induce superlattice effects, which include superconductivity, strong interactions, and other novel electronic and optical properties [10, 11, 12, 13]. More generally, the study of the mechanics of these nanoscale structures is driven in part by the possibility of engineering advanced materials with novel properties by stacking the same or different types of individual layers in appropriate sequences [14, 15, 16, 17].

Relaxation can be understood by considering a bilayer of graphene in which the two layers are given an initial small relative rotation. Variations in the local stacking between the layers generate a quasiperiodic moiré pattern with a period that scales inversely with the size of the angle of the relative rotation (see Figure 1.1). Mechanically, the bilayer has strong intralayer bonding and weak van der Waals interactions between the layers. As a consequence, the atoms in each lattice adjust through in-plane and out-of-plane deformations. As the lattice structure relaxes, local regions with the energetically favorable AB or BA alignment grow, while regions with AA alignment decrease in size. Typically, the relaxed structure exhibits a network of narrow ridges or wrinkles forming domain walls that separate the relatively large commensurate regions with AB and BA stacking between the lattices [18, 19, 20, 21, 22].

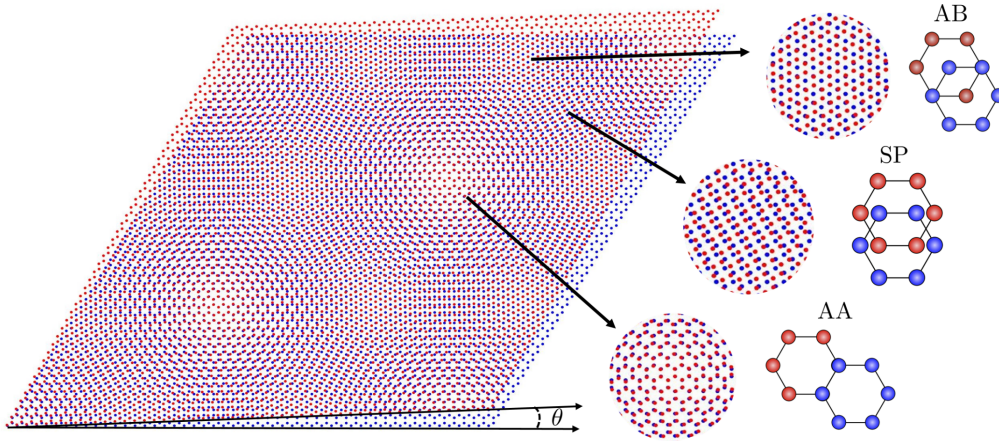


Fig. 1.1: A moiré pattern formed by bilayer graphene with a twist of angle θ , containing three main stacking configurations: AA, AB, and SP.

We derive our continuum model starting from an expression for the discrete energy for two interacting hexagonal lattices. The lattices may have different lattice parameters and there may be a slight relative rotation between the lattices. For simplicity, we keep the atoms on one lattice fixed. In our discrete energy, we model intralayer interactions between neighboring atoms on the deformable lattice with extensional, torsional, and dihedral springs. These

*School of Mathematical and Statistical Sciences, Arizona State University, Tempe, AZ 85281, USA.

†Department of Mathematics, University of Akron, Akron, OH 44325, USA.

describe how the bonds between neighboring atoms resist stretching and bending and how the system maintains an hexagonal lattice structure. The discrete energy also includes a term for the weak interaction between atoms on different lattices. This term is based on a pairwise potential between non-bonded atoms, and we consider both a Lennard-Jones-type potential and a version of the Kolmogorov-Crespi potential [23].

To move from the discrete to the continuum, we introduce a small parameter defined as the ratio of the typical interlayer spacing to the lateral extent of the parallel lattices. Exploiting this small parameter, we develop Taylor expansions of the terms in our discrete energy. After appropriately truncating these expansions, a Riemann sum argument is used to replace sums over the lattice with integrals. This procedure yields a continuum energy for the interacting bilayer. The minimizers of this continuum energy represent equilibrium configurations of the deformable lattice. We note that our continuum weak interlayer interaction energy is a version of the generalized stacking fault energy [24, 25]. Although a continuum description, the weak energy retains information about the local mismatch between the original discrete lattices.

We validate the discrete-to-continuum modeling procedure just described through numerical simulations. We use the open-source discrete modeling software LAMMPS [26] to simulate the lattice relaxation predicted by the discrete model. Also, we use the multiphysics software COMSOL [27] to solve numerically the Euler-Lagrange equations derived from the continuum energy. For both the Lennard-Jones and the Kolmogorov-Crespi potentials, we obtain good agreement between the results of the discrete and continuum numerical simulations for several parameter regimes. In particular, we show that our continuum model can reproduce relaxed moiré patterns observed in the simulations based on the discrete model and observed in other studies [18, 22]. For the Lennard-Jones potential, there is poor agreement with the out-of-plane displacement of the domain walls in some parameter ranges. However, we show that decreasing the well depth of the potential yields a better match between the discrete and continuum. For the Kolmogorov-Crespi potential, we get good agreement between the discrete and the continuum. Our numerical results indicate that this agreement improves as ε decreases, as expected. How well our continuum model works depends on the size of the elastic constants. When the elastic constants are relatively small, the solutions to the discrete simulations exhibit small scale spatial oscillations. This suggests that one of the basic assumptions of our discrete-to-continuum modeling procedure—that the atomic lattice can be embedded in a smooth surface—is violated. In this case, we observe poor agreement between the predictions of the discrete and continuum models. On the other hand, when the elastic constants are relatively large, small-scale spatial oscillations do not occur in the discrete solutions. The continuum model in this case predicts solutions that agree well with the solutions predicted by the discrete model.

This paper extends the discrete-to-continuum procedure developed in our previous papers [28, 1]. In [28], we use a discrete-to-continuum procedure similar to the procedure in this paper to derive a continuum variational model for two chains of atoms with slightly incommensurate lattices. The continuum model recovers both qualitatively and quantitatively the behavior observed in the corresponding discrete model. The numerical solutions for both models demonstrate the presence of large commensurate regions separated by localized incommensurate domain walls. In [1], we develop a continuum variational model for a two-dimensional deformable square lattice of atoms interacting with a two-dimensional rigid square lattice. We use the same discrete-to-continuum procedure as in this paper. The two lattices have slightly different lattice parameters and there is a small relative rotation between them. We show that the continuum model recovers both qualitatively and quantitatively the behavior observed in the corresponding discrete model.

In [29, 30], the authors present a multiscale model that predicts the deformation of bilayers of graphene and bilayers of other two-dimensional materials. In their model, the total energy of the bilayer has an elastic contribution, associated with the stretching and bending of the individual layers, and a misfit energy, which describes the van der Waals interactions between the two layers. The misfit energy is defined using the generalized stacking-fault energy for bilayers, which the authors develop in an earlier publication [25] from density-functional theory calculations. The misfit energy is a function of the separation and registry between layers. In [29], the authors use their model to explain the structure of deformed bilayer graphene in terms of dislocation theory. The model is applied to determine the structure and energetics of four interlayer dislocations in bilayer graphene, where the different cases are determined by the angle between the Burgers vector and the line of dislocation. In [30], the authors use the model to study deformations that result from a small rotation between the layers. The model predicts two distinct equilibrium structures, which the authors call a breathing mode and a bending mode. The latter, more stable at small rotation angles, is characterized by a twist in the dislocation structure near the dislocation nodes, at which there are also large out-of-plane displacements. The authors note that this newly discovered structure has both different symmetry and period from the classical moiré structure that is often assumed for rotated bilayer graphene.

The continuum model we develop in this paper has essential elements in common with the model presented in [29, 30]. Specifically, our model contains terms for the elastic energy of the deformable layer and a term for

the van der Waals interactions between the two layers. However, we derive all terms in our continuum energy by upscaling from an atomistic description of the problem. Our upscaling procedure introduces a small parameter that determines the relative size of the various contributions to the continuum energy. Hence, we gain insight into how the balance of these terms produces phenomena like relaxed moiré patterns in interacting bilayers. Furthermore, our modeling sets the stage for additional analysis to rigorously determine the relation between atomistic and continuum descriptions of the problem [31, 32].

In [8], the authors use multiscale simulations to study the structural relaxation in twisted graphene bilayers. They also study the electron diffraction patterns associated with the relaxation. Their simulations show that the relaxation exhibits a localized rotation and shrinking of the AA domains. For small twisting angles, the localized rotation are approximately a constant, while for large twisting angles, the rotation scales linearly with the angle. The authors use a continuum model to explain their results theoretically. A nonlinear elasticity model describes the mechanical response within a graphene layer. The elastic energy density consists of a Saint Venant–Kirchhoff membrane term and a Helfrich bending term. For the interlayer energy, the authors develop a discrete-continuum approximation based on the Kolmogorov-Crespi potential. The interlayer energy is calculated in two parts. Locally, the potential is evaluated exactly over a short-range discrete region. Outside this region, a continuum integral approximation is used [33].

In [5], the authors study bilayer relaxation by minimizing a total continuum energy over a collection of all possible local atomic environments, which they call configuration space. For the configuration-space approach, every atomic site in the bilayer is associated with a vector that describes the local relative stacking registry at that site. The authors use this approach to study the relaxation patterns in configuration space. They present computational results for small-angle twisted bilayer graphene and molybdenum disulfide, and demonstrate the computational efficiency of their method for computing relaxations. In [7], these authors extend the configuration-space approach from bilayers to general weakly coupled incommensurate deformable multi-layers. Their main result is the derivation of an elastic model for the relaxation of vertical stacks of any number of incommensurate, weakly coupled deformable layers. When specialized to a bilayer heterostructure, the model in [7] reduces to a well-posed variational problem for the continuum displacement field on a periodic moiré domain even for aperiodic atomistic configurations. Their model in this case is similar to the continuum model we derive in this paper, although our approach is entirely different from theirs.

In [34], a model similar to that developed in [5] is used to describe how the shapes of moiré domains and domain boundaries yield information about the generalized stacking fault energy function at the low twist-angle limit.

In [22], the authors use multiscale modeling to study lattice reconstruction in twisted bilayers of transition metal dichalcogenides at low twist angles. Using density functional theory, they develop interpolation formulae for the interlayer adhesion energies of the bilayers. The authors combine the interlayer adhesion energies with elasticity theory. The resulting model is used to analyze the mesoscale domain structures formed during lattice relaxation.

This paper is organized as follows. In Section 2, we formulate a discrete energy of the system of a graphene sheet over a substrate. In Section 3 we derive a continuum energy that keeps track of the mismatch of the spacing between the atoms on each curve. Section 4 includes numerical results that compare the atomistic model with the continuum model. We summarize in Section 5.

2. Atomistic Model. We consider a discrete system that consists of parallel 2-dimensional atomic lattices, $\hat{\mathcal{A}}_1$ and $\hat{\mathcal{A}}_2$, both infinite in extent. The atoms in $\hat{\mathcal{A}}_2$ can move and each of these atoms interacts with its neighbors within $\hat{\mathcal{A}}_2$ via a strong bond potential. $\hat{\mathcal{A}}_2$ describes a layer of a 2-dimensional material that is nearly inextensible and has a finite resistance to bending. In the absence of interactions with atoms on $\hat{\mathcal{A}}_1$, the atoms in $\hat{\mathcal{A}}_2$ in equilibrium form a flat hexagonal lattice that has lattice parameter h_2 . The atoms in $\hat{\mathcal{A}}_1$ are fixed and form a flat hexagonal lattice with lattice parameter h_1 . In this work, $\hat{\mathcal{A}}_1$ describes a rigid substrate. All atoms in $\hat{\mathcal{A}}_2$ are assumed to interact with all atoms in $\hat{\mathcal{A}}_1$ via a weak interatomic potential. Below we refer to $\hat{\mathcal{A}}_1$ as the rigid lattice and to $\hat{\mathcal{A}}_2$ as the deformable lattice.

We assume that $\hat{\mathcal{A}}_2$ deforms periodically and that, in its reference configuration, one periodic cell of $\hat{\mathcal{A}}_2$ occupies a parallelogram-shaped, planar domain \mathcal{A}_2^0 with sides of length L . To define \mathcal{A}_2^0 , we set $\mathbf{a}_1^2 = (1, 0)$ and $\mathbf{a}_2^2 = (1/2, \sqrt{3}/2)$, we let A be the 2×2 matrix with \mathbf{a}_1^2 and \mathbf{a}_2^2 as its columns, and we define

$$(2.1) \quad D = \{ \mathbf{x} = A\mathbf{y} \text{ with } \mathbf{y} \in [0, L]^2 \}.$$

Then $\mathcal{A}_2^0 = \{ (\mathbf{x}, \sigma) : \mathbf{x} = (x_1, x_2) \in D \}$. We set $N_2 = L/h_2$. The set D can be divided into N_2^2 unit cells each containing two atoms. See Figure 2.1. The deformed and reference positions of the $(2N_2)^2$ atoms in \mathcal{A}_2^0 are given by the set of vectors

$$\mathbf{Q} := \{ \mathbf{q}_{ij}^1 \}_{i,j=1}^{N_2} \cup \{ \mathbf{q}_{ij}^2 \}_{i,j=1}^{N_2} \subset \mathbb{R}^3 \text{ and } \mathbf{R} := \{ \mathbf{r}_{ij}^1 \}_{i,j=1}^{N_2} \cup \{ \mathbf{r}_{ij}^2 \}_{i,j=1}^{N_2} \subset \mathbb{R}^3,$$

respectively. Then the positions of the atoms in the reference configuration are

$$(2.2) \quad \mathbf{r}_{ij}^k = (h_2 ((i + k/3) \mathbf{a}_1^2 + (j + k/3) \mathbf{a}_2^2), \sigma) \text{ for } k = 1, 2,$$

and the positions of the atoms in the deformed configuration are

$$(2.3) \quad \mathbf{q}_{ij}^k = \mathbf{r}_{ij}^k + (\mathbf{u}_{ij}^k, v_{ij}^k) \text{ for } k = 1, 2,$$

where \mathbf{u}_{ij}^k is the displacement in the x, y plane, and v_{ij}^k in the z -direction. Because $\hat{\mathcal{A}}_2$ deforms periodically, we identify $i = N_2 + 1$ with $i = 1$ and $j = N_2 + 1$ with $j = 1$.

For the rigid lattice, the current and the reference configurations are the same. To describe these, we define the rotation matrix

$$R(\theta) = \begin{pmatrix} \cos \theta & -\sin \theta \\ \sin \theta & \cos \theta \end{pmatrix}$$

and we define \mathbf{a}_i^1 as the transpose of $R(\theta)(\mathbf{a}_i^2)^T$ for $i = 1, 2$. We assume that there is a unit cell of $\hat{\mathcal{A}}_2$ whose lower left corner sits directly above the lower left corner of a unit cell in $\hat{\mathcal{A}}_1$. Then, the positions of atoms on the rigid lattice are $\mathbf{P} := \{\mathbf{p}_{\ell m}^1\}_{\ell, m=-\infty}^{\infty} \cup \{\mathbf{p}_{\ell m}^2\}_{\ell, m=-\infty}^{\infty} \subset \mathbb{R}^3$, where

$$(2.4) \quad \mathbf{p}_{\ell m}^{\tilde{k}} = \left(h_1 \left((\ell + \tilde{k}/3) \mathbf{a}_1^1 + (m + \tilde{k}/3) \mathbf{a}_2^1 \right), 0 \right) \text{ for } \tilde{k} = 1, 2.$$

Note that we assume that the rigid lattice is infinite in extent in order to appropriately compute the nonlocal weak energy.

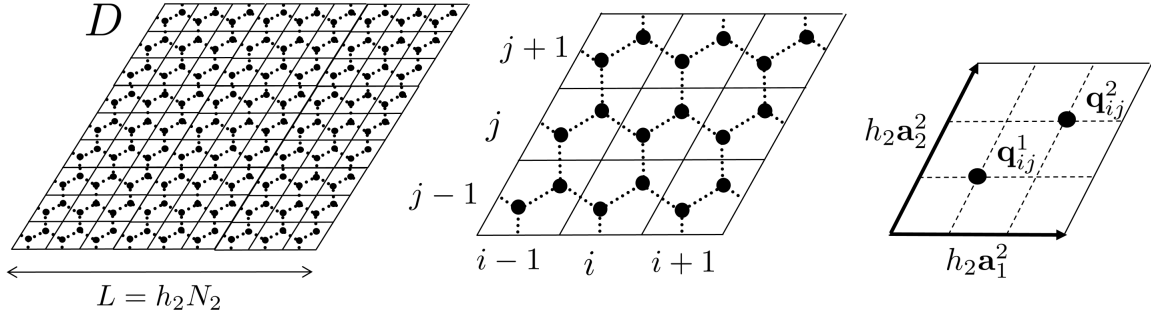


Fig. 2.1: Lattice $\hat{\mathcal{A}}_2$. Left: $\hat{\mathcal{A}}_2$ consists of N_2^2 cells. Middle: each cell is indexed by i, j . Right: the cell i, j contains two atoms \mathbf{q}_{ij}^1 and \mathbf{q}_{ij}^2 . The lattice vectors \mathbf{a}_1^2 and \mathbf{a}_2^2 are also shown.

We assume that, in the reference configuration, the lattices are planar and parallel. Also, the lattices are separated by a distance σ , where σ is a length scale associated with the weak potential. When $h_1 = h_2$ (e.g., bilayer graphene) and $\theta = 0$, the equilibrium configuration of the system is $\hat{\mathcal{A}}_2$ shifted relatively to $\hat{\mathcal{A}}_1$ such that half of the atoms in $\hat{\mathcal{A}}_2$ sit above the centers of the hexagons in $\hat{\mathcal{A}}_1$ (AB stacking). The system would be in *global registry*. In this paper, we consider the situation where $\hat{\mathcal{A}}_1$ and $\hat{\mathcal{A}}_2$ in the reference configuration have slightly different orientations (small values of θ) and/or when they have slightly different lattice parameter ($h_1 \neq h_2$, but $|h_1 - h_2|/h_1 \ll 1$). See Figure 1.1.

We assume that the total energy of the discrete system depends on the position of the atoms in the deformable lattice and is given by

$$(2.5) \quad E(\mathbf{Q}) := E_s(\mathbf{Q}) + E_t(\mathbf{Q}) + E_d(\mathbf{Q}) + E_w(\mathbf{Q}).$$

That is, the total energy is the sum of the intralayer energy—composed of the *stretching* E_s , *torsional* E_t , and *dihedral* E_d energies—and the interlayer (weak) energy E_w .

The stretching energy E_s is the energy associated with stretching or compressing bonds between neighboring atoms in $\hat{\mathcal{A}}_2$. Using a harmonic potential, we define

$$(2.6) \quad E_s(\mathbf{Q}) := \sum_{i,j=1}^{N_2} \frac{k_s}{2} \left[\left(\frac{\|\mathbf{b}_{ij}^1\| - \frac{h_2}{\sqrt{3}}}{\frac{h_2}{\sqrt{3}}} \right)^2 + \left(\frac{\|\mathbf{b}_{ij}^2\| - \frac{h_2}{\sqrt{3}}}{\frac{h_2}{\sqrt{3}}} \right)^2 + \left(\frac{\|\mathbf{b}_{ij}^3\| - \frac{h_2}{\sqrt{3}}}{\frac{h_2}{\sqrt{3}}} \right)^2 \right],$$

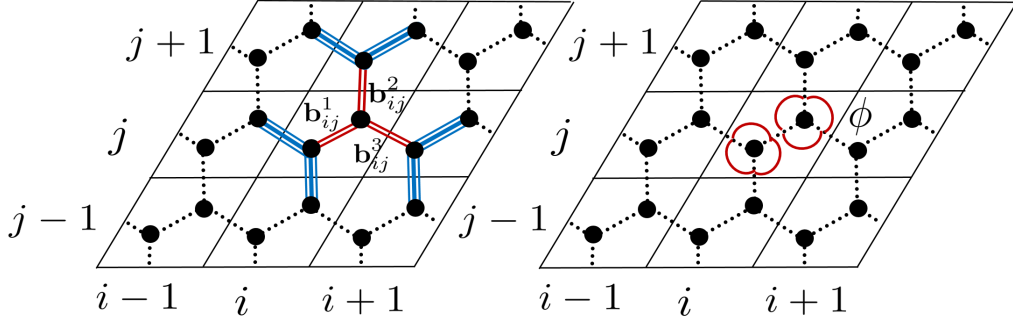


Fig. 2.2: Left: The lattice with the main three bonds (red double lines) corresponding to the i, j cell, used to define the stretching energy and the adjacent bonds (blue triple lines) used to defined the dihedral angles. Right: The six angles ϕ (red solid lines) corresponding to the i, j cell used to define the torsional energy.

where the vectors

$$\mathbf{b}_{ij}^1 = \mathbf{q}_{ij}^1 - \mathbf{q}_{ij}^2, \quad \mathbf{b}_{ij}^2 = \mathbf{q}_{ij+1}^1 - \mathbf{q}_{ij}^2, \quad \text{and} \quad \mathbf{b}_{ij}^3 = \mathbf{q}_{i+1j}^1 - \mathbf{q}_{ij}^2$$

represent the bonds between the atom \mathbf{q}_{ij}^2 and its neighbors for every cell $i, j = 1, \dots, N_2$ (see Figure 2.2 (left)). In (2.6), k_s is the spring constant.

The torsional energy is the energy associated with changing the angle between adjacent bonds. We model this energy by assuming we have torsional springs between adjacent bonds. Each atom is related to three torsional springs, and therefore each cell contains 6 torsional springs. The torsional energy is

$$(2.7) \quad E_t(\mathbf{Q}) := \sum_{i,j=1}^{N_2} \frac{k_t}{2} \left[(\phi(\mathbf{b}_{ij}^1, \mathbf{b}_{ij}^2) - 2\pi/3)^2 + (\phi(\mathbf{b}_{ij}^2, \mathbf{b}_{ij}^3) - 2\pi/3)^2 + (\phi(\mathbf{b}_{ij}^1, \mathbf{b}_{ij}^3) - 2\pi/3)^2 \right. \\ \left. + (\phi(-\mathbf{b}_{i-1j}^3, -\mathbf{b}_{ij}^1) - 2\pi/3)^2 + (\phi(-\mathbf{b}_{ij-1}^2, -\mathbf{b}_{ij}^1) - 2\pi/3)^2 + (\phi(-\mathbf{b}_{i-1j}^3, -\mathbf{b}_{ij-1}^2) - 2\pi/3)^2 \right],$$

where k_t is the torsional spring constant and $\phi(\mathbf{a}, \mathbf{c})$ is the angle between the vectors \mathbf{a} and \mathbf{c} . Right of Figure 2.2 shows the six angles corresponding to the cell i, j .

Assuming that admissible in-plane deformations of $\hat{\mathcal{A}}_2$ are small, we can use the approximation

$$\phi = \arccos(x) \approx \arccos(-1/2) + \frac{1}{\sin(\arccos(-1/2))} (x + 1/2) = \frac{2\pi}{3} + \frac{2}{\sqrt{3}} \left(\cos(\phi) + \frac{1}{2} \right)$$

to rewrite E_t as

$$(2.8) \quad E_t(\mathbf{Q}) = \sum_{i,j=1}^{N_2} \frac{k_t}{2} \frac{4}{3} \left[\left(\frac{\mathbf{b}_{ij}^1 \cdot \mathbf{b}_{ij}^2}{\|\mathbf{b}_{ij}^1\| \|\mathbf{b}_{ij}^2\|} + \frac{1}{2} \right)^2 + \left(\frac{\mathbf{b}_{ij}^2 \cdot \mathbf{b}_{ij}^3}{\|\mathbf{b}_{ij}^2\| \|\mathbf{b}_{ij}^3\|} + \frac{1}{2} \right)^2 + \left(\frac{\mathbf{b}_{ij}^1 \cdot \mathbf{b}_{ij}^3}{\|\mathbf{b}_{ij}^1\| \|\mathbf{b}_{ij}^3\|} + \frac{1}{2} \right)^2 \right. \\ \left. + \left(\frac{\mathbf{b}_{i-1j}^3 \cdot \mathbf{b}_{ij}^1}{\|\mathbf{b}_{i-1j}^3\| \|\mathbf{b}_{ij}^1\|} + \frac{1}{2} \right)^2 + \left(\frac{\mathbf{b}_{ij-1}^2 \cdot \mathbf{b}_{ij}^1}{\|\mathbf{b}_{ij-1}^2\| \|\mathbf{b}_{ij}^1\|} + \frac{1}{2} \right)^2 + \left(\frac{\mathbf{b}_{i-1j}^3 \cdot \mathbf{b}_{ij-1}^2}{\|\mathbf{b}_{i-1j}^3\| \|\mathbf{b}_{ij-1}^2\|} + \frac{1}{2} \right)^2 \right].$$

Certain out-of-plane deformations are not penalized by the extensional and torsional energies. For example, there is no energy cost for folding along a direction parallel to the sides of the domain D . To penalize for such deformations, we introduce the dihedral energy by assuming that a dihedral spring connects every triplet of adjacent bonds. This spring energy is minimized when the third bond lies in the plane formed by the first two bonds. See Figure 2.3. We assume that the energy of a dihedral spring is

$$e_d(\mathbf{a}, \mathbf{b}, \mathbf{c}) := \frac{k_d}{2} \cos^2 \psi = \frac{k_d}{2} \frac{((\mathbf{a} \times \mathbf{b}) \cdot \mathbf{c})^2}{\|\mathbf{a} \times \mathbf{b}\|^2 \|\mathbf{c}\|^2},$$

where k_d is the dihedral spring constant and ψ is the dihedral angle defined as in Figure 2.3. For each $i, j = 1, \dots, N_2$, each bond \mathbf{b}_{ij}^p , $p = 1, 2, 3$ is the ‘middle’ bond in 4 different triplets of adjacent bonds. See Figure 2.2.

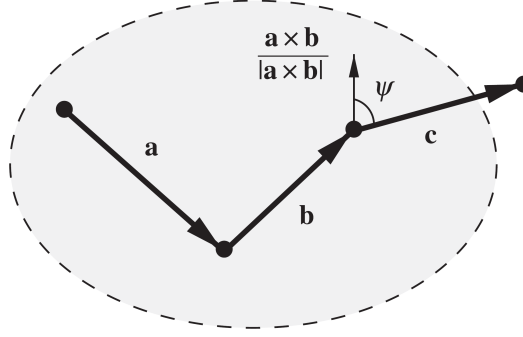


Fig. 2.3: A dihedral spring connecting vectors \mathbf{a} , \mathbf{b} , and \mathbf{c} . The spring energy is minimized when $\psi = \pi/2$.

Hence the total dihedral energy is

$$(2.9) \quad E_d(\mathbf{Q}) := \sum_{i,j=1}^{N_2} \frac{k_d}{2} \left\{ \frac{((\mathbf{b}_{ij}^1 \times \mathbf{b}_{ij}^2) \cdot \mathbf{b}_{ij-1}^2)^2}{\|\mathbf{b}_{ij}^1 \times \mathbf{b}_{ij}^2\|^2 \|\mathbf{b}_{ij-1}^2\|^2} + \frac{((\mathbf{b}_{ij}^1 \times \mathbf{b}_{ij}^2) \cdot \mathbf{b}_{i-1j}^3)^2}{\|\mathbf{b}_{ij}^1 \times \mathbf{b}_{ij}^2\|^2 \|\mathbf{b}_{i-1j}^3\|^2} + \frac{((\mathbf{b}_{ij}^1 \times \mathbf{b}_{ij}^3) \cdot \mathbf{b}_{ij-1}^2)^2}{\|\mathbf{b}_{ij}^1 \times \mathbf{b}_{ij}^3\|^2 \|\mathbf{b}_{ij-1}^2\|^2} + \right. \\ \left. \frac{((\mathbf{b}_{ij}^1 \times \mathbf{b}_{ij}^3) \cdot \mathbf{b}_{i-1j}^3)^2}{\|\mathbf{b}_{ij}^1 \times \mathbf{b}_{ij}^3\|^2 \|\mathbf{b}_{i-1j}^3\|^2} + \frac{((\mathbf{b}_{ij}^2 \times \mathbf{b}_{i-1j+1}^3) \cdot \mathbf{b}_{ij}^1)^2}{\|\mathbf{b}_{ij}^2 \times \mathbf{b}_{i-1j+1}^3\|^2 \|\mathbf{b}_{ij}^1\|^2} + \frac{((\mathbf{b}_{ij}^2 \times \mathbf{b}_{i-1j+1}^3) \cdot \mathbf{b}_{ij}^3)^2}{\|\mathbf{b}_{ij}^2 \times \mathbf{b}_{i-1j+1}^3\|^2 \|\mathbf{b}_{ij}^3\|^2} + \right. \\ \left. \frac{((\mathbf{b}_{ij}^2 \times \mathbf{b}_{ij+1}^1) \cdot \mathbf{b}_{ij}^1)^2}{\|\mathbf{b}_{ij}^2 \times \mathbf{b}_{ij+1}^1\|^2 \|\mathbf{b}_{ij}^1\|^2} + \frac{((\mathbf{b}_{ij}^2 \times \mathbf{b}_{ij+1}^1) \cdot \mathbf{b}_{ij}^3)^2}{\|\mathbf{b}_{ij}^2 \times \mathbf{b}_{ij+1}^1\|^2 \|\mathbf{b}_{ij}^3\|^2} + \frac{((\mathbf{b}_{ij}^3 \times \mathbf{b}_{ij}^2) \cdot \mathbf{b}_{i+1j}^1)^2}{\|\mathbf{b}_{ij}^3 \times \mathbf{b}_{ij}^2\|^2 \|\mathbf{b}_{i+1j}^1\|^2} + \right. \\ \left. \frac{((\mathbf{b}_{ij}^3 \times \mathbf{b}_{ij}^2) \cdot \mathbf{b}_{i+1j-1}^2)^2}{\|\mathbf{b}_{ij}^3 \times \mathbf{b}_{ij}^2\|^2 \|\mathbf{b}_{i+1j-1}^2\|^2} + \frac{((\mathbf{b}_{ij}^3 \times \mathbf{b}_{ij}^1) \cdot \mathbf{b}_{i+1j}^1)^2}{\|\mathbf{b}_{ij}^3 \times \mathbf{b}_{ij}^1\|^2 \|\mathbf{b}_{i+1j}^1\|^2} + \frac{((\mathbf{b}_{ij}^3 \times \mathbf{b}_{ij}^1) \cdot \mathbf{b}_{i+1j-1}^2)^2}{\|\mathbf{b}_{ij}^3 \times \mathbf{b}_{ij}^1\|^2 \|\mathbf{b}_{i+1j-1}^2\|^2} \right\}.$$

The bending between interatomic bonds is penalized by introducing harmonic torsional springs and dihedral angles between the bonds. The expressions for the extensional and torsional springs, respectively, show that the sum of the corresponding energy components is minimized when the atoms on $\hat{\mathcal{A}}_2$ form a hexagonal lattice with sides of length $h_2/\sqrt{3}$.

Finally, we consider 2 choices for the energy of the weak interaction between $\hat{\mathcal{A}}_1$ and $\hat{\mathcal{A}}_2$. Our first choice is to define

$$(2.10) \quad E_w(\mathbf{Q}) = \omega \sum_{i,j=1}^{N_2} \sum_{k=1}^2 \sum_{\ell,m=-\infty}^{\infty} \sum_{\bar{k}=1}^2 g_{\text{LJ}} \left(\frac{\|\mathbf{q}_{ij}^k - \mathbf{p}_{\ell m}^{\bar{k}}\|}{\sigma} \right),$$

where g_{LJ} is the classical Lennard-Jones 12-6 potential

$$(2.11) \quad g_{\text{LJ}}(r) = r^{-12} - 2r^{-6}.$$

The parameters σ and ω define the equilibrium interatomic distance and the strength of the Lennard-Jones potential, respectively. Note that the inner double sum in (2.10) is taken over the entire rigid lattice to properly account for weak interactions between the lattices.

The Lennard-Jones potential fails to adequately account for the registry dependence in the interaction between bilayers. The Kolmogorov-Crespi potential addresses this deficiency [23]. Therefore, the second choice we consider for the weak interaction is

$$(2.12) \quad E_w(\mathbf{Q}) = \omega \sum_{i,j=1}^{N_2} \sum_{k=1}^2 \sum_{\ell,m=-\infty}^{\infty} \sum_{\bar{k}=1}^2 g_{\text{KC}} \left(\frac{\|\mathbf{q}_{ij}^k - \mathbf{p}_{\ell m}^{\bar{k}}\|}{\sigma}, \frac{\hat{\rho}(\mathbf{q}_{ij}^k - \mathbf{p}_{\ell m}^{\bar{k}})}{\delta} \right),$$

where g_{KC} is a version of the Kolmogorov-Crespi potential having the form

$$(2.13) \quad g_{\text{KC}}(r, \rho) = e^{-\tilde{\lambda}(r-1)} \left[\tilde{C} + 2f(\rho) \right] - r^{-6} \quad \text{with} \quad f(\rho) = e^{-\rho^2} \left(\tilde{C}_0 + \tilde{C}_2 \rho^2 + \tilde{C}_4 \rho^4 \right).$$

In (2.12), $\hat{\rho}(\mathbf{a})$ is the length of the projection of \mathbf{a} onto the xy -plane, which is the plane containing the fixed lattice $\hat{\mathcal{A}}_1$. For g_{KC} , ω can be associated with the strength of the potential. The parameters σ and δ are lengths; σ is related to the equilibrium spacing between the layers. The constants $\tilde{\lambda}$, \tilde{C} , \tilde{C}_0 , \tilde{C}_2 , and \tilde{C}_4 are dimensionless parameters [23].

3. Continuum Model. First, we briefly describe the approach we take to derive the continuum model. We assume that the atoms on the deformable lattice $\hat{\mathcal{A}}_2$ are embedded in a smooth surface $\mathcal{A}_2 \subset \mathbb{R}^3$ and we describe this surface parametrically in terms of the displacement field. Nondimensionalizing the discrete problem introduces a small geometric parameter $\varepsilon = \sigma/L$, equal to the ratio of the equilibrium distance of the weak interaction to the length of the side of the domain D . Evaluating the displacements at atomic positions, substituting these into the expression (2.5) for the discrete energy, expanding the result in terms of ε , and converting summation into integration, leads to an expansion in terms of ε for the continuum energy, written as a functional of the displacement field.

We identify the leading-order terms in this expansion, up to the order at which contributions from the extensional, torsional, and dihedral springs, as well the van der Waals interactions are included. The resulting continuum energy is of Ginzburg-Landau type and contains terms of different powers in ε . The minimizers of the continuum energy typically exhibit bulk regions of registry, separated by thin walls where the gradient of the displacement field is large. Thus, within the walls, the contributions from higher-order terms generally cannot be neglected. We choose to cut off the expansion that leads to the continuum energy at the order when all components of the displacement contribute to the energy density inside the walls at leading order. Finally, in the next section, we present the results of simulations confirming that the behavior of minimizers of the continuum energy match that of minimizers of the discrete energy.

We assume that the deformed configuration of a periodic cell of $\hat{\mathcal{A}}_2$ is embedded in a sufficiently smooth surface $\mathcal{A}_2 = \{(\mathbf{x} + \mathbf{u}(\mathbf{x}), \sigma + v(\mathbf{x})) : (\mathbf{x}, \sigma) \in \mathcal{A}_2^0\}$, where $(\mathbf{u}(\mathbf{x}), v(\mathbf{x}))$ is the displacement of the point (\mathbf{x}, σ) on \mathcal{A}_2^0 . Next, we assume $\sigma \ll L$, that is, the length scale associated with the equilibrium spacing between the lattices is much smaller than the lateral extent of the system. Then, we define $\varepsilon = \sigma/L$ and introduce the rescalings

$$(3.1) \quad \boldsymbol{\chi} = \frac{\mathbf{x}}{L}, \quad \boldsymbol{\xi} = \frac{\mathbf{u}}{\varepsilon L}, \quad \eta = \frac{v}{\varepsilon L}, \quad \mathcal{E} = \frac{\varepsilon E}{\omega}.$$

We define the nondimensional parameters

$$(3.2) \quad \delta_1 = \frac{h_1}{\sigma}, \quad \delta_2 = \frac{h_2}{\sigma}, \quad \gamma_s = \frac{6\sqrt{3}k_s}{\omega\delta_2^2}, \quad \gamma_t = \frac{64\sqrt{3}k_t}{\omega\delta_2^2}, \quad \gamma_d = \frac{\sqrt{3}k_d}{4\omega}.$$

The numerical coefficients in the definitions of γ_s , γ_t , and γ_d are explained later. The scaling for the displacements are appropriate for small deformations considered here. With a slight abuse of notation, we now set

$$(3.3) \quad \mathcal{A}_2^0 = \{(\boldsymbol{\chi}, \varepsilon) : \boldsymbol{\chi} \in D_1\}, \quad \mathcal{A}_2 = \{(\boldsymbol{\chi} + \varepsilon\boldsymbol{\xi}(\boldsymbol{\chi}), \varepsilon + \varepsilon\eta(\boldsymbol{\chi})) : (\boldsymbol{\chi}, \varepsilon) \in \mathcal{A}_2^0\},$$

where D_1 is the rescaled parallelogram D now of side 1. We assume that $\delta_i = \mathcal{O}(1)$, $i = 1, 2$, that is, the lattice parameters for $\hat{\mathcal{A}}_1$ and $\hat{\mathcal{A}}_2$ are comparable to the distance between $\hat{\mathcal{A}}_1$ and $\hat{\mathcal{A}}_2$ (and hence both are much smaller than the lateral extent of the system). Furthermore, in order to observe the registry effects on a macroscale, we assume that

$$(3.4) \quad \alpha := \frac{\delta_1 - \delta_2}{\varepsilon\delta_2} = \mathcal{O}(1),$$

so that the mismatch between the equilibrium lattice parameters of $\hat{\mathcal{A}}_1$ and $\hat{\mathcal{A}}_2$ is small.

In the rescaled coordinates, the atoms on \mathcal{A}_2^0 are located at the points $\mathbf{r}_{ij}^k = (\boldsymbol{\chi}_{ij}^k, \varepsilon)$, where

$$(3.5) \quad \boldsymbol{\chi}_{ij}^k = \varepsilon\delta_2 \left((i + k/3)\mathbf{a}_1^2 + (j + k/3)\mathbf{a}_2^2 \right)$$

for $i, j = 1, \dots, N_2$ and $k = 1, 2$, are obtained by dividing \mathbf{r}_{ij}^k by L in (2.2). Atom k in the i, j cell is then displaced to the point

$$(3.6) \quad \mathbf{q}_{ij}^k = (\boldsymbol{\chi}_{ij}^k + \varepsilon\boldsymbol{\xi}(\boldsymbol{\chi}_{ij}^k), \varepsilon + \varepsilon\eta(\boldsymbol{\chi}_{ij}^k)).$$

Note that here and in what follows we continue to use the notation \mathbf{q}_{ij}^k , \mathbf{r}_{ij}^k , and \mathbf{b}_{ij}^p , but now to denote the corresponding nondimensional quantities.

3.1. Elastic Energy Contribution. The developments in this section closely follow those in [1]. Using that ε is small, we Taylor expand the rescaled versions of the components (2.6), (2.8), and (2.9) of the discrete elastic energy in ε about $\boldsymbol{\xi}(\boldsymbol{\chi}_{ij}^2)$. After truncating the expansions, we end up with approximate energies as a function of $\boldsymbol{\xi}$ and η evaluated at $\boldsymbol{\chi}_{ij}^2$, where $i, j = 1, \dots, N_2$. The details of the derivations that led to these truncated expansions and the definitions of \mathbf{v}_1 , \mathbf{v}_2 , and \mathbf{v}_3 are given in the Supplementary Material 7.1. This yields

$$(3.7) \quad \mathcal{E}_s[\boldsymbol{\xi}, \eta] \sim \sum_{i,j=1}^{N_2} \frac{9k_s\varepsilon^3}{2\omega} \left[\left(\mathbf{v}_1 \cdot \nabla \boldsymbol{\xi} \mathbf{v}_1 + \frac{\varepsilon}{2} \mathbf{v}_1 \cdot (\nabla \eta \otimes \nabla \eta) \mathbf{v}_1 \right)^2 + \left(\mathbf{v}_2 \cdot \nabla \boldsymbol{\xi} \mathbf{v}_2 + \frac{\varepsilon}{2} \mathbf{v}_2 \cdot (\nabla \eta \otimes \nabla \eta) \mathbf{v}_2 \right)^2 + \left(\mathbf{v}_3 \cdot \nabla \boldsymbol{\xi} \mathbf{v}_3 + \frac{\varepsilon}{2} \mathbf{v}_3 \cdot (\nabla \eta \otimes \nabla \eta) \mathbf{v}_3 \right)^2 \right],$$

$$(3.8) \quad \mathcal{E}_t[\boldsymbol{\xi}, \eta] \sim \sum_{i,j=1}^{N_2} \frac{48k_t}{\omega} \varepsilon^3 \left[\left(\frac{\mathbf{v}_1 \cdot \nabla \boldsymbol{\xi} \mathbf{v}_2 + \mathbf{v}_2 \cdot \nabla \boldsymbol{\xi} \mathbf{v}_1}{2} + \frac{\varepsilon}{2} (\mathbf{v}_1 \cdot (\nabla \eta \otimes \nabla \eta) \mathbf{v}_2) \right)^2 + \left(\frac{\mathbf{v}_2 \cdot \nabla \boldsymbol{\xi} \mathbf{v}_3 + \mathbf{v}_3 \cdot \nabla \boldsymbol{\xi} \mathbf{v}_2}{2} + \frac{\varepsilon}{2} (\mathbf{v}_2 \cdot (\nabla \eta \otimes \nabla \eta) \mathbf{v}_3) \right)^2 + \left(\frac{\mathbf{v}_1 \cdot \nabla \boldsymbol{\xi} \mathbf{v}_3 + \mathbf{v}_3 \cdot \nabla \boldsymbol{\xi} \mathbf{v}_1}{2} + \frac{\varepsilon}{2} (\mathbf{v}_1 \cdot (\nabla \eta \otimes \nabla \eta) \mathbf{v}_3) \right)^2 \right],$$

and

$$(3.9) \quad \mathcal{E}_d[\boldsymbol{\xi}, \eta] \sim \sum_{i,j=1}^{N_2} \frac{3k_d\delta_2^2\varepsilon^5}{8\omega} [7\eta_{,11}^2 + 16\eta_{,12}^2 - 2\eta_{,11}\eta_{,22} + 7\eta_{,22}^2].$$

As we did in [1], we neglect some third-order terms in ε , in particular, the terms that contain second-order derivatives in $\boldsymbol{\xi}$ or are cubic in derivatives of $\boldsymbol{\xi}$. Further, we include some quartic terms in the derivative of η , that allow us to complete squares in (3.7) and (3.8). We showed in [1] that including/deleting these higher order terms from the truncated energy gives minimizers with the structure close to that of the minimizers of the discrete energy as $\varepsilon \rightarrow 0$.

We now observe that \mathcal{A}_2^0 has area $\sqrt{3}/2$ in nondimensional coordinates and that the spacing between the atoms is $\varepsilon\delta_2/\sqrt{3} \ll 1$. Hence, the number of atoms on \mathcal{A}_2^0 is $\sim \frac{1}{\varepsilon^2}$. These observations justify replacing the sums in (3.7), (3.8), and (3.9) with integrals to define the continuum elastic energies

$$(3.10) \quad \mathcal{F}_s^\varepsilon[\boldsymbol{\xi}, \eta] =: \frac{\gamma_s\varepsilon}{2} \int_{D_1} \left[\left(\mathbf{v}_1 \cdot \nabla \boldsymbol{\xi} \mathbf{v}_1 + \frac{\varepsilon}{2} |\nabla \eta \cdot \mathbf{v}_1|^2 \right)^2 + \left(\mathbf{v}_2 \cdot \nabla \boldsymbol{\xi} \mathbf{v}_2 + \frac{\varepsilon}{2} |\nabla \eta \cdot \mathbf{v}_2|^2 \right)^2 + \left(\mathbf{v}_3 \cdot \nabla \boldsymbol{\xi} \mathbf{v}_3 + \frac{\varepsilon}{2} |\nabla \eta \cdot \mathbf{v}_3|^2 \right)^2 \right] d\boldsymbol{\chi},$$

$$(3.11) \quad \mathcal{F}_t^\varepsilon[\boldsymbol{\xi}, \eta] =: \gamma_t\varepsilon \int_{D_1} \left[\left(\frac{\mathbf{v}_1 \cdot \nabla \boldsymbol{\xi} \mathbf{v}_2 + \mathbf{v}_2 \cdot \nabla \boldsymbol{\xi} \mathbf{v}_1}{2} + \frac{\varepsilon}{2} (\mathbf{v}_1 \cdot (\nabla \eta \otimes \nabla \eta) \mathbf{v}_2) \right)^2 + \left(\frac{\mathbf{v}_2 \cdot \nabla \boldsymbol{\xi} \mathbf{v}_3 + \mathbf{v}_3 \cdot \nabla \boldsymbol{\xi} \mathbf{v}_2}{2} + \frac{\varepsilon}{2} (\mathbf{v}_2 \cdot (\nabla \eta \otimes \nabla \eta) \mathbf{v}_3) \right)^2 + \left(\frac{\mathbf{v}_1 \cdot \nabla \boldsymbol{\xi} \mathbf{v}_3 + \mathbf{v}_3 \cdot \nabla \boldsymbol{\xi} \mathbf{v}_1}{2} + \frac{\varepsilon}{2} (\mathbf{v}_1 \cdot (\nabla \eta \otimes \nabla \eta) \mathbf{v}_3) \right)^2 \right] d\boldsymbol{\chi},$$

and

$$(3.12) \quad \mathcal{F}_d^\varepsilon[\boldsymbol{\xi}, \eta] =: \gamma_d\varepsilon^3 \int_{D_1} [7\eta_{,11}^2 + 16\eta_{,12}^2 - 2\eta_{,11}\eta_{,22} + 7\eta_{,22}^2] d\boldsymbol{\chi}.$$

3.2. Van der Waals Energy Contribution. We derive the continuum versions of (2.10) and (2.12), which we shall see have the form

$$(3.13) \quad \mathcal{F}_w^\varepsilon[\boldsymbol{\xi}, \eta] = \frac{1}{\varepsilon} \int_{D_1} G(\boldsymbol{\chi}, \boldsymbol{\xi}, \eta) d\boldsymbol{\chi}.$$

An important feature of our approach is that, to define the function G , we develop an expression for the local mismatch between the two lattices in their reference configurations. This expression depends on χ and on the relative rotation and lattice parameter mismatch.

The Lennard-Jones potential is considered first. Starting with the inner double sum on the right-hand side of (2.10), we observe that the total interaction energy corresponding to the atom ijk on $\hat{\mathcal{A}}_2$ with all the atoms on the rigid lattice $\hat{\mathcal{A}}_1$ is

$$(3.14) \quad \sum_{\ell, m=-\infty}^{\infty} \sum_{\tilde{k}=1}^2 g_{LJ} \left(\frac{\|\mathbf{q}_{ij}^k - \mathbf{p}_{\ell\tilde{m}}^{\tilde{k}}\|}{\varepsilon} \right).$$

Next, we define \mathbf{t}_{ijk} , the local horizontal mismatch between the lattices $\hat{\mathcal{A}}_1$ and $\hat{\mathcal{A}}_2$ in the reference configuration as measured at atom ijk on $\hat{\mathcal{A}}_2$. To determine \mathbf{t}_{ijk} , we project the vector \mathbf{r}_{ij}^k onto the plane of $\hat{\mathcal{A}}_1$. The projection falls inside one of the unit cells of $\hat{\mathcal{A}}_1$. Let $\tilde{\ell}, \tilde{m}$ be the indices of that unit cell. We define \mathbf{t}_{ijk} as the vector from the atom $\mathbf{p}_{\tilde{\ell}\tilde{m}}^{\tilde{k}}$ on $\hat{\mathcal{A}}_1$ to the endpoint of the projection of \mathbf{r}_{ij}^k onto the plane of $\hat{\mathcal{A}}_1$. See Figure 3.1.

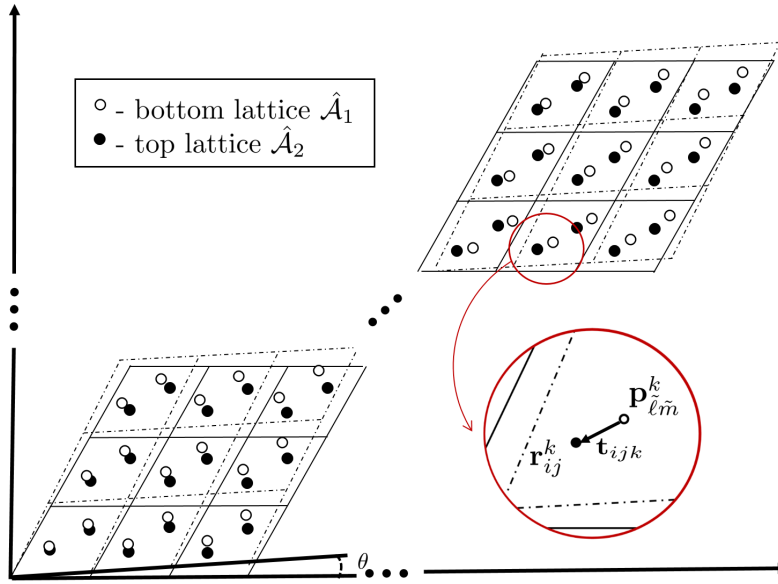


Fig. 3.1: The reference configuration of the system of two hexagonal lattices $\hat{\mathcal{A}}_1$ and $\hat{\mathcal{A}}_2$, mismatched by an angle θ , in nondimensional coordinates. Only two patches of the lattice structure are shown: near and away from the origin. The region of two atoms in the reference configurations, \mathbf{r}_{ij}^k and $\mathbf{p}_{\tilde{\ell}\tilde{m}}^{\tilde{k}}$, is zoomed in to show the corresponding local horizontal mismatched \mathbf{t}_{ijk} between them.

We can now write

$$(3.15) \quad \begin{aligned} \|\mathbf{q}_{ij}^k - \mathbf{p}_{\ell\tilde{m}}^{\tilde{k}}\| &= \left\| \left(\mathbf{q}_{ij}^k - \mathbf{r}_{ij}^k \right) + \left(\mathbf{r}_{ij}^k - \mathbf{p}_{\tilde{\ell}\tilde{m}}^{\tilde{k}} \right) + \left(\mathbf{p}_{\tilde{\ell}\tilde{m}}^{\tilde{k}} - \mathbf{p}_{\ell\tilde{m}}^{\tilde{k}} \right) \right\| \\ &= \left\| \left(\varepsilon \boldsymbol{\xi}(\boldsymbol{\chi}_{ij}^k), \varepsilon \eta(\boldsymbol{\chi}_{ij}^k) \right) + \left(\mathbf{t}_{ijk}, \varepsilon \right) + \left(\varepsilon \delta_1 \left(\left(\tilde{\ell} - \ell + (k - \tilde{k})/3 \right) \mathbf{a}_1^1 + \left(\tilde{m} - m + (k - \tilde{k})/3 \right) \mathbf{a}_2^1 \right), 0 \right) \right\| \\ &= \left(\left\| \varepsilon \delta_1 \left(\left(\tilde{\ell} - \ell + (k - \tilde{k})/3 \right) \mathbf{a}_1^1 + \left(\tilde{m} - m + (k - \tilde{k})/3 \right) \mathbf{a}_2^1 \right) + \mathbf{t}_{ijk} + \varepsilon \boldsymbol{\xi}(\boldsymbol{\chi}_{ij}^k) \right\|^2 + \left(\varepsilon + \varepsilon \eta(\boldsymbol{\chi}_{ij}^k) \right)^2 \right)^{1/2}. \end{aligned}$$

Recall from (3.4) that $\alpha\varepsilon$, the relative mismatch between the lattice parameters, is $\mathcal{O}(\varepsilon)$. In a similar way, we define

$$(3.16) \quad \Theta := \frac{\theta}{\varepsilon} = \mathcal{O}(1),$$

so that $\Theta\varepsilon$, the relative rotation between the lattices, is $\mathcal{O}(\varepsilon)$. Hence, we can linearize \mathbf{t}_{ijk} in ε to write $\mathbf{t}_{ijk} = \mathbf{t}_{ijk}^t + \mathbf{t}_{ijk}^r$, where \mathbf{t}_{ijk}^t is the relative mismatch when $\theta = 0$ and \mathbf{t}_{ijk}^r is the relative mismatch when $\alpha = 0$. We next

derive expressions for \mathbf{t}_{ijk}^t and \mathbf{t}_{ijk}^r . Recall that we assume that the left bottom corner of the 0,0 cell of $\hat{\mathcal{A}}_2$ lies directly above the left bottom corner of the 0,0 cell of $\hat{\mathcal{A}}_1$.

To write down \mathbf{t}_{ijk}^t , we assume that $\theta = 0$ and hence $\mathbf{a}_i^1 = \mathbf{a}_i^2$ for $i = 1, 2$. We then have

$$\begin{aligned}
\mathbf{t}_{ijk}^t &= \varepsilon \delta_2 \left((i+k/3) \mathbf{a}_1^2 + (j+k/3) \mathbf{a}_2^2 \right) - \varepsilon \delta_1 \left((\tilde{\ell} + k/3) \mathbf{a}_1^1 + (\tilde{m} + k/3) \mathbf{a}_2^1 \right) \\
&= ((i+k/3)(\delta_2 - \delta_1)\varepsilon + i_1 \delta_1 \varepsilon) \mathbf{a}_1^2 + ((j+k/3)(\delta_2 - \delta_1)\varepsilon + j_1 \delta_1 \varepsilon) \mathbf{a}_2^2 \\
&= \left((i+k/3) \left(\frac{\delta_2 - \delta_1}{\delta_2 \varepsilon} \right) \delta_2 \varepsilon^2 + i_1 \delta_1 \varepsilon \right) \mathbf{a}_1^2 + \left((j+k/3) \left(\frac{\delta_2 - \delta_1}{\delta_2 \varepsilon} \right) \delta_2 \varepsilon^2 + j_1 \delta_1 \varepsilon \right) \mathbf{a}_2^2 \\
(3.17) \quad &= \alpha \varepsilon (\delta_2 \varepsilon (i+k/3)) \mathbf{a}_1^2 + \alpha \varepsilon (\delta_2 \varepsilon (j+k/3)) \mathbf{a}_2^2 + \delta_1 \varepsilon i_1 \mathbf{a}_1^2 + \delta_1 \varepsilon j_1 \mathbf{a}_2^2 = \alpha \varepsilon \chi_{ij}^k + \delta_1 \varepsilon (i_1 \mathbf{a}_1^2 + j_1 \mathbf{a}_2^2),
\end{aligned}$$

where $i_1 = i - \tilde{\ell}$ and $j_1 = j - \tilde{m}$, and where the final equal sign uses (3.5). Note that we could instead write

$$(3.18) \quad \mathbf{t}_{ijk}^t = \alpha \varepsilon \chi_{ij}^k + \delta_1 \varepsilon (i_1 \mathbf{a}_1^1 + j_1 \mathbf{a}_2^1).$$

To write down \mathbf{t}_{ijk}^r , we assume $\delta_1 = \delta_2$, and in this case, we have

$$\begin{aligned}
\mathbf{t}_{ijk}^r &= \varepsilon \delta_1 \left((i+k/3) \mathbf{a}_1^2 + (j+k/3) \mathbf{a}_2^2 \right) - \varepsilon \delta_1 \left((\tilde{\ell} + k/3) \mathbf{a}_1^1 + (\tilde{m} + k/3) \mathbf{a}_2^1 \right) \\
(3.19) \quad &= \varepsilon \delta_1 \left((i+k/3) (\mathbf{a}_1^2 - \mathbf{a}_1^1) + (j+k/3) (\mathbf{a}_2^2 - \mathbf{a}_2^1) \right) + \varepsilon \delta_1 (i_2 \mathbf{a}_1^1 + j_2 \mathbf{a}_2^1),
\end{aligned}$$

where $i_2 = i - \tilde{\ell}$ and $j_2 = j - \tilde{m}$. Recalling that the lattice $\hat{\mathcal{A}}_1$ is rotated with respect to $\hat{\mathcal{A}}_2$ by the angle $\theta = \varepsilon \Theta$, we see that

$$\mathbf{a}_i^2 - \mathbf{a}_i^1 = \mathbf{a}_i^2 - R(\theta) \mathbf{a}_i^2 = \begin{pmatrix} 1 - \cos \varepsilon \Theta & \sin \varepsilon \Theta \\ -\sin \varepsilon \Theta & 1 - \cos \varepsilon \Theta \end{pmatrix} \mathbf{a}_i^2 \sim \varepsilon \Theta \begin{pmatrix} 0 & 1 \\ -1 & 0 \end{pmatrix} \mathbf{a}_i^2 \quad \text{for } i = 1, 2.$$

Inserting these expressions into (3.19) yields

$$(3.20) \quad \mathbf{t}_{ijk}^r \sim \varepsilon \Theta (\chi_{ij}^k)^\perp + \varepsilon \delta_1 (i_2 \mathbf{a}_1^1 + j_2 \mathbf{a}_2^1),$$

where $(\chi_{ij}^k)^\perp = \begin{pmatrix} 0 & 1 \\ -1 & 0 \end{pmatrix} \chi_{ij}^k$.

Combining (3.18) and (3.20) gives

$$(3.21) \quad \mathbf{t}_{ijk} = \mathbf{t}_{ijk}^t + \mathbf{t}_{ijk}^r \sim \varepsilon \alpha \chi_{ij}^k + \varepsilon \Theta (\chi_{ij}^k)^\perp + \varepsilon \delta_1 (i_1 \mathbf{a}_1^1 + j_1 \mathbf{a}_2^1 + i_2 \mathbf{a}_1^1 + j_2 \mathbf{a}_2^1).$$

Now we substitute (3.21) into (3.15). Also, we use that $i_1 = i_2 = i - \tilde{\ell}$, $j_1 = j_2 = j - \tilde{m}$ and that the basis of $\hat{\mathcal{A}}_1$ is a small perturbation of the basis of $\hat{\mathcal{A}}_2$, which follows from the smallness of θ . Lastly, we use that δ_1 and δ_2 are close. From (3.15), we thereby obtain

$$\begin{aligned}
\left\| \mathbf{q}_{ij}^k - \mathbf{p}_{\ell m}^{\tilde{k}} \right\| &\sim \varepsilon \left(\left\| \delta_1 \left((\tilde{\ell} - \ell + (k - \tilde{k})/3) \mathbf{a}_1^1 + (\tilde{m} - m + (k - \tilde{k})/3) \mathbf{a}_2^1 + 2i_1 \mathbf{a}_1^1 + 2j_1 \mathbf{a}_2^1 \right) \right. \right. \\
&\quad \left. \left. + \alpha \chi_{ij}^k + \Theta (\chi_{ij}^k)^\perp + \boldsymbol{\xi} (\chi_{ij}^k) \right\|^2 + (1 + \eta (\chi_{ij}^k))^2 \right)^{\frac{1}{2}} \\
&\sim \varepsilon \left(\left\| \delta_1 \left((2i - \ell - \tilde{\ell} + (k - \tilde{k})/3) \mathbf{a}_1^1 + (2j - m - \tilde{m} + (k - \tilde{k})/3) \mathbf{a}_2^1 \right) \right. \right. \\
&\quad \left. \left. + \alpha \chi_{ij}^k + \Theta (\chi_{ij}^k)^\perp + \boldsymbol{\xi} (\chi_{ij}^k) \right\|^2 + (1 + \eta (\chi_{ij}^k))^2 \right)^{\frac{1}{2}} \\
&\sim \varepsilon \left(\left\| \delta_2 \left((2i - \ell - \tilde{\ell} + (k - \tilde{k})/3) \mathbf{a}_1^2 + (2j - m - \tilde{m} + (k - \tilde{k})/3) \mathbf{a}_2^2 \right) \right. \right. \\
&\quad \left. \left. + \alpha \chi_{ij}^k + \Theta (\chi_{ij}^k)^\perp + \boldsymbol{\xi} (\chi_{ij}^k) \right\|^2 + (1 + \eta (\chi_{ij}^k))^2 \right)^{\frac{1}{2}} \\
(3.22) \quad &= \varepsilon \left(\left\| \delta_2 \left((\ell + (k - \tilde{k})/3) \mathbf{a}_1^2 + (m + (k - \tilde{k})/3) \mathbf{a}_2^2 \right) \right. \right. \\
&\quad \left. \left. + \alpha \chi_{ij}^k + \Theta (\chi_{ij}^k)^\perp + \boldsymbol{\xi} (\chi_{ij}^k) \right\|^2 + (1 + \eta (\chi_{ij}^k))^2 \right)^{\frac{1}{2}},
\end{aligned}$$

where in the last line we changed the indices $\ell \rightarrow 2i - \ell - \tilde{\ell}$ and $m \rightarrow 2j - m - \tilde{m}$. Therefore, we can write

$$(3.23) \quad g_{\text{LJ}} \left(\frac{\|\mathbf{q}_{ij}^k - \mathbf{p}_{\ell m}^{\tilde{k}}\|}{\varepsilon} \right) = g_{\text{LJ}} \left(\sqrt{\rho(\alpha\chi_{ij}^k + \Theta(\chi_{ij}^k)^\perp + \boldsymbol{\xi}(\chi_{ij}^k))^2 + (1 + \eta(\chi_{ij}^k))^2} \right),$$

where

$$\rho(\mathbf{p}) = \left\| \delta_2(\ell + (k - \tilde{k})/3) \mathbf{a}_1^2 + \delta_2(m + (k - \tilde{k})/3) \mathbf{a}_2^2 + \mathbf{p} \right\|$$

for every $\mathbf{p} \in \mathbb{R}^2$.

To complete the definition of G for the Lennard-Jones potential, we now set

$$(3.24) \quad G(\boldsymbol{\chi}, \boldsymbol{\xi}, \eta) := \mathcal{G}_{\text{LJ}}(\alpha\boldsymbol{\chi} + \Theta\boldsymbol{\chi}^\perp + \boldsymbol{\xi}, \eta),$$

where

$$(3.25) \quad \mathcal{G}_{\text{LJ}}(\mathbf{p}, t) := \sum_{k=1}^2 \sum_{\ell, m=-\infty}^{\infty} \sum_{\tilde{k}=1}^2 g_{\text{LJ}} \left(\sqrt{\rho(\mathbf{p})^2 + (1+t)^2} \right)$$

for $t > -1$.

For the Kolmogorov-Crespi potential, we note that $\rho(\alpha\chi_{ij}^k + \Theta(\chi_{ij}^k)^\perp + \boldsymbol{\xi}(\chi_{ij}^k))$ is the length of the projection of $\mathbf{q}_{ij}^k - \mathbf{p}_{\ell m}^{\tilde{k}}$ onto the xy -plane, which is the plane containing the fixed lattice $\hat{\mathcal{A}}_1$. In this case, we set

$$G(\boldsymbol{\chi}, \boldsymbol{\xi}, \eta) := \mathcal{G}_{\text{KC}}(\alpha\boldsymbol{\chi} + \Theta\boldsymbol{\chi}^\perp + \boldsymbol{\xi}, \eta),$$

where

$$(3.26) \quad \mathcal{G}_{\text{KC}}(\mathbf{p}, t) := \sum_{k=1}^2 \sum_{\ell, m=-\infty}^{\infty} \sum_{\tilde{k}=1}^2 g_{\text{KC}} \left(\sqrt{\rho(\mathbf{p})^2 + (1+t)^2}, \frac{\varepsilon\rho(\mathbf{p})}{\delta/L} \right).$$

Finally, the nondimensional version of either (2.10) or (2.12) takes the form

$$(3.27) \quad \mathcal{E}_w(\mathbf{Q}) = \varepsilon \sum_{i,j=1}^{N_2} \sum_{k=1}^2 \sum_{\ell, m=-\infty}^{\infty} \sum_{\tilde{k}=1}^2 g \sim \frac{1}{\varepsilon} \sum_{i,j=1}^{N_2} G(\boldsymbol{\chi}, \boldsymbol{\xi}, \eta) \varepsilon^2 \sim \frac{1}{\varepsilon} \int_{D_1} G(\boldsymbol{\chi}, \boldsymbol{\xi}, \eta) d\boldsymbol{\chi} =: \mathcal{F}_w^\varepsilon[\boldsymbol{\xi}, \eta],$$

where g is either g_{LJ} or g_{KC} with the appropriate arguments and G is defined using either \mathcal{G}_{LJ} or \mathcal{G}_{KC} . This establishes (3.13).

3.3. Continuum Energy. Combining (3.10)–(3.12) and (3.27) yields a continuum energy functional that can be written as

$$(3.28) \quad \begin{aligned} \mathcal{F}^\varepsilon[\boldsymbol{\xi}, \eta] &:= \frac{\varepsilon}{2} \int_{D_1} f \left(D(V\nabla\xi V^T) + \frac{\varepsilon}{2} V(\nabla\eta \otimes \nabla\eta) V^T \right) d\boldsymbol{\chi} \\ &+ \gamma_d \varepsilon^3 \int_{D_1} [7\eta_{,11}^2 + 16\eta_{,12}^2 - 2\eta_{,11}\eta_{,22} + 7\eta_{,22}^2] d\boldsymbol{\chi} + \frac{1}{\varepsilon} \int_{D_1} G(\boldsymbol{\chi}, \boldsymbol{\xi}, \eta) d\boldsymbol{\chi}. \end{aligned}$$

Here $D(A) = (A + A^T)/2$ is the symmetric part of A for any $A \in M^{3 \times 3}$, V is the 3×2 matrix whose i th row is \mathbf{v}_i and

$$f(M) = \gamma_s (m_{11}^2 + m_{22}^2 + m_{33}^2) + \gamma_t (m_{12}^2 + m_{21}^2 + m_{13}^2 + m_{31}^2 + m_{23}^2 + m_{32}^2)$$

for any $M = (m_{ij}) \in M_{\text{sym}}^{3 \times 3}$.

Note that the elastic contribution to the energy (3.28) is like that of the Föppl–von Kármán theory. The corresponding variational problem is of Ginzburg–Landau type, where the minimizers are determined via a competition between the elastic energy and the potential energy, which has multiple wells associated with the low-energy commensurate regions. The system is forced to reside in these wells, with the sharp transition between the wells being smoothed out due to the penalty imposed by the elastic energy. Consequently, we expect the minimizers of (3.28) to develop walls of characteristic width ε .

Now let $B(\nabla\xi, \nabla\eta) = D(V\nabla\xi V^T) + \frac{\varepsilon}{2} V\nabla\eta \otimes \nabla\eta V^T$ and

$$\hat{M} = \begin{pmatrix} \gamma_s B_{11} & \gamma_t B_{12} & \gamma_t B_{13} \\ \gamma_t B_{21} & \gamma_s B_{22} & \gamma_t B_{23} \\ \gamma_t B_{31} & \gamma_t B_{32} & \gamma_s B_{33} \end{pmatrix},$$

where B_{ij} are the entries in the matrix $B(\nabla\xi, \nabla\eta)$. Let $\mathbf{b}_1(\nabla\xi, \nabla\eta)$ and $\mathbf{b}_2(\nabla\xi, \nabla\eta)$ be the first two columns of $V^T \hat{M} V$. It is shown in Supplementary Material 7.3 that the Euler-Lagrange equations for the functional \mathcal{F}^ε are

$$(3.29) \quad \begin{cases} -\varepsilon \operatorname{div} [\mathbf{b}_1(\nabla\xi, \nabla\eta)] + \frac{1}{\varepsilon} G_{\xi_1}(\chi, \xi, \eta) = 0, \\ -\varepsilon \operatorname{div} [\mathbf{b}_2(\nabla\xi, \nabla\eta)] + \frac{1}{\varepsilon} G_{\xi_2}(\chi, \xi, \eta) = 0, \\ 14\varepsilon^3 \gamma_d \Delta^2 \eta - \varepsilon^2 \operatorname{div} (\mathbf{b}_1(\nabla\xi, \nabla\eta) \cdot \nabla\eta, \mathbf{b}_2(\nabla\xi, \nabla\eta) \cdot \nabla\eta) + \frac{1}{\varepsilon} G_\eta(\chi, \xi, \eta) = 0. \end{cases}$$

Here the first two equations describe the force balance in the plane of the deformable lattice, while the last equation is the vertical force balance.

4. Numerical Results. To validate our discrete-to-continuum procedure, in this section we compare the predictions of the discrete and the continuum models. We consider results for both the Lennard-Jones 12–6 potential (2.11) and the Kolmogorov-Crespi potential (2.13). To solve the atomistic model numerically, we use LAMMPS [26] to minimize the discrete energy (2.5). We use COMSOL [27] to numerically solve the system of partial differential equations (3.29) derived from the continuum model (3.28). For the continuum simulations, we use dissipation-dominated (gradient flow) dynamics to drive the energy of the system toward a possibly local minimum. The same task was accomplished for the atomistic model by performing molecular dynamics simulations at a sufficiently low temperature.

4.1. Periodic Boundary Conditions. In this subsection we describe how the boundary conditions are implemented in the simulations below. Recall that we assume that $\hat{\mathcal{A}}_2$ is infinite in extent and deforms periodically. This requires that the surface \mathcal{A}_2^0 satisfies the following constraint. If we pick two points identified on the edges of \mathcal{A}_2^0 and project the position vectors for these points onto $\hat{\mathcal{A}}_1$, then $\hat{\mathcal{A}}_1$ is invariant when translated by the vector between the two projected points. See Figure 4.1 (a). This in turn places constraints on the combinations of rotation and lattice mismatch that can be used to define the reference configuration.

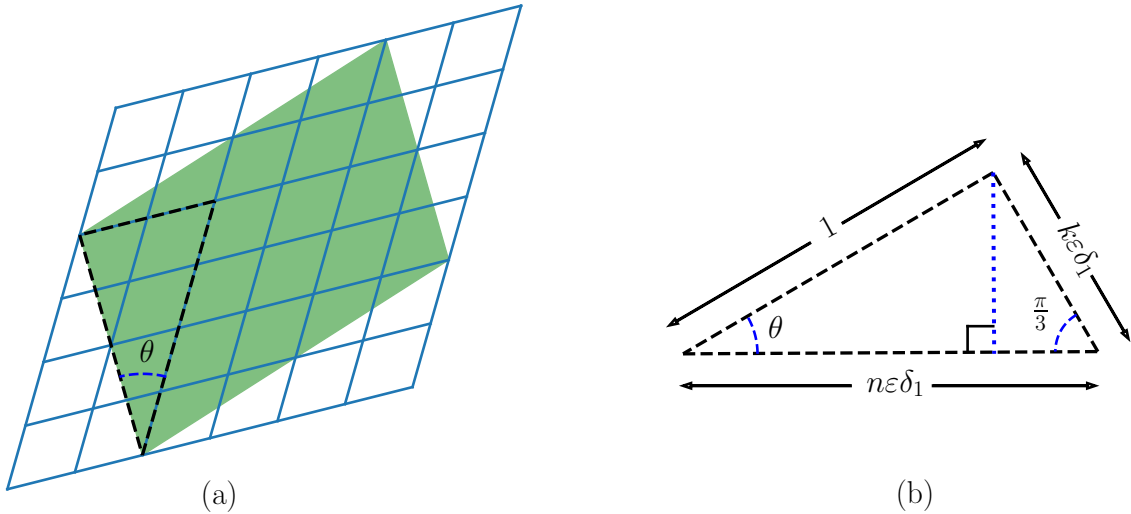


Fig. 4.1: (a) A rotation of the reference configuration \mathcal{A}_2^0 (shaded) such that each corner sits above a corner of a unit cell in $\hat{\mathcal{A}}_1$. (b) Geometry of the dashed triangle in (a). In the case depicted, $k = 2$ and $n = 4$.

As suggested by Figure 4.1(a), a sufficient condition for periodicity is that each corner of the reference configuration \mathcal{A}_2^0 sits above a corner of a unit cell in $\hat{\mathcal{A}}_1$. From the triangle in Figure 4.1(b), we derive the relations

$$(4.1) \quad \cos \theta = n\varepsilon\delta_1 - \frac{1}{2}k\varepsilon\delta_1, \quad \sin \theta = \frac{\sqrt{3}}{2}k\varepsilon\delta_1, \quad \text{and} \quad \tan \theta = \frac{\frac{\sqrt{3}}{2}k}{n - \frac{k}{2}}$$

among $\theta, \varepsilon\delta_1, n$, and k .

We use (4.1) to generate parameter values ensuring that periodicity is satisfied. Recall that we denote the number of cells in each side of the deformable lattice $\hat{\mathcal{A}}_2$ in D_1 by N_2 , so that $\varepsilon\delta_2 N_2 = 1$. We pick N_2 and δ_2 and set $\varepsilon = (\delta_2 N_2)^{-1}$. Given ε , we pick $k, n \in \mathbb{N}$ and set

$$(4.2) \quad \theta := \arctan\left(\frac{\frac{\sqrt{3}}{2}k}{n - \frac{k}{2}}\right) \text{ and } \delta_1 := \frac{2}{\sqrt{3}k\varepsilon} \sin\theta = \frac{1}{\varepsilon\sqrt{(n - \frac{k}{2})^2 + \frac{3}{4}k^2}}.$$

Note that the first condition in (4.1) is also satisfied. Hence the reference configuration will satisfy the ‘corner-to-corner’ periodicity condition.

Next we use (4.2) to derive useful expressions for the parameters α and Θ appearing in (3.24). We define m by $n = N_2 - m$. From (3.16) we have

$$(4.3) \quad \Theta = \frac{\theta}{\varepsilon} = \frac{1}{\varepsilon} \arctan\left(\frac{\frac{\sqrt{3}}{2}k\varepsilon\delta_2}{n\varepsilon\delta_2 - \frac{k}{2}\varepsilon\delta_2}\right) = \frac{1}{\varepsilon} \arctan\left(\frac{\frac{\sqrt{3}}{2}k\delta_2\varepsilon}{1 - (m + \frac{k}{2})\delta_2\varepsilon}\right) \sim \frac{\sqrt{3}}{2}k\delta_2,$$

using that $\varepsilon\delta_2 N_2 = 1$. Further,

$$(4.4) \quad \alpha = \frac{\delta_1 - \delta_2}{\varepsilon\delta_2} = \frac{1}{\varepsilon^2\delta_2\sqrt{(N_2 - m - \frac{k}{2})^2 + \frac{3}{4}k^2}} - 1 = \frac{1}{\varepsilon\sqrt{(1 - (m + \frac{k}{2})\varepsilon\delta_2)^2 + \frac{3}{4}(\varepsilon\delta_2 k)^2}} - 1 \sim \left(m + \frac{k}{2}\right)\delta_2.$$

4.2. Results for the Lennard-Jones Potential. For the Lennard-Jones potential, we start by comparing results for two different values of ε . Figure 4.2 shows results for $\varepsilon = 0.0094$ and Figure 4.3 shows results for $\varepsilon = 0.0047$. Each set of plots shows the out-of-plane displacement η and the two in-plane displacements ξ_1 and ξ_2 for both the discrete and continuum models. The parameter values used in these simulations are given in Tables 4.1(a), (b).

In the plots shown in Figure 4.3, the lateral extent of the system is twice the lateral extent of the plots in Figure 4.2. This difference reflects how changes in ε are implemented in the discrete simulations. The continuum simulations are based on the partial differential equations (3.29), in which ε appears explicitly. Hence we directly set the value of ε . However, ε does not appear explicitly in the discrete energy. Instead, recalling that $\varepsilon = \sigma/L$ we run simulations corresponding to different values of ε by changing the lateral size L of the system, i.e., by making the fixed and the deformable lattices smaller or larger.

The main observation from Figures 4.2 and 4.3 is that for both values of ε , we see good agreement between the discrete and the continuum models. We note that, for the out-of-plane displacement η , our simulations predict spatial patterns that have been observed for twisted graphene bilayers in many studies [18, 19, 20, 21, 22]. The plots of η in Figures 4.2(a), 4.2(d), 4.3(a), and 4.3(d) exhibit hot spots, which are regions of relatively large out-of-plane displacement localized about a point. Neighboring hot spots are connected by straight ridges or wrinkles, which are regions of relatively large out-of-plane displacement localized about the lines joining the hot spots. These wrinkles form domain walls between relatively large triangular commensurate regions.

In this same set of plots, we see that the hot spots occur at 2 different possible heights. In this case, we refer to the wrinkles emanating from the higher hot spots as *primary wrinkles* and the other wrinkles, which connect 2 lower hot spots, as *secondary wrinkles*. We note that the secondary wrinkles are less discernible in the plots from the discrete simulations compared to the plots from the continuum simulations. We can see this when comparing Figures 4.2(a) and 4.2(d) and when comparing Figures 4.3(a) and 4.3(d). In Figure 4.3(a), it is difficult to discern any secondary wrinkles. Another observation is that as ε decreases, the hot spots and the connecting wrinkles become more spatially concentrated, as expected by the form of the energy for the continuum model.

Next we consider the effect of changing the value of the parameter ω , which appears in the Lennard-Jones potential and measures the strength of the interaction, or the well-depth. See (2.10). Recall that we rescale the discrete energy by ω when we derived the continuum model. Decreasing ω increases the value of the dimensionless elastic constants γ_s, γ_t , and γ_d . We consider results for two values of ω . In Figure 4.3, we see results for $\omega = 0.5$.

We now compare these plots to the results depicted in Figure 4.4, for which the parameter values are the same as those used for Figure 4.3 except that $\omega = 0.0083$ and that consequently the values of γ_s, γ_t , and γ_d are different. See Tables 4.1(a), (b). Note that the difference in lateral extent seen in these two sets of plots is not because ε is different. Rather, in Figure 4.4, we show only a subset of the full domain in order to better exhibit the details of each plot. We see that for a smaller value of ω , the hot spots and the wrinkles become more spatially diffuse and the triangular commensurate regions occupy a relatively smaller part of the lattice. For smaller ω , there

is better agreement between the results predicted by the discrete and the continuum models. In particular, we see good agreement between the heights of the secondary wrinkles when comparing Figure 4.4(a) to Figure 4.4(d). Decreasing the value of ω improves the match because it increases the ratio of the elastic constants to the interaction constant. See [28] for further discussion of this issue.

	h_1, h_2	L	θ	k_s	k_t	k_d	σ	ω
Figures 4.2	$3^{1/2}2^{1/6}$	120	-3.22	25.2	1.5375	4.1	$2^{1/6}$	0.5
Figures 4.3	$3^{1/2}2^{1/6}$	240	-1.6	25.2	1.5375	4.1	$2^{1/6}$	0.5
Figures 4.4	$3^{1/2}2^{1/6}$	240	-1.6	25.2	1.5375	4.1	$2^{1/6}$	0.008

(a) Parameters for the Discrete Model. All lengths are in Å. θ is in degrees. k_s, k_t, k_d , and ω are in eV.

	ε	δ_1, δ_2	k	m	α	Θ	γ_s	γ_t	γ_d
Figures 4.2	0.0094	$3^{1/2}$	4	-2	0	-6	174.58	113.62	3.55
Figures 4.3	0.0047	$3^{1/2}$	4	-2	0	-6	174.58	113.62	3.55
Figures 4.4	0.0047	$3^{1/2}$	4	-2	0	-6	10474.79	6817.35	213.04

(b) Dimensionless Parameters for the Continuum Model. Θ is in radians.

Table 4.1: Parameter Values for Simulations using LJ Potential.

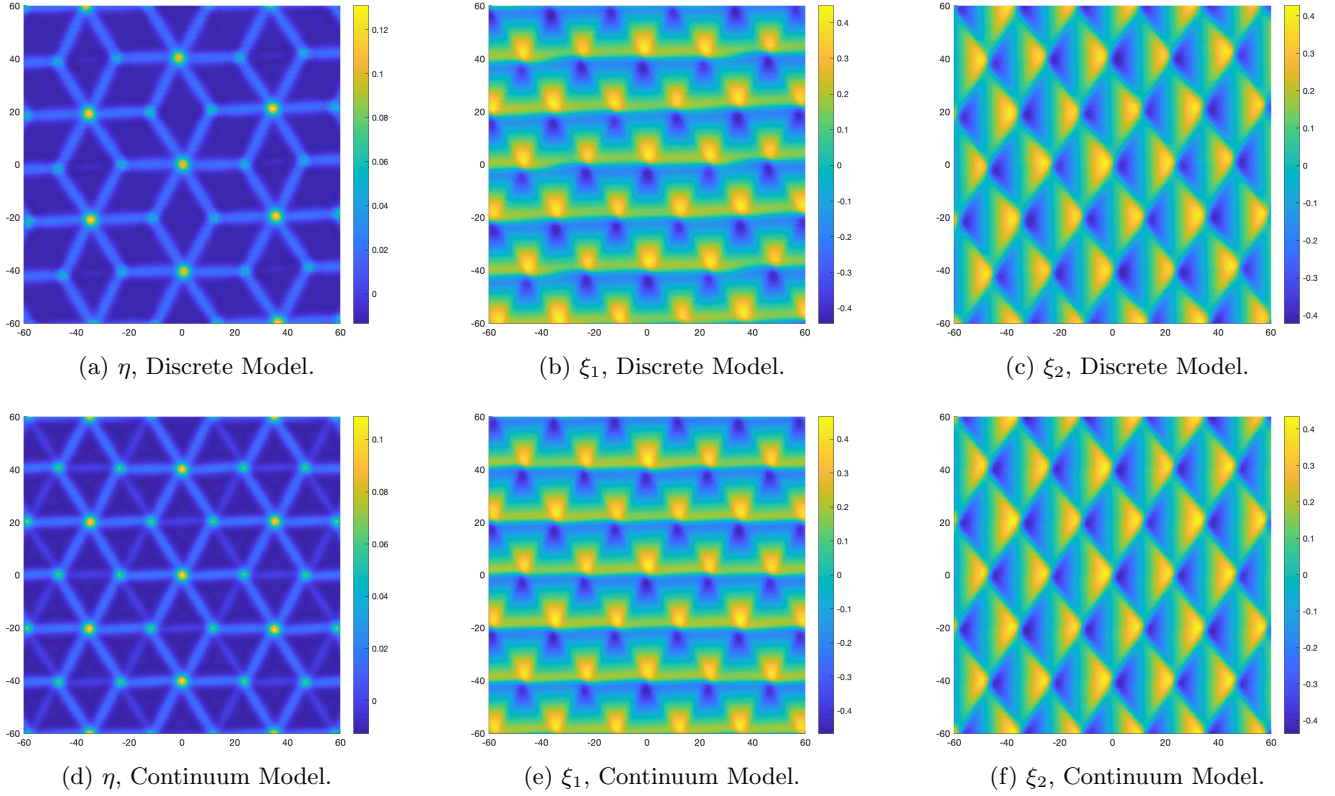


Fig. 4.2: Simulation Results for Lennard-Jones Potential with $\varepsilon = 0.0094$ and $\omega = 0.5$.

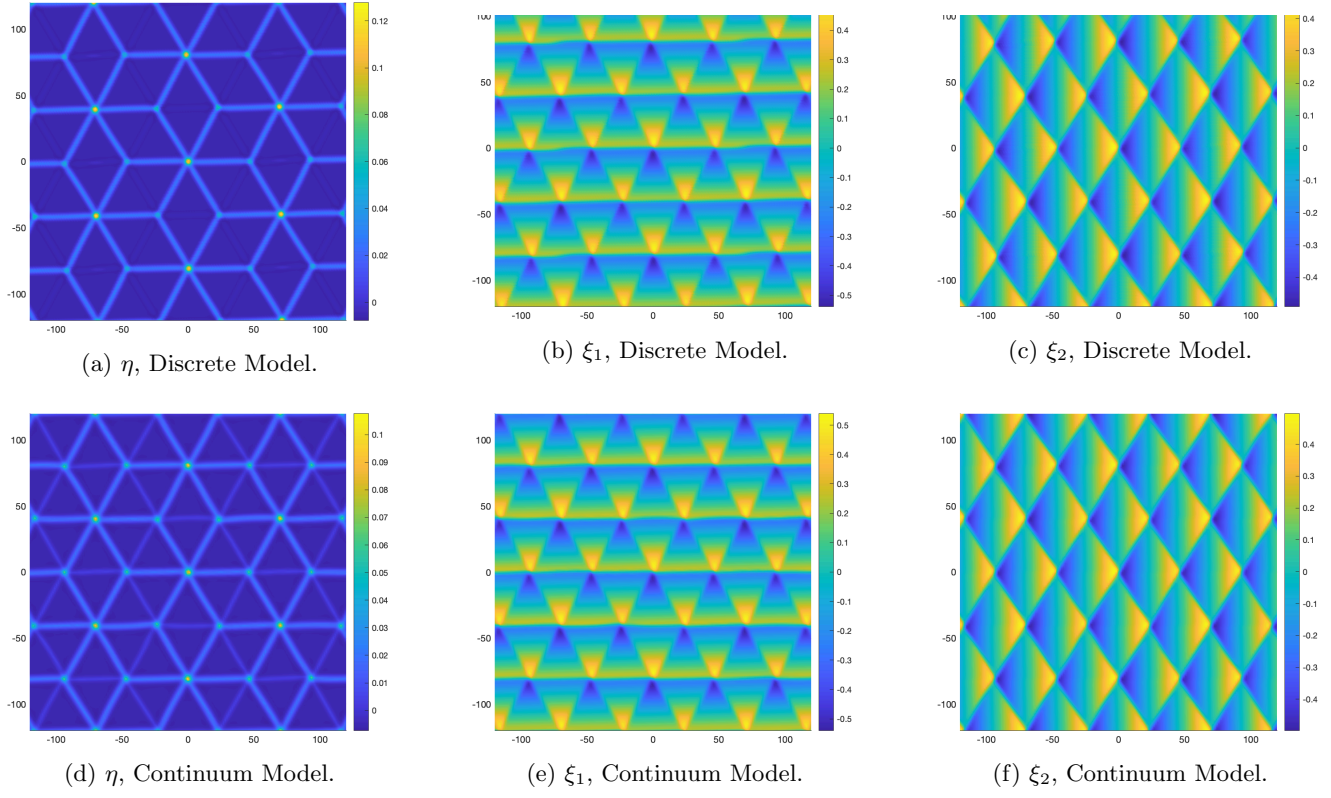


Fig. 4.3: Simulation Results for Lennard-Jones Potential with $\varepsilon = 0.0047$ and $\omega = 0.5$.

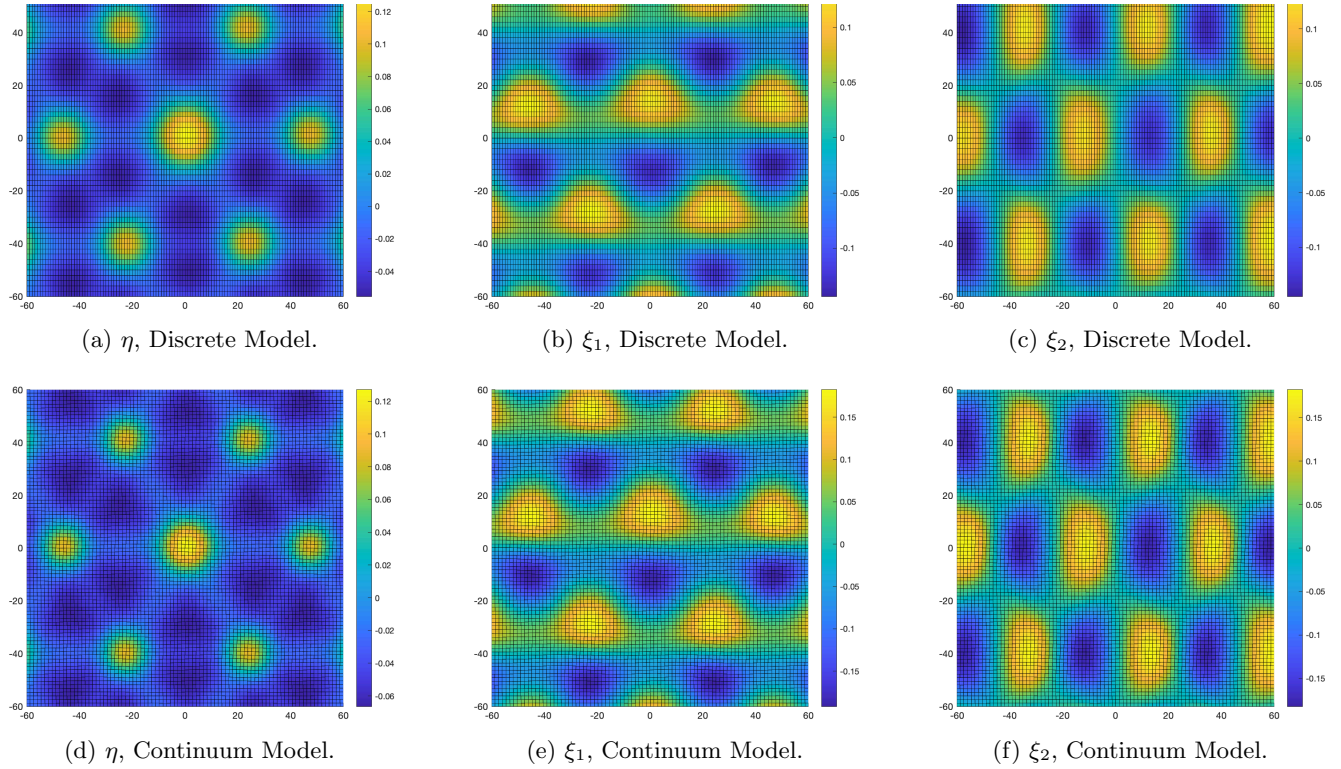


Fig. 4.4: Simulation Results for Lennard-Jones Potential with $\varepsilon = 0.0047$ and $\omega = 0.0083$.

4.3. Results for the Kolmogorov-Crespi Potential. In this subsection, we compare the predictions of the discrete and continuum models for the Kolmogorov-Crespi potential. For the discrete simulations, we generate results using the potential in (2.13), which we refer to as the Kolmogorov-Crespi-z potential.

To demonstrate that the match between the discrete and the continuum improves as ε gets smaller, we consider results for two different values of ε . Figure 4.5 shows results for $\varepsilon = 0.024$. Figure 4.6 shows results for $\varepsilon = 0.012$. The other parameter values used in these simulations are listed in Tables 4.2(a), (b), and (c). As in the previous subsection, the main point is the good match we see between the predictions of the discrete and continuum models. Also, as we saw above, here we see by comparing Figures 4.5(a) and 4.6(a) and by comparing Figures 4.5(d) and 4.6(d) that reducing ε spatially concentrates the hotspots and the wrinkles.

	h_1, h_2	L	θ	k_s	k_t	k_d	σ	ω	δ
Figure 4.5	2.46	140	-1.74	3.23	0.75	12.0	3.34	0.01	0.58
Figure 4.6	2.46	280	-0.87	3.23	0.75	12.0	3.34	0.01	0.58

(a) Parameters for the Discrete Model. All lengths are in Å. θ is in degrees. k_s, k_t, k_d , and ω are in eV.

	ε	δ_1, δ_2	k	m	α	Θ	γ_s	γ_t	γ_d
Figure 4.5	0.024	0.74	2	-1	0	-1.28	123.66	306.64	10.39
Figure 4.6	0.012	0.74	2	-1	0	-1.28	123.66	306.64	10.39

(b) Dimensionless Parameters for the Continuum Model. Θ is in radians.

$\tilde{\lambda}$	\tilde{C}	\tilde{C}_0	\tilde{C}_2	\tilde{C}_4
12.12	0.30	1.53	1.20	0.48

(c) Dimensionless Parameters for the KC Potential.

Table 4.2: Parameter Values for Simulations using KC Potential.

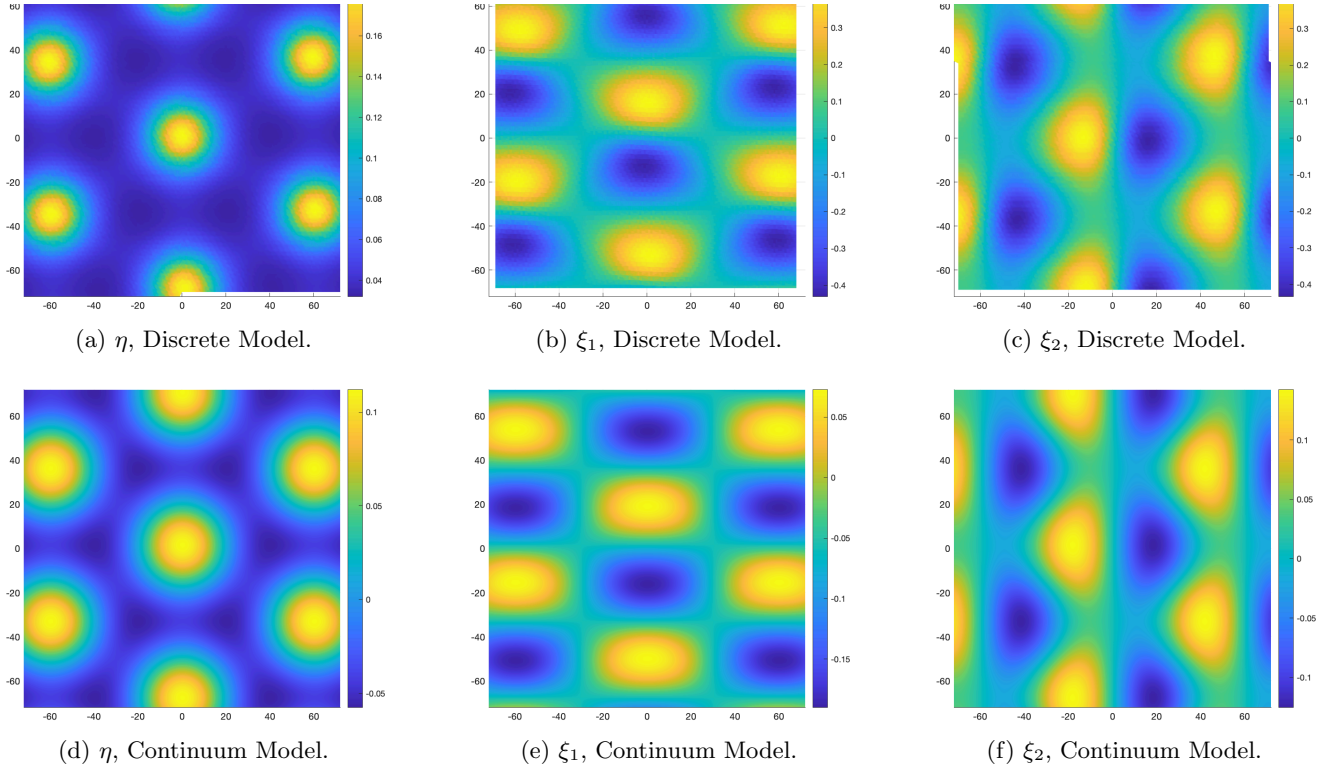


Fig. 4.5: Simulation Results for Kolmogorov-Crespi Potential with $\varepsilon = 0.024$.

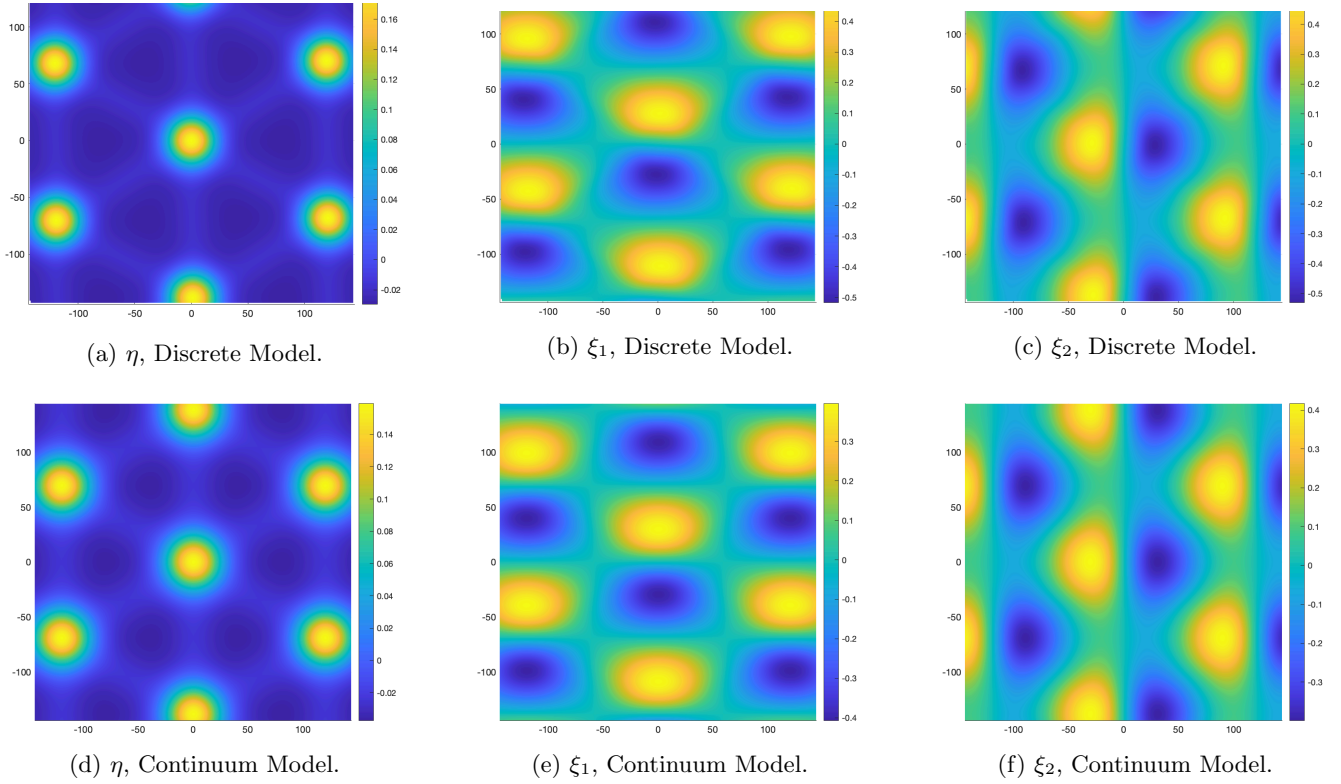


Fig. 4.6: Simulation Results for Kolmogorov-Crespi Potential with $\varepsilon = 0.012$.

4.4. Results for two versions of the Kolmogorov-Crespi potential. Here we compare results based on the full Kolmogorov-Crespi potential [23] to results based on the Kolmogorov-Crespi-z potential (2.13). We compare the predictions of the discrete model using both these potentials to the predictions of the continuum model, which is derived using the Kolmogorov-Crespi-z potential. Note that we do not have a version of the continuum model derived from the full Kolmogorov-Crespi potential. The goal of these comparisons is to explain why in some cases we fail to see a good match between the predictions of the discrete and the continuum models.

We present a set of results that indicates how the size of the elastic constants affects the smoothness of the deformed configurations. We consider two cases, one case in which the elastic constants are relatively small and one case in which the elastic constants are relatively large. The parameter values used in the simulations are listed in Tables 4.3 (a), (b) and Table 4.2 (c).

In Figure 4.7, we show results based on the Kolmogorov-Crespi-z potential for the case when the elastic constants are relatively large. The key plot here is Figure 4.7(b), which shows that the discrete model predicts smooth deformations. Comparing the LAMMPS results to the COMSOL results in this set of figures, we see that we get a good match between the predictions of the discrete and continuum models. Note in particular that in both Figures 4.7(a) and 4.7(c), the secondary wrinkles deflect away from the fixed lattice, i.e., the wrinkles are higher than the surrounding commensurate regions.

In Figures 4.8, we show results based on the Kolmogorov-Crespi-z potential for the case when the elastic constants are relatively small. In this case, we get a poor match between the predictions of the discrete and continuum models. In particular, Figure 4.8(a) indicates that the primary and secondary wrinkles deflect toward the fixed lattice for the discrete model, while Figure 4.8(c) indicates that the primary and secondary wrinkles deflect away from the fixed lattice for the continuum model. A key observation here is that when the elastic constants are small, the deformed configuration predicted by the discrete simulation exhibits small-scale spatial oscillation, as can be seen in Figure 4.8(b).

To explain these results, recall that a basic assumption justifying our discrete-to-continuum modeling procedure is that the discrete lattice can be embedded in a smooth surface. The small scale oscillations we see in Figure 4.8(b) suggest that this assumption is violated. As a consequence, we do not expect to get a good match between the predictions of the two models. The results in Figure 4.7 suggest that sufficiently large elastic constants can suppress these small scale oscillations, in which case a good match between the discrete and the continuum is attained.

One could conjecture that the problem is with the use of the Kolmogorov-Crespi-z potential. To show that this is not the case, we compare the predictions of the discrete model using the full Kolmogorov-Crespi potential versus the predictions of the Kolmogorov-Crespi-z potential. See Figure 4.9. Figures 4.9(a) and 4.9(b) show the predictions of the discrete model using the full Kolmogorov-Crespi potential and relatively large elastic constants. These simulations use the same parameter values as those used for Figure 4.7. Figures 4.9(c) and 4.9(d) show the predictions of the discrete model using the full Kolmogorov-Crespi potential and relatively small elastic constants. These simulations use the same parameter values as those used for Figure 4.8. By comparing Figures 4.9(a) and 4.9(b) to Figures 4.7(a) and 4.7(b) and by comparing Figures 4.9(c) and 4.9(d) to Figures 4.8(a) and 4.8(b), we see the same predictions from the discrete model if we use the full Kolmogorov-Crespi potential versus the Kolmogorov-Crespi-z potential.

In Figure 4.10 we show the predictions of the discrete and continuum models for relatively large elastic constants. These simulations use the same parameter values as those used for Figure 4.7. Note that here we are using the full Kolmogorov-Crespi potential. As expected from the above discussion, we see a good match between the discrete and the continuum.

	h_1, h_2	L	θ	k_s	k_t	k_d	σ	ω	δ
Figures 4.7, 4.9(a),(b), 4.10	2.46	120	-2.03	3.23	0.75	12	3.34	0.01	0.58
Figures 4.8, 4.9(c),(d)	2.46	120	-2.03	0.403	0.015	1.20	3.34	0.01	0.58

(a) Parameters for the Discrete Model. All lengths are in Å. θ is in degrees. $k_s, k_t, k_d,$ and ω are in eV.

	ε	δ_1, δ_2	k	m	α	Θ	γ_s	γ_t	γ_d
Figures 4.7, 4.9(a),(b), 4.10	0.028	0.74	2	-1	0	-1.28	123.66	306.64	10.39
Figures 4.8, 4.9(c),(d)	0.028	0.74	2	-1	0	-1.28	15.46	6.13	1.04

(b) Dimensionless Parameters for the Continuum Model. Θ is in radians.

Table 4.3: Parameter Values for Additional Simulations using KC Potential.

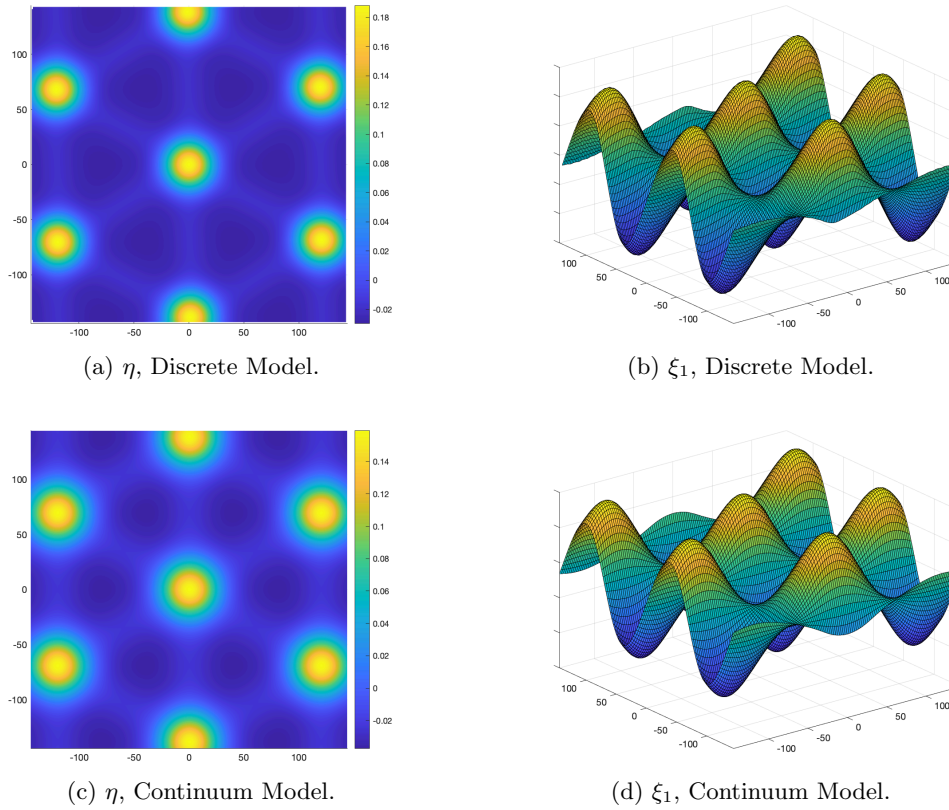


Fig. 4.7: Simulation Results for the Kolmogorov-Crespi Potential, Large Elastic Constants.

5. Conclusions. We derive a continuum model of a graphene bilayer in which one layer is fixed. We start with a discrete energy containing elastic terms and a weak interaction term. After expanding these terms in a small geometric parameter, we truncate the expansions and approximate sums with integrals to arrive at a continuum energy having a Ginzburg-Landau structure.

To validate our modeling, we perform numerical simulations to compare the predictions of the original discrete model and our continuum model. This comparison shows excellent agreement between the two models if the dimensionless elastic constants that appear in the continuum model are sufficiently large. The continuum model predicts spatial patterns that have been observed for twisted graphene bilayers in other papers [18, 19, 20, 21, 22]. For the out-of-plane displacement, the model predicts hot spots and wrinkles connecting neighboring hot spots. These wrinkles form domain walls between relatively large triangular commensurate regions.

For certain cases, we see discrepancies between what the discrete and continuum models predict for the out-of-plane displacements of some hot spots and wrinkles. This occurs for both the Lennard-Jones potential and the Kolmogorov-Crespi potential. Surface plots of solutions show small-scale spatial oscillations in the horizontal displacement when the elastic constants are not sufficiently large relative to the strength of the weak interaction. The existence of these oscillations violates a basic assumption of our discrete-to-continuum modeling procedure, and we believe that this explains why the discrepancies occur. For the Lennard-Jones potential, decreasing ω , which controls the strength of the weak interaction, increases the dimensionless elastic constants that appear in the continuum model. In this case, we see a good match for the out-of-plane displacement of all hot spots and wrinkles. Likewise, we see a good match for the Kolmogorov-Crespi potential when we directly increase the size of the elastic constants in the discrete model.

In this paper, we apply our discrete-to-continuum modeling procedure to a discrete energy in which the weak-interaction term is based on either the Lennard-Jones potential or a version of the Kolmogorov-Crespi potential that assumes that the layers are locally parallel. Each of these potentials has the feature that the interaction between

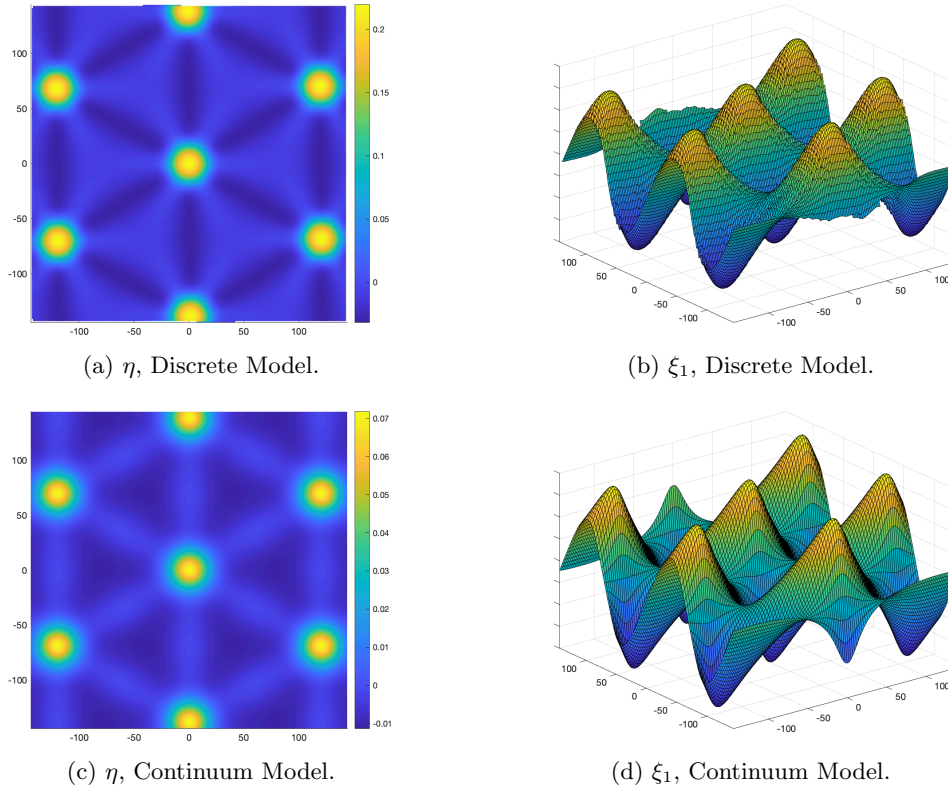


Fig. 4.8: Simulation Results for the Kolmogorov-Crespi Potential, Small Elastic Constants.

two non-bonded atoms is computed from a simple function of the positions of the two atoms. In particular, neither of these potentials requires additional information about the layers near the atoms, for example, information about the local orientation of the normals. Our approach is based on finding the local horizontal offset in the reference configuration. We decompose this offset into contributions from the lattice mismatch of the layers and from the misalignment between the layers. Because of the relatively simple form of the potentials we work with here, we can in a straightforward way incorporate these contributions as parameters in the final form of the potential in the continuum model. It would be of interest to explore whether this approach can be adapted to more complicated potentials. For example, the full Kolmogorov-Crespi potential depends not just on the positions of the interacting atoms but also on the local orientation of the lattices near the atoms.

6. Acknowledgment. This work was supported by the National Science Foundation grant DMS-1615952.

REFERENCES

- [1] M. I. Español, D. Golovaty, and J. P. Wilber, “Discrete-to-continuum modelling of weakly interacting incommensurate two-dimensional lattices,” *Proceedings of the Royal Society A: Mathematical, Physical and Engineering Sciences*, vol. 474, no. 2209, p. 20170612, 2018.
- [2] E. Y. Andrei and A. H. MacDonald, “Graphene bilayers with a twist,” *Nature materials*, vol. 19, no. 12, pp. 1265–1275, 2020.
- [3] S. Sunku, G. Ni, B.-Y. Jiang, H. Yoo, A. Sternbach, A. McLeod, T. Stauber, L. Xiong, T. Taniguchi, K. Watanabe, *et al.*, “Photonic crystals for nano-light in moiré graphene superlattices,” *Science*, vol. 362, no. 6419, pp. 1153–1156, 2018.
- [4] S. Carr, S. Fang, and E. Kaxiras, “Electronic-structure methods for twisted moiré layers,” *Nature Reviews Materials*, vol. 5, no. 10, pp. 748–763, 2020.
- [5] S. Carr, D. Massatt, S. B. Torrisi, P. Cazeaux, M. Luskin, and E. Kaxiras, “Relaxation and domain formation in incommensurate two-dimensional heterostructures,” *Physical Review B*, vol. 98, no. 22, p. 224102, 2018.
- [6] S. Carr, S. Fang, Z. Zhu, and E. Kaxiras, “Exact continuum model for low-energy electronic states of twisted bilayer graphene,” *Physical Review Research*, vol. 1, no. 1, p. 013001, 2019.
- [7] P. Cazeaux, M. Luskin, and D. Massatt, “Energy minimization of two dimensional incommensurate heterostructures,” *Archive for Rational Mechanics and Analysis*, vol. 235, no. 2, pp. 1289–1325, 2020.
- [8] K. Zhang and E. B. Tadmor, “Structural and electron diffraction scaling of twisted graphene bilayers,” *Journal of the Mechanics and Physics of Solids*, vol. 112, pp. 225–238, 2018.
- [9] A. Weston, Y. Zou, V. Enaldiev, A. Summerfield, N. Clark, V. Zólyomi, A. Graham, C. Yelgel, S. Magorrian, M. Zhou, *et al.*,

- “Atomic reconstruction in twisted bilayers of transition metal dichalcogenides,” *Nature Nanotechnology*, vol. 15, no. 7, pp. 592–597, 2020.
- [10] Y. Cao, V. Fatemi, S. Fang, K. Watanabe, T. Taniguchi, E. Kaxiras, and P. Jarillo-Herrero, “Unconventional superconductivity in magic-angle graphene superlattices,” *Nature*, vol. 556, no. 7699, pp. 43–50, 2018.
- [11] H. Yoo, R. Engelke, S. Carr, S. Fang, K. Zhang, P. Cazeaux, S. H. Sung, R. Hovden, A. W. Tsen, T. Taniguchi, *et al.*, “Atomic and electronic reconstruction at the van der waals interface in twisted bilayer graphene,” *Nature materials*, vol. 18, no. 5, pp. 448–453, 2019.
- [12] T. Li, S. Jiang, L. Li, Y. Zhang, K. Kang, J. Zhu, K. Watanabe, T. Taniguchi, D. Chowdhury, L. Fu, *et al.*, “Continuous mott transition in semiconductor moiré superlattices,” *Nature*, vol. 597, no. 7876, pp. 350–354, 2021.
- [13] K. Dong, T. Zhang, J. Li, Q. Wang, F. Yang, Y. Rho, D. Wang, C. P. Grigoropoulos, J. Wu, and J. Yao, “Flat bands in magic-angle bilayer photonic crystals at small twists,” *Physical review letters*, vol. 126, no. 22, p. 223601, 2021.
- [14] K. Novoselov, A. Mishchenko, A. Carvalho, and A. C. Neto, “2D materials and van der Waals heterostructures,” *Science*, vol. 353, no. 6298, p. aac9439, 2016.
- [15] M. V. Sulleiro, A. Develioglu, R. Quirós-Ovies, L. Martín-Pérez, N. M. Sabanés, M. L. Gonzalez-Juarez, I. J. Gómez, M. Vera-Hidalgo, V. Sebastián, J. Santamaría, *et al.*, “Fabrication of devices featuring covalently linked mos 2-graphene heterostructures,” *Nature chemistry*.
- [16] R. Xiang, T. Inoue, Y. Zheng, A. Kumamoto, Y. Qian, Y. Sato, M. Liu, D. Tang, D. Gokhale, J. Guo, *et al.*, “One-dimensional van der waals heterostructures,” *Science*, vol. 367, no. 6477, pp. 537–542, 2020.
- [17] K. Tran, G. Moody, F. Wu, X. Lu, J. Choi, K. Kim, A. Rai, D. A. Sanchez, J. Quan, A. Singh, *et al.*, “Evidence for moiré excitons in van der waals heterostructures,” *Nature*, vol. 567, no. 7746, pp. 71–75, 2019.
- [18] M. M. van Wijk, A. Schuring, M. I. Katsnelson, and A. Fasolino, “Relaxation of moiré patterns for slightly misaligned identical lattices: graphene on graphite,” *2D Materials*, vol. 2, no. 3, p. 034010, 2015.
- [19] M. M. van Wijk, A. Schuring, M. I. Katsnelson, and A. Fasolino, “Moiré patterns as a probe of interplanar interactions for graphene on h-BN,” *Physical Review Letters*, vol. 113, no. 13, p. 135504, 2014.
- [20] N. N. T. Nam and M. Koshino, “Lattice relaxation and energy band modulation in twisted bilayer graphene,” *Phys. Rev. B*, vol. 96, p. 075311, Aug 2017.
- [21] S. K. Jain, V. Juričić, and G. T. Barkema, “Structure of twisted and buckled bilayer graphene,” *2D Materials*, vol. 4, no. 1, p. 015018, 2016.
- [22] V. Enaldiev, V. Zólyomi, C. Yelgel, S. Magorrian, and V. Fal’ko, “Stacking domains and dislocation networks in marginally twisted bilayers of transition metal dichalcogenides,” *Physical Review Letters*, vol. 124, no. 20, p. 206101, 2020.
- [23] A. N. Kolmogorov and V. H. Crespi, “Registry-dependent interlayer potential for graphitic systems,” *Phys. Rev. B*, vol. 71, p. 235415, Jun 2005.
- [24] V. Vitek, “Intrinsic stacking faults in body-centred cubic crystals,” *The Philosophical Magazine: A Journal of Theoretical Experimental and Applied Physics*, vol. 18, no. 154, pp. 773–786, 1968.

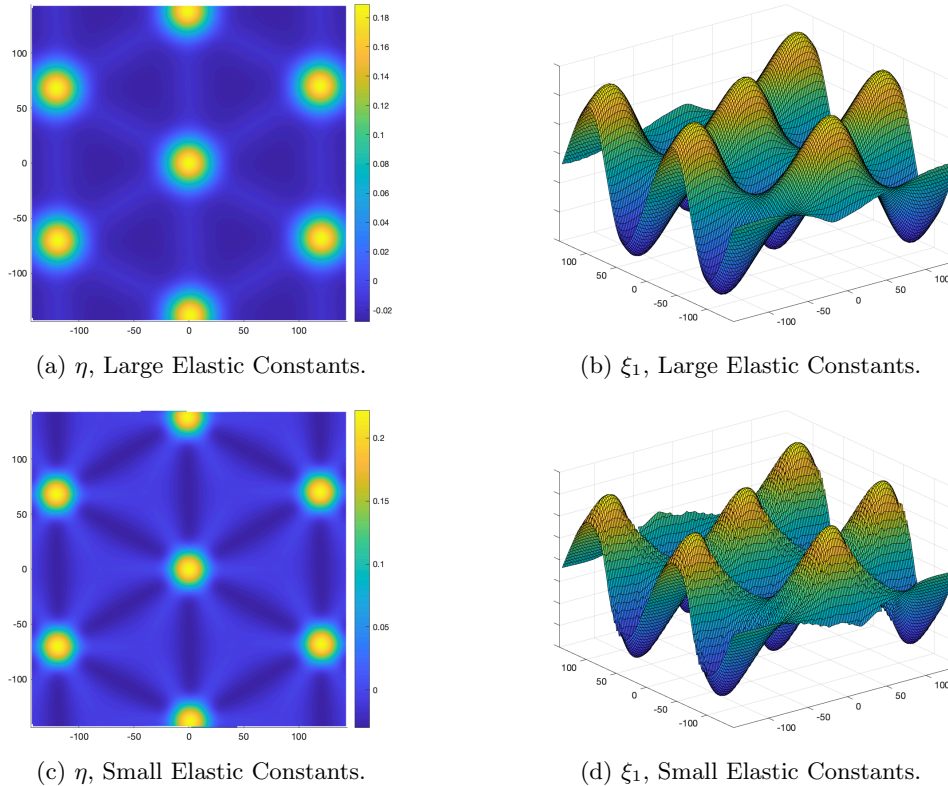


Fig. 4.9: Simulation Results for the Discrete Model Using the Full Kolmogorov-Crespi Potential.

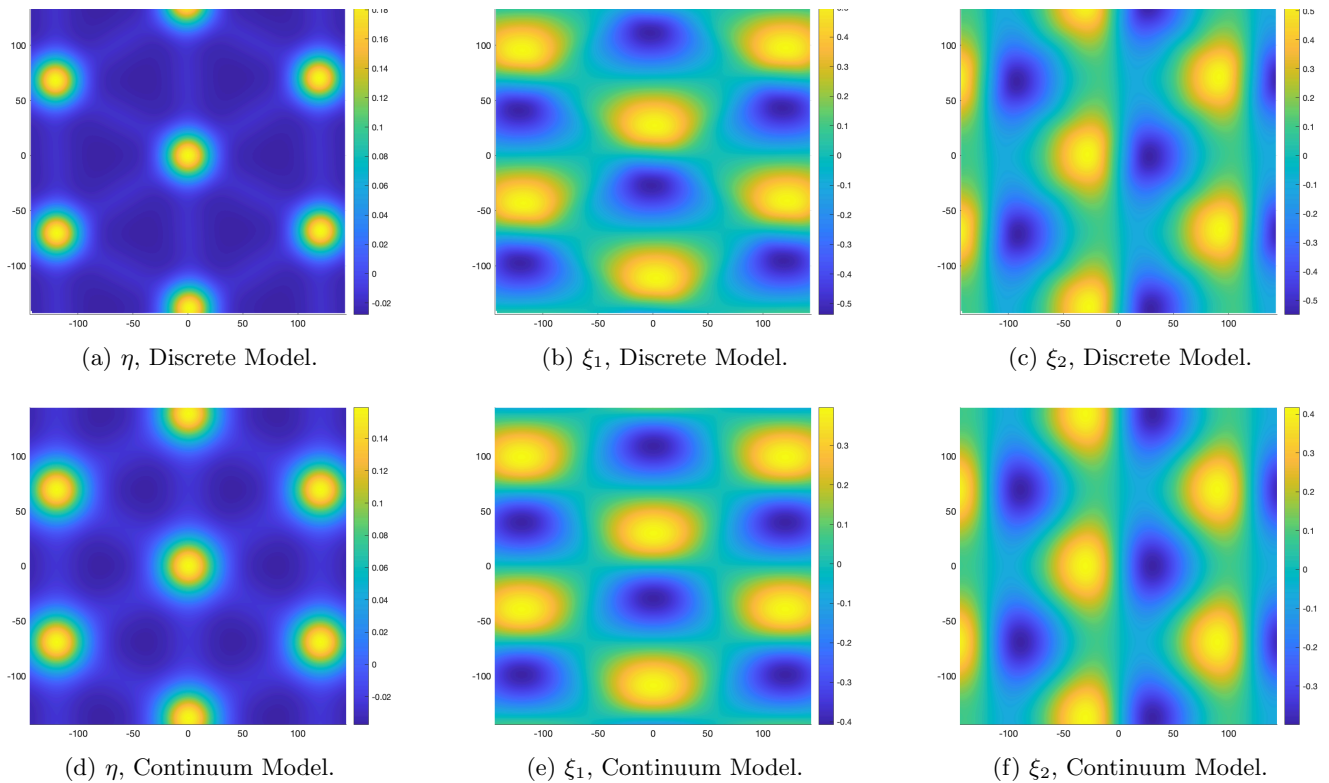


Fig. 4.10: Simulation Results for the Kolmogorov-Crespi Potential, Large Elastic Constants.

- [25] S. Zhou, J. Han, S. Dai, J. Sun, and D. J. Srolovitz, “Van der Waals bilayer energetics: Generalized stacking-fault energy of graphene, boron nitride, and graphene/boron nitride bilayers,” *Physical Review B*, vol. 92, no. 15, p. 155438, 2015.
- [26] S. Plimpton, “Fast parallel algorithms for short-range molecular dynamics,” *Journal of Computational Physics*, vol. 117, no. 1, pp. 1 – 19, 1995. Available at <http://lammps.sandia.gov>.
- [27] “COMSOL Multiphysics® v. 5.3.” <http://www.comsol.com/>. COMSOL AB, Stockholm, Sweden.
- [28] M. I. Español, D. Golovaty, and J. P. Wilber, “Discrete-to-continuum modeling of weakly interacting incommensurate chains,” *Physical Review E*, vol. 96, no. 3, p. 033003, 2017.
- [29] S. Dai, Y. Xiang, and D. J. Srolovitz, “Structure and energetics of interlayer dislocations in bilayer graphene,” *Physical Review B*, vol. 93, no. 8, p. 085410, 2016.
- [30] S. Dai, Y. Xiang, and D. J. Srolovitz, “Twisted bilayer graphene: Moiré with a twist,” *Nano letters*, vol. 16, no. 9, pp. 5923–5927, 2016.
- [31] A. Braides, M. Solci, and E. Vitali, “A derivation of linear elastic energies from pair-interaction atomistic systems,” *Networks and Heterogeneous Media*, vol. 2, no. 3, p. 551, 2007.
- [32] A. Braides, “Discrete-to-continuum variational methods for lattice systems,” in *Proceedings International Congress of Mathematicians. Seoul*, pp. 997–1015, 2014.
- [33] K. Zhang and E. B. Tadmor, “Energy and moiré patterns in 2d bilayers in translation and rotation: A study using an efficient discrete-continuum interlayer potential,” *Extreme Mechanics Letters*, vol. 14, pp. 16–22, 2017.
- [34] D. Halbertal, N. R. Finney, S. S. Sunku, A. Kerelsky, C. Rubio-Verdú, S. Shabani, L. Xian, S. Carr, S. Chen, C. Zhang, *et al.*, “Moiré metrology of energy landscapes in van der waals heterostructures,” *Nature communications*, vol. 12, no. 1, pp. 1–8, 2021.

7. Supplemental Material.

7.1. Asymptotic Expressions. In this section, we expand in ε all contributions to the discrete energy that led to the asymptotic expressions (3.7)–(3.9) in Section 3.1. Recall that \mathbf{q}_{ij}^k and \mathbf{b}_{ij}^p are nondimensional quantities in all the calculations that follow.

7.1.1. Extensional Springs. We expand the first term in (2.6) in ε . We first expand \mathbf{b}_{ij}^1 . Since all of the bonds relate to $\boldsymbol{\chi}_{ij}^2$, we will use it for the expansion. We have that

$$\begin{aligned}\mathbf{b}_{ij}^1 &= \mathbf{q}_{ij}^1 - \mathbf{q}_{ij}^2 \\ &= (\boldsymbol{\chi}_{ij}^1 + \varepsilon \boldsymbol{\xi}(\boldsymbol{\chi}_{ij}^1), \varepsilon + \varepsilon \eta(\boldsymbol{\chi}_{ij}^1)) - (\boldsymbol{\chi}_{ij}^2 + \varepsilon \boldsymbol{\xi}(\boldsymbol{\chi}_{ij}^2), \varepsilon + \varepsilon \eta(\boldsymbol{\chi}_{ij}^2)) \\ &= (\boldsymbol{\chi}_{ij}^1 - \boldsymbol{\chi}_{ij}^2 + \varepsilon (\boldsymbol{\xi}(\boldsymbol{\chi}_{ij}^1) - \boldsymbol{\xi}(\boldsymbol{\chi}_{ij}^2)), \varepsilon (\eta(\boldsymbol{\chi}_{ij}^1) - \eta(\boldsymbol{\chi}_{ij}^2))) \\ &= \left(\boldsymbol{\chi}_{ij}^1 - \boldsymbol{\chi}_{ij}^2 + \varepsilon \left(\nabla \boldsymbol{\xi}(\boldsymbol{\chi}_{ij}^1 - \boldsymbol{\chi}_{ij}^2) + \frac{1}{2} (\boldsymbol{\chi}_{ij}^1 - \boldsymbol{\chi}_{ij}^2) \cdot H_{\boldsymbol{\xi}} \cdot (\boldsymbol{\chi}_{ij}^1 - \boldsymbol{\chi}_{ij}^2) + \text{h.o.t.} \right), \right. \\ &\quad \left. \varepsilon \left(\nabla \eta \cdot (\boldsymbol{\chi}_{ij}^1 - \boldsymbol{\chi}_{ij}^2) + \frac{1}{2} (\boldsymbol{\chi}_{ij}^1 - \boldsymbol{\chi}_{ij}^2) \cdot H_{\eta} \cdot (\boldsymbol{\chi}_{ij}^1 - \boldsymbol{\chi}_{ij}^2) + \text{h.o.t.} \right) \right).\end{aligned}$$

Since

$$\begin{aligned}\boldsymbol{\chi}_{ij}^1 - \boldsymbol{\chi}_{ij}^2 &= \varepsilon \delta_2 \left(i + \frac{1}{3} \right) \mathbf{a}_1 + \left(j + \frac{1}{3} \right) \mathbf{a}_2 - \varepsilon \delta_2 \left(\left(i + \frac{2}{3} \right) \mathbf{a}_1 + \left(j + \frac{2}{3} \right) \mathbf{a}_2 \right) \\ &= \varepsilon \delta_2 \left(-\frac{1}{3} (\mathbf{a}_1 + \mathbf{a}_2) \right) = \varepsilon \delta_2 \left(-\frac{1}{2}, -\frac{\sqrt{3}}{6} \right) = \varepsilon \delta_2 (v_{11}, v_{12}) = \varepsilon \delta_2 \mathbf{v}_1,\end{aligned}$$

then,

$$(7.1) \quad \mathbf{b}_{ij}^1 = \varepsilon \delta_2 \left(v_{11} + \varepsilon \nabla \xi_1 \cdot \mathbf{v}_1 + \frac{\varepsilon^2 \delta_2}{2} \mathbf{v}_1 \cdot H_{\xi_1} \cdot \mathbf{v}_1 + \mathcal{O}(\varepsilon^3), v_{12} + \varepsilon \nabla \xi_2 \cdot \mathbf{v}_1 + \frac{\varepsilon^2 \delta_2}{2} \mathbf{v}_1 \cdot H_{\xi_2} \cdot \mathbf{v}_1 + \mathcal{O}(\varepsilon^3), \right. \\ \left. \varepsilon \nabla \eta \cdot \mathbf{v}_1 + \frac{\varepsilon^2 \delta_2}{2} \mathbf{v}_1 \cdot H_{\eta} \cdot \mathbf{v}_1 + \mathcal{O}(\varepsilon^3) \right).$$

Similarly,

$$(7.2) \quad \mathbf{b}_{ij}^2 = \varepsilon \delta_2 \left(v_{21} + \varepsilon \nabla \xi_1 \cdot \mathbf{v}_2 + \frac{\varepsilon^2 \delta_2}{2} \mathbf{v}_2 \cdot H_{\xi_1} \cdot \mathbf{v}_2 + \mathcal{O}(\varepsilon^3), v_{22} + \varepsilon \nabla \xi_2 \cdot \mathbf{v}_2 + \frac{\varepsilon^2 \delta_2}{2} \mathbf{v}_2 \cdot H_{\xi_2} \cdot \mathbf{v}_2 + \mathcal{O}(\varepsilon^3), \right. \\ \left. \varepsilon \nabla \eta \cdot \mathbf{v}_2 + \frac{\varepsilon^2 \delta_2}{2} \mathbf{v}_2 \cdot H_{\eta} \cdot \mathbf{v}_2 + \mathcal{O}(\varepsilon^3) \right),$$

where $\mathbf{v}_2 = (v_{21}, v_{22}) = (0, 1/\sqrt{3})$ and

$$(7.3) \quad \mathbf{b}_{ij}^3 = \varepsilon \delta_2 \left(v_{31} + \varepsilon \nabla \xi_1 \cdot \mathbf{v}_3 + \frac{\varepsilon^2 \delta_2}{2} \mathbf{v}_3 \cdot H_{\xi_1} \cdot \mathbf{v}_3 + \mathcal{O}(\varepsilon^3), v_{32} + \varepsilon \nabla \xi_2 \cdot \mathbf{v}_3 + \frac{\varepsilon^2 \delta_2}{2} \mathbf{v}_3 \cdot H_{\xi_2} \cdot \mathbf{v}_3 + \mathcal{O}(\varepsilon^3), \right. \\ \left. \varepsilon \nabla \eta \cdot \mathbf{v}_3 + \frac{\varepsilon^2 \delta_2}{2} \mathbf{v}_3 \cdot H_{\eta} \cdot \mathbf{v}_3 + \mathcal{O}(\varepsilon^3) \right),$$

where $\mathbf{v}_3 = (v_{31}, v_{32}) = \left(\frac{1}{2}, -\frac{\sqrt{3}}{6} \right)$. Note that in (7.1) and in the expressions that follow, all partial derivatives are evaluated at $\boldsymbol{\chi}_{ij}^2$.

We next expand

$$(7.4) \quad \|\mathbf{b}_{ij}^1\| = \varepsilon \delta_2 \|\mathbf{v}_1\| + \frac{\varepsilon^2 \delta_2}{\|\mathbf{v}_1\|} (v_{11} \nabla \xi_1 \cdot \mathbf{v}_1 + v_{12} \nabla \xi_2 \cdot \mathbf{v}_1) + \frac{\varepsilon^3 \delta_2}{2 \|\mathbf{v}_1\|} \left((\nabla \xi_1 \cdot \mathbf{v}_1)^2 + (\nabla \xi_2 \cdot \mathbf{v}_1)^2 + (\nabla \eta \cdot \mathbf{v}_1)^2 \right. \\ \left. - \frac{1}{\|\mathbf{v}_1\|^2} (v_{11} \nabla \xi_1 \cdot \mathbf{v}_1 + v_{12} \nabla \xi_2 \cdot \mathbf{v}_1)^2 + \delta_2 (v_{11} \mathbf{v}_1 \cdot H_{\xi_1} \cdot \mathbf{v}_1 + v_{12} \mathbf{v}_1 \cdot H_{\xi_2} \cdot \mathbf{v}_1) \right) + \mathcal{O}(\varepsilon^4).$$

Using that $\|\mathbf{v}_1\| = \frac{1}{\sqrt{3}}$, $v_{11} \nabla \xi_1 \cdot \mathbf{v}_1 + v_{12} \nabla \xi_2 \cdot \mathbf{v}_1 = \mathbf{v}_1 \cdot \nabla \boldsymbol{\xi} \cdot \mathbf{v}_1$, and that $(\nabla \xi_1 \cdot \mathbf{v}_1)^2 + (\nabla \xi_2 \cdot \mathbf{v}_1)^2 = |\nabla \boldsymbol{\xi} \mathbf{v}_1|^2$, we have that

$$(7.5) \quad \frac{\|\mathbf{b}_{ij}^1\| - \frac{\varepsilon \delta_2}{\sqrt{3}}}{\frac{\varepsilon \delta_2}{\sqrt{3}}} = \frac{\varepsilon}{\|\mathbf{v}_1\|^2} \mathbf{v}_1 \cdot \nabla \boldsymbol{\xi} \cdot \mathbf{v}_1 + \frac{\varepsilon^2}{2 \|\mathbf{v}_1\|^2} \left(|\nabla \boldsymbol{\xi} \cdot \mathbf{v}_1|^2 + (\nabla \eta \cdot \mathbf{v}_1)^2 \right. \\ \left. - \frac{1}{\|\mathbf{v}_1\|^2} (\mathbf{v}_1 \cdot \nabla \boldsymbol{\xi} \cdot \mathbf{v}_1)^2 + \delta_2 (v_{11} \mathbf{v}_1 \cdot H_{\xi_1} \cdot \mathbf{v}_1 + v_{12} \mathbf{v}_1 \cdot H_{\xi_2} \cdot \mathbf{v}_1) \right) + \mathcal{O}(\varepsilon^3).$$

$$(7.6) \quad \left(\frac{\|\mathbf{b}_{ij}^1\| - \frac{\varepsilon\delta_2}{\sqrt{3}}}{\frac{\varepsilon\delta_2}{\sqrt{3}}} \right)^2 = \frac{\varepsilon^2}{\|\mathbf{v}_1\|^4} (\mathbf{v}_1 \cdot \nabla \boldsymbol{\xi} \mathbf{v}_1)^2 + \frac{\varepsilon^3}{\|\mathbf{v}_1\|^4} \mathbf{v}_1 \cdot \nabla \boldsymbol{\xi} \mathbf{v}_1 \left(|\nabla \boldsymbol{\xi} \mathbf{v}_1|^2 + (\nabla \eta \cdot \mathbf{v}_1)^2 \right) + \mathbf{v}_1 \cdot \left(-\frac{1}{\|\mathbf{v}_1\|^2} \nabla \boldsymbol{\xi} (\mathbf{v}_1 \otimes \mathbf{v}_1) \nabla \boldsymbol{\xi} + \delta_2 v_{11} H_{\xi_1} + \delta_2 v_{12} H_{\xi_2} \right) \mathbf{v}_1 + \mathcal{O}(\varepsilon^4).$$

A similar computation for the second term in (2.6) yields

$$(7.7) \quad \left(\frac{\|\mathbf{b}_{ij}^2\| - \frac{\varepsilon\delta_2}{\sqrt{3}}}{\frac{\varepsilon\delta_2}{\sqrt{3}}} \right)^2 = \frac{\varepsilon^2}{\|\mathbf{v}_2\|^4} (\mathbf{v}_2 \cdot \nabla \boldsymbol{\xi} \mathbf{v}_2)^2 + \frac{\varepsilon^3}{\|\mathbf{v}_2\|^4} \mathbf{v}_2 \cdot \nabla \boldsymbol{\xi} \mathbf{v}_2 \left(|\nabla \boldsymbol{\xi} \mathbf{v}_2|^2 + (\nabla \eta \cdot \mathbf{v}_2)^2 \right) + \mathbf{v}_2 \cdot \left(-\frac{1}{\|\mathbf{v}_2\|^2} \nabla \boldsymbol{\xi} (\mathbf{v}_2 \otimes \mathbf{v}_2) \nabla \boldsymbol{\xi} + \delta_2 v_{21} H_{\xi_1} + \delta_2 v_{22} H_{\xi_2} \right) \mathbf{v}_2 + \mathcal{O}(\varepsilon^4).$$

and third term

$$(7.8) \quad \left(\frac{\|\mathbf{b}_{ij}^3\| - \frac{\varepsilon\delta_2}{\sqrt{3}}}{\frac{\varepsilon\delta_2}{\sqrt{3}}} \right)^2 = \frac{\varepsilon^2}{\|\mathbf{v}_3\|^4} (\mathbf{v}_3 \cdot \nabla \boldsymbol{\xi} \mathbf{v}_3)^2 + \frac{\varepsilon^3}{\|\mathbf{v}_3\|^4} \mathbf{v}_3 \cdot \nabla \boldsymbol{\xi} \mathbf{v}_3 \left(|\nabla \boldsymbol{\xi} \mathbf{v}_3|^2 + (\nabla \eta \cdot \mathbf{v}_3)^2 \right) + \mathbf{v}_3 \cdot \left(-\frac{1}{\|\mathbf{v}_3\|^2} \nabla \boldsymbol{\xi} (\mathbf{v}_3 \otimes \mathbf{v}_3) \nabla \boldsymbol{\xi} + \delta_2 v_{31} H_{\xi_1} + \delta_2 v_{32} H_{\xi_2} \right) \mathbf{v}_3 + \mathcal{O}(\varepsilon^4).$$

We now combine (7.6), (7.7), and (7.8), which yields

$$(7.9) \quad \begin{aligned} \mathcal{E}_s[\boldsymbol{\xi}, \eta] = & \sum_{i,j=1}^{N_2} \frac{9k_s}{2\omega} \left\{ \varepsilon^3 \left[(\mathbf{v}_1 \cdot \nabla \boldsymbol{\xi} \mathbf{v}_1)^2 + (\mathbf{v}_2 \cdot \nabla \boldsymbol{\xi} \mathbf{v}_2)^2 + (\mathbf{v}_3 \cdot \nabla \boldsymbol{\xi} \mathbf{v}_3)^2 \right] \right. \\ & + \varepsilon^4 \left[\mathbf{v}_1 \cdot \nabla \boldsymbol{\xi} \mathbf{v}_1 \left(|\nabla \boldsymbol{\xi} \mathbf{v}_1|^2 + (\nabla \eta \cdot \mathbf{v}_1)^2 \right) + \mathbf{v}_2 \cdot \nabla \boldsymbol{\xi} \mathbf{v}_2 \left(|\nabla \boldsymbol{\xi} \mathbf{v}_2|^2 + (\nabla \eta \cdot \mathbf{v}_2)^2 \right) \right. \\ & + \mathbf{v}_3 \cdot \nabla \boldsymbol{\xi} \mathbf{v}_3 \left(|\nabla \boldsymbol{\xi} \mathbf{v}_3|^2 + (\nabla \eta \cdot \mathbf{v}_3)^2 \right) \\ & + \mathbf{v}_1 \cdot \left(-\frac{1}{\|\mathbf{v}_1\|^2} \nabla \boldsymbol{\xi} (\mathbf{v}_1 \otimes \mathbf{v}_1) \nabla \boldsymbol{\xi} + \delta_2 v_{11} H_{\xi_1} + \delta_2 v_{12} H_{\xi_2} \right) \mathbf{v}_1 \\ & + \mathbf{v}_2 \cdot \left(-\frac{1}{\|\mathbf{v}_2\|^2} \nabla \boldsymbol{\xi} (\mathbf{v}_2 \otimes \mathbf{v}_2) \nabla \boldsymbol{\xi} + \delta_2 v_{21} H_{\xi_1} + \delta_2 v_{22} H_{\xi_2} \right) \mathbf{v}_2 \\ & \left. \left. + \mathbf{v}_3 \cdot \left(-\frac{1}{\|\mathbf{v}_3\|^2} \nabla \boldsymbol{\xi} (\mathbf{v}_3 \otimes \mathbf{v}_3) \nabla \boldsymbol{\xi} + \delta_2 v_{31} H_{\xi_1} + \delta_2 v_{32} H_{\xi_2} \right) \mathbf{v}_3 \right] + \mathcal{O}(\varepsilon^5) \right\}. \end{aligned}$$

Notice that $(\nabla \eta \cdot \mathbf{v}_1)^2 = \mathbf{v}_1 \cdot (\nabla \eta \otimes \nabla \eta) \cdot \mathbf{v}_1$ and the same for the other similar terms. To transform this sum to an integral, we use that the area of the small cells have dimension $\frac{\sqrt{3}}{2} \delta_2^2 \varepsilon^2$, and define $\gamma_s = \frac{6\sqrt{3}k_s}{\omega \delta_2^2}$.

7.1.2. Torsional Springs. We expand the first term in (2.8) in ε using the expansions (7.1) and (7.2), and then (7.4) for the norm.

$$(7.10) \quad \begin{aligned} \mathbf{b}_{ij}^1 \cdot \mathbf{b}_{ij}^2 &= \varepsilon^2 \delta_2^2 \{ \mathbf{v}_1 \cdot \mathbf{v}_2 + \varepsilon (\mathbf{v}_1 \nabla \boldsymbol{\xi} \cdot \mathbf{v}_2 + \mathbf{v}_2 \nabla \boldsymbol{\xi} \cdot \mathbf{v}_1) + \\ & \quad \varepsilon^2 ((\nabla \xi_1 \cdot \mathbf{v}_1)(\nabla \xi_1 \cdot \mathbf{v}_2) + (\nabla \xi_2 \cdot \mathbf{v}_1)(\nabla \xi_2 \cdot \mathbf{v}_2) + (\nabla \eta \cdot \mathbf{v}_1)(\nabla \eta \cdot \mathbf{v}_2)) + \mathcal{O}(\varepsilon^2) \}. \\ &= \varepsilon^2 \delta_2^2 \{ \mathbf{v}_1 \cdot \mathbf{v}_2 + \varepsilon (\mathbf{v}_1 \nabla \boldsymbol{\xi} \cdot \mathbf{v}_2 + \mathbf{v}_2 \nabla \boldsymbol{\xi} \cdot \mathbf{v}_1) + \\ & \quad \varepsilon^2 \mathbf{v}_1 \cdot ((\nabla \xi_1 \otimes \nabla \xi_1) + (\nabla \xi_2 \otimes \nabla \xi_2) + (\nabla \eta \otimes \nabla \eta)) \cdot \mathbf{v}_2 + \mathcal{O}(\varepsilon^2) \}. \end{aligned}$$

Notice that here, there are other terms of order ε^2 that are left out by following the work in [1] for the square case, where we learned that we do not need them to still be able to model what we want.

We also have that

$$\|\mathbf{b}_{ij}^1\| \|\mathbf{b}_{ij}^2\| = \varepsilon^2 \delta_2^2 (\|\mathbf{v}_1\| \|\mathbf{v}_2\| + \varepsilon (\mathbf{v}_1 \nabla \boldsymbol{\xi} \cdot \mathbf{v}_1 + \mathbf{v}_2 \nabla \boldsymbol{\xi} \cdot \mathbf{v}_2) + \mathcal{O}(\varepsilon^2)) = \varepsilon^2 \delta_2^2 \|\mathbf{v}_1\| \|\mathbf{v}_2\| (1 + \mathcal{O}(\varepsilon))$$

and therefore,

$$(7.11) \quad (\|\mathbf{b}_{ij}^1\| \|\mathbf{b}_{ij}^2\|)^{-1} = \frac{\varepsilon^{-2} \delta_2^{-2}}{\|\mathbf{v}_1\| \|\mathbf{v}_2\|} (1 + \mathcal{O}(\varepsilon)).$$

Then,

$$(7.12) \quad \frac{\mathbf{b}_{ij}^1 \cdot \mathbf{b}_{ij}^2}{\|\mathbf{b}_{ij}^1\| \|\mathbf{b}_{ij}^2\|} = \frac{\mathbf{v}_1 \cdot \mathbf{v}_2}{\|\mathbf{v}_1\| \|\mathbf{v}_2\|} + \varepsilon \left(\frac{\mathbf{v}_2 \cdot \nabla \xi \mathbf{v}_1}{\|\mathbf{v}_1\| \|\mathbf{v}_2\|} + \frac{\mathbf{v}_1 \cdot \nabla \xi \mathbf{v}_2}{\|\mathbf{v}_1\| \|\mathbf{v}_2\|} \right) + \frac{\varepsilon^2}{\|\mathbf{v}_1\| \|\mathbf{v}_2\|} \mathbf{v}_1 \cdot (\nabla \xi_1 \otimes \nabla \xi_1 + \nabla \xi_2 \otimes \nabla \xi_2 + \nabla \eta \otimes \nabla \eta) \cdot \mathbf{v}_2 + \mathcal{O}(\varepsilon^2).$$

Using that $\frac{\mathbf{v}_1 \cdot \mathbf{v}_2}{\|\mathbf{v}_1\| \|\mathbf{v}_2\|} = -1/2$ and that $\|\mathbf{v}_1\| = \|\mathbf{v}_2\| = 1/\sqrt{3}$, we obtain that

$$(7.13) \quad \left(\frac{\mathbf{b}_{ij}^1 \cdot \mathbf{b}_{ij}^2}{\|\mathbf{b}_{ij}^1\| \|\mathbf{b}_{ij}^2\|} + \frac{1}{2} \right)^2 = 9\varepsilon^2 (\mathbf{v}_2 \cdot \nabla \xi \mathbf{v}_1 + \mathbf{v}_1 \cdot \nabla \xi \mathbf{v}_2)^2 + 18\varepsilon^3 (\mathbf{v}_2 \cdot \nabla \xi \mathbf{v}_1 + \mathbf{v}_1 \cdot \nabla \xi \mathbf{v}_2) (\mathbf{v}_1 \cdot (\nabla \xi_1 \otimes \nabla \xi_1 + \nabla \xi_2 \otimes \nabla \xi_2 + \nabla \eta \otimes \nabla \eta) \cdot \mathbf{v}_2) + \mathcal{O}(\varepsilon^3)$$

Similarly,

$$(7.14) \quad \left(\frac{\mathbf{b}_{ij}^2 \cdot \mathbf{b}_{ij}^3}{\|\mathbf{b}_{ij}^2\| \|\mathbf{b}_{ij}^3\|} + \frac{1}{2} \right)^2 = 9\varepsilon^2 (\mathbf{v}_2 \cdot \nabla \xi \mathbf{v}_3 + \mathbf{v}_3 \cdot \nabla \xi \mathbf{v}_2)^2 + 18\varepsilon^3 (\mathbf{v}_2 \cdot \nabla \xi \mathbf{v}_3 + \mathbf{v}_3 \cdot \nabla \xi \mathbf{v}_2) (\mathbf{v}_2 \cdot (\nabla \xi_1 \otimes \nabla \xi_1 + \nabla \xi_2 \otimes \nabla \xi_2 + \nabla \eta \otimes \nabla \eta) \cdot \mathbf{v}_3) + \mathcal{O}(\varepsilon^3)$$

and

$$(7.15) \quad \left(\frac{\mathbf{b}_{ij}^1 \cdot \mathbf{b}_{ij}^3}{\|\mathbf{b}_{ij}^1\| \|\mathbf{b}_{ij}^3\|} + \frac{1}{2} \right)^2 = 9\varepsilon^2 (\mathbf{v}_3 \cdot \nabla \xi \mathbf{v}_1 + \mathbf{v}_1 \cdot \nabla \xi \mathbf{v}_3)^2 + 18\varepsilon^3 (\mathbf{v}_3 \cdot \nabla \xi \mathbf{v}_1 + \mathbf{v}_1 \cdot \nabla \xi \mathbf{v}_3) (\mathbf{v}_1 \cdot (\nabla \xi_1 \otimes \nabla \xi_1 + \nabla \xi_2 \otimes \nabla \xi_2 + \nabla \eta \otimes \nabla \eta) \cdot \mathbf{v}_3) + \mathcal{O}(\varepsilon^3)$$

For the following term, we need the expansion of \mathbf{b}_{i-1j}^3 . For it, we can write

$$(7.16) \quad \mathbf{b}_{i-1j}^3 = \mathbf{q}_{ij}^1 - \mathbf{q}_{i-1j}^2 = (\mathbf{q}_{ij}^1 - \mathbf{q}_{ij}^2) - (\mathbf{q}_{i-1j}^2 - \mathbf{q}_{ij}^2) = \mathbf{b}_{ij}^1 - (\mathbf{q}_{i-1j}^2 - \mathbf{q}_{ij}^2).$$

$$(7.17) \quad \begin{aligned} \mathbf{q}_{i-1j}^2 - \mathbf{q}_{ij}^2 &= (\boldsymbol{\chi}_{i-1j}^2 + \varepsilon \boldsymbol{\xi}(\boldsymbol{\chi}_{i-1j}^2), \varepsilon + \varepsilon \eta(\boldsymbol{\chi}_{i-1j}^2)) - (\boldsymbol{\chi}_{ij}^2 + \varepsilon \boldsymbol{\xi}(\boldsymbol{\chi}_{ij}^2), \varepsilon + \varepsilon \eta(\boldsymbol{\chi}_{ij}^2)) \\ &= \left(\boldsymbol{\chi}_{i-1j}^2 - \boldsymbol{\chi}_{ij}^2 + \varepsilon \left(\nabla \boldsymbol{\xi} \cdot (\boldsymbol{\chi}_{i-1j}^2 - \boldsymbol{\chi}_{ij}^2) + \frac{1}{2} (\boldsymbol{\chi}_{i-1j}^2 - \boldsymbol{\chi}_{ij}^2) \cdot H_{\boldsymbol{\xi}} (\boldsymbol{\chi}_{i-1j}^2 - \boldsymbol{\chi}_{ij}^2) + \text{h.o.t.} \right), \right. \\ &\quad \left. \varepsilon \left(\nabla \eta \cdot (\boldsymbol{\chi}_{i-1j}^2 - \boldsymbol{\chi}_{ij}^2) + \frac{1}{2} (\boldsymbol{\chi}_{i-1j}^2 - \boldsymbol{\chi}_{ij}^2) \cdot H_{\eta} (\boldsymbol{\chi}_{i-1j}^2 - \boldsymbol{\chi}_{ij}^2) + \text{h.o.t.} \right) \right) \\ &= \left(-\varepsilon \delta_2 \mathbf{a}_1 + \varepsilon^2 \delta_2 \left(-\nabla \boldsymbol{\xi} \cdot \mathbf{a}_1 + \frac{1}{2} \varepsilon \delta_2 \mathbf{a}_1 \cdot H_{\boldsymbol{\xi}} \mathbf{a}_1 + \text{h.o.t.} \right), \right. \\ &\quad \left. \varepsilon^2 \delta_2 \left(-\nabla \eta \cdot \mathbf{a}_1 + \varepsilon \delta_2 \frac{1}{2} \mathbf{a}_1 \cdot H_{\eta} \mathbf{a}_1 + \text{h.o.t.} \right) \right) \end{aligned}$$

$$(7.18) \quad \begin{aligned} \mathbf{b}_{i-1j}^3 &= \varepsilon \delta_2 \left(v_{11} + 1 + \varepsilon \nabla \xi_1 \cdot (\mathbf{v}_1 + \mathbf{a}_1) + \varepsilon^2 \delta_2 \frac{1}{2} (\mathbf{v}_1 H_{\xi_1} \mathbf{v}_1 - \mathbf{a}_1 H_{\xi_1} \mathbf{a}_1) + \mathcal{O}(\varepsilon^3), \right. \\ &\quad v_{12} + \varepsilon \nabla \xi_2 \cdot (\mathbf{v}_1 + \mathbf{a}_1) + \varepsilon^2 \delta_2 \frac{1}{2} (\mathbf{v}_1 H_{\xi_2} \mathbf{v}_1 - \mathbf{a}_1 H_{\xi_2} \mathbf{a}_1) + \mathcal{O}(\varepsilon^3), \\ &\quad \left. \varepsilon \nabla \eta \cdot (\mathbf{v}_1 + \mathbf{a}_1) + \varepsilon^2 \delta_2 \frac{1}{2} (\mathbf{v}_1 H_{\eta} \mathbf{v}_1 - \mathbf{a}_1 H_{\eta} \mathbf{a}_1) + \mathcal{O}(\varepsilon^3) \right). \end{aligned}$$

But because $\mathbf{v}_1 + \mathbf{a}_1 = \mathbf{v}_3$, we have that

$$(7.19) \quad \begin{aligned} \mathbf{b}_{i-1j}^3 = \varepsilon \delta_2 \left(v_{31} + \varepsilon \nabla \xi_1 \cdot \mathbf{v}_3 + \varepsilon^2 \delta_2 \frac{1}{2} (\mathbf{v}_1 H_{\xi_1} \mathbf{v}_1 - \mathbf{a}_1 H_{\xi_1} \mathbf{a}_1) + \mathcal{O}(\varepsilon^3), \right. \\ v_{32} + \varepsilon \nabla \xi_2 \cdot \mathbf{v}_3 + \varepsilon^2 \delta_2 \frac{1}{2} (\mathbf{v}_1 H_{\xi_2} \mathbf{v}_1 - \mathbf{a}_1 H_{\xi_2} \mathbf{a}_1) + \mathcal{O}(\varepsilon^3), \\ \left. \varepsilon \nabla \eta \cdot \mathbf{v}_3 + \varepsilon^2 \delta_2 \frac{1}{2} (\mathbf{v}_1 H_{\eta} \mathbf{v}_1 - \mathbf{a}_1 H_{\eta} \mathbf{a}_1) + \mathcal{O}(\varepsilon^3) \right). \end{aligned}$$

Then,

$$(7.20) \quad \begin{aligned} \left(\frac{\mathbf{b}_{i-1j}^3 \cdot \mathbf{b}_{ij}^1}{\|\mathbf{b}_{i-1j}^3\| \|\mathbf{b}_{ij}^1\|} + \frac{1}{2} \right)^2 = 9\varepsilon^2 (\mathbf{v}_3 \cdot \nabla \xi \mathbf{v}_1 + \mathbf{v}_1 \cdot \nabla \xi \mathbf{v}_3)^2 + \\ 18\varepsilon^3 (\mathbf{v}_3 \cdot \nabla \xi \mathbf{v}_1 + \mathbf{v}_1 \cdot \nabla \xi \mathbf{v}_3) (\mathbf{v}_1 \cdot (\nabla \xi_1 \otimes \nabla \xi_1 + \nabla \xi_2 \otimes \nabla \xi_2 + \nabla \eta \otimes \nabla \eta) \cdot \mathbf{v}_3) + \mathcal{O}(\varepsilon^3) \end{aligned}$$

We also need

$$(7.21) \quad \begin{aligned} \mathbf{b}_{ij-1}^2 = \mathbf{q}_{ij}^1 - \mathbf{q}_{ij-1}^2 = (\mathbf{q}_{ij}^1 - \mathbf{q}_{ij}^2) - (\mathbf{q}_{ij-1}^2 - \mathbf{q}_{ij}^2) = \mathbf{b}_{ij}^1 - (\mathbf{q}_{ij-1}^2 - \mathbf{q}_{ij}^2) \\ = \varepsilon \delta_2 \left(v_{11} + \frac{1}{2} + \varepsilon \nabla \xi_1 \cdot (\mathbf{v}_1 + \mathbf{a}_2) + \varepsilon^2 \delta_2 \frac{1}{2} (\mathbf{v}_1 H_{\xi_1} \mathbf{v}_1 - \mathbf{a}_2 H_{\xi_1} \mathbf{a}_2) + \mathcal{O}(\varepsilon^3), \right. \\ v_{12} + \frac{\sqrt{3}}{2} + \varepsilon \nabla \xi_2 \cdot (\mathbf{v}_1 + \mathbf{a}_2) + \varepsilon^2 \delta_2 \frac{1}{2} (\mathbf{v}_1 H_{\xi_2} \mathbf{v}_1 - \mathbf{a}_2 H_{\xi_2} \mathbf{a}_2) + \mathcal{O}(\varepsilon^3), \\ \left. \varepsilon \nabla \eta \cdot (\mathbf{v}_1 + \mathbf{a}_2) + \varepsilon^2 \delta_2 \frac{1}{2} (\mathbf{v}_1 H_{\eta} \mathbf{v}_1 - \mathbf{a}_2 H_{\eta} \mathbf{a}_2) + \mathcal{O}(\varepsilon^3) \right). \end{aligned}$$

But because $\mathbf{v}_1 + \mathbf{a}_2 = \mathbf{v}_2$, we have that

$$(7.22) \quad \begin{aligned} \mathbf{b}_{ij-1}^2 = \varepsilon \delta_2 \left(v_{21} + \varepsilon \nabla \xi_1 \cdot \mathbf{v}_2 + \varepsilon^2 \delta_2 \frac{1}{2} (\mathbf{v}_1 H_{\xi_1} \mathbf{v}_1 - \mathbf{a}_2 H_{\xi_1} \mathbf{a}_2) + \mathcal{O}(\varepsilon^3), \right. \\ v_{22} + \varepsilon \nabla \xi_2 \cdot \mathbf{v}_2 + \varepsilon^2 \delta_2 \frac{1}{2} (\mathbf{v}_1 H_{\xi_2} \mathbf{v}_1 - \mathbf{a}_2 H_{\xi_2} \mathbf{a}_2) + \mathcal{O}(\varepsilon^3), \\ \left. \varepsilon \nabla \eta \cdot \mathbf{v}_2 + \varepsilon^2 \delta_2 \frac{1}{2} (\mathbf{v}_1 H_{\eta} \mathbf{v}_1 - \mathbf{a}_2 H_{\eta} \mathbf{a}_2) + \mathcal{O}(\varepsilon^3) \right). \end{aligned}$$

$$(7.23) \quad \begin{aligned} \left(\frac{\mathbf{b}_{ij-1}^2 \cdot \mathbf{b}_{ij}^1}{\|\mathbf{b}_{ij-1}^2\| \|\mathbf{b}_{ij}^1\|} + \frac{1}{2} \right)^2 = 9\varepsilon^2 (\mathbf{v}_2 \cdot \nabla \xi \mathbf{v}_1 + \mathbf{v}_1 \cdot \nabla \xi \mathbf{v}_2)^2 + \\ 18\varepsilon^3 (\mathbf{v}_2 \cdot \nabla \xi \mathbf{v}_1 + \mathbf{v}_1 \cdot \nabla \xi \mathbf{v}_2) (\mathbf{v}_1 \cdot (\nabla \xi_1 \otimes \nabla \xi_1 + \nabla \xi_2 \otimes \nabla \xi_2 + \nabla \eta \otimes \nabla \eta) \cdot \mathbf{v}_2) + \mathcal{O}(\varepsilon^3) \end{aligned}$$

$$(7.24) \quad \begin{aligned} \left(\frac{\mathbf{b}_{i-1j}^3 \cdot \mathbf{b}_{ij-1}^2}{\|\mathbf{b}_{i-1j}^3\| \|\mathbf{b}_{ij-1}^2\|} + \frac{1}{2} \right)^2 = 9\varepsilon^2 (\mathbf{v}_2 \cdot \nabla \xi \mathbf{v}_3 + \mathbf{v}_3 \cdot \nabla \xi \mathbf{v}_2)^2 + \\ 18\varepsilon^3 (\mathbf{v}_2 \cdot \nabla \xi \mathbf{v}_3 + \mathbf{v}_3 \cdot \nabla \xi \mathbf{v}_2) (\mathbf{v}_3 \cdot (\nabla \xi_1 \otimes \nabla \xi_1 + \nabla \xi_2 \otimes \nabla \xi_2 + \nabla \eta \otimes \nabla \eta) \cdot \mathbf{v}_2) + \mathcal{O}(\varepsilon^3) \end{aligned}$$

Combining (2.8) with (7.13), (7.14), (7.15), (7.20), (7.23), and (7.24), we arrive at

$$(7.25) \quad \begin{aligned} \mathcal{E}_t[\xi, \eta] \sim \sum_{i,j=1}^{N_2} \frac{48kt}{\omega} \left\{ \varepsilon^3 \left(\left(\frac{\mathbf{v}_1 \cdot \nabla \xi \mathbf{v}_2 + \mathbf{v}_2 \cdot \nabla \xi \mathbf{v}_1}{2} \right)^2 + \left(\frac{\mathbf{v}_2 \cdot \nabla \xi \mathbf{v}_3 + \mathbf{v}_3 \cdot \nabla \xi \mathbf{v}_2}{2} \right)^2 + \left(\frac{\mathbf{v}_1 \cdot \nabla \xi \mathbf{v}_3 + \mathbf{v}_3 \cdot \nabla \xi \mathbf{v}_1}{2} \right)^2 \right) + \right. \\ \varepsilon^4 \left[\left(\frac{\mathbf{v}_1 \cdot \nabla \xi \mathbf{v}_2 + \mathbf{v}_2 \cdot \nabla \xi \mathbf{v}_1}{2} \right) (\mathbf{v}_1 \cdot (\nabla \xi_1 \otimes \nabla \xi_1 + \nabla \xi_2 \otimes \nabla \xi_2 + \nabla \eta \otimes \nabla \eta) \cdot \mathbf{v}_2) \right. \\ + \left(\frac{\mathbf{v}_2 \cdot \nabla \xi \mathbf{v}_3 + \mathbf{v}_3 \cdot \nabla \xi \mathbf{v}_2}{2} \right) (\mathbf{v}_3 \cdot (\nabla \xi_1 \otimes \nabla \xi_1 + \nabla \xi_2 \otimes \nabla \xi_2 + \nabla \eta \otimes \nabla \eta) \cdot \mathbf{v}_2) \\ \left. \left. + \left(\frac{\mathbf{v}_1 \cdot \nabla \xi \mathbf{v}_3 + \mathbf{v}_3 \cdot \nabla \xi \mathbf{v}_1}{2} \right) (\mathbf{v}_3 \cdot (\nabla \xi_1 \otimes \nabla \xi_1 + \nabla \xi_2 \otimes \nabla \xi_2 + \nabla \eta \otimes \nabla \eta) \cdot \mathbf{v}_1) \right] \right\} \end{aligned}$$

Again, to transform this sum to an integral, we use that the area of the small cells have dimension $\frac{\sqrt{3}}{2}\delta_2^2\varepsilon^2$, and define $\gamma_t = \frac{4\sqrt{3}k_t}{\omega\delta_2^2}$.

7.1.3. Dihedral Springs. We expand the third term in (2.9) in ε . To do this, we need the expansions of $\mathbf{b}_{i-1j+1}^3, \mathbf{b}_{ij+1}^1, \mathbf{b}_{i+1j}^1$ and \mathbf{b}_{i+1j+1}^1 . First, we write

$$(7.26) \quad \mathbf{b}_{i-1j+1}^3 = \mathbf{q}_{ij+1}^1 - \mathbf{q}_{i-1j+1}^2 = (\mathbf{q}_{ij+1}^1 - \mathbf{q}_{ij}^2) - (\mathbf{q}_{i-1j+1}^2 - \mathbf{q}_{ij}^2) = \mathbf{b}_{ij}^2 - (\mathbf{q}_{i-1j+1}^2 - \mathbf{q}_{ij}^2).$$

The first term in (7.26) is \mathbf{b}_{ij}^2 . For the second, we have

$$(7.27) \quad \begin{aligned} \mathbf{q}_{i-1j+1}^2 - \mathbf{q}_{ij}^2 &= (\boldsymbol{\chi}_{i-1j+1}^2 + \varepsilon\xi(\boldsymbol{\chi}_{i-1j+1}^2), \varepsilon + \varepsilon\eta(\boldsymbol{\chi}_{i-1j+1}^2)) - (\boldsymbol{\chi}_{ij}^2 + \varepsilon\xi(\boldsymbol{\chi}_{ij}^2), \varepsilon + \varepsilon\eta(\boldsymbol{\chi}_{ij}^2)) \\ &= \left(\boldsymbol{\chi}_{i-1j+1}^2 - \boldsymbol{\chi}_{ij}^2 + \varepsilon \left(\nabla\xi \cdot (\boldsymbol{\chi}_{i-1j+1}^2 - \boldsymbol{\chi}_{ij}^2) + \frac{1}{2} (\boldsymbol{\chi}_{i-1j+1}^2 - \boldsymbol{\chi}_{ij}^2) H_\xi (\boldsymbol{\chi}_{i-1j+1}^2 - \boldsymbol{\chi}_{ij}^2) + \text{h.o.t.} \right), \right. \\ &\quad \left. \varepsilon \left(\nabla\eta \cdot (\boldsymbol{\chi}_{i-1j+1}^2 - \boldsymbol{\chi}_{ij}^2) + \frac{1}{2} (\boldsymbol{\chi}_{i-1j+1}^2 - \boldsymbol{\chi}_{ij}^2) H_\eta (\boldsymbol{\chi}_{i-1j+1}^2 - \boldsymbol{\chi}_{ij}^2) + \text{h.o.t.} \right) \right) \\ &= \left(\varepsilon\delta_2(\mathbf{a}_2 - \mathbf{a}_1) + \varepsilon^2\delta_2 \left(\nabla\xi \cdot (\mathbf{a}_2 - \mathbf{a}_1) + \frac{1}{2}\varepsilon\delta_2\mathbf{a}_1 H_\xi(\mathbf{a}_2 - \mathbf{a}_1) + \text{h.o.t.} \right), \right. \\ &\quad \left. \varepsilon^2\delta_2 \left(\nabla\eta \cdot (\mathbf{a}_2 - \mathbf{a}_1) + \varepsilon\delta_2\frac{1}{2}(\mathbf{a}_2 - \mathbf{a}_1) H_\eta(\mathbf{a}_2 - \mathbf{a}_1) + \text{h.o.t.} \right) \right) \end{aligned}$$

Because $\mathbf{v}_2 + \mathbf{a}_1 - \mathbf{a}_2 = \mathbf{v}_3$, we have that

$$(7.28) \quad \begin{aligned} \mathbf{b}_{i-1j+1}^3 &= \varepsilon\delta_2 \left(v_{31} + \varepsilon\nabla\xi_1 \cdot \mathbf{v}_3 + \varepsilon^2\delta_2\frac{1}{2} (v_2 H_{\xi_1} \mathbf{v}_2 - (\mathbf{a}_2 - \mathbf{a}_1) H_{\xi_1}(\mathbf{a}_2 - \mathbf{a}_1)) + \mathcal{O}(\varepsilon^3), \right. \\ &\quad v_{32} + \varepsilon\nabla\xi_2 \cdot \mathbf{v}_3 + \varepsilon^2\delta_2\frac{1}{2} (v_1 H_{\xi_2} \mathbf{v}_2 - (\mathbf{a}_2 - \mathbf{a}_1) H_{\xi_2}(\mathbf{a}_2 - \mathbf{a}_1)) + \mathcal{O}(\varepsilon^3), \\ &\quad \left. \varepsilon\nabla\eta \cdot \mathbf{v}_3 + \varepsilon^2\delta_2\frac{1}{2} (v_2 H_\eta \mathbf{v}_2 - (\mathbf{a}_2 - \mathbf{a}_1) H_\eta(\mathbf{a}_2 - \mathbf{a}_1)) + \mathcal{O}(\varepsilon^3) \right). \end{aligned}$$

Now, we expand \mathbf{b}_{ij+1}^1

$$(7.29) \quad \mathbf{b}_{ij+1}^1 = \mathbf{q}_{ij+1}^1 - \mathbf{q}_{ij+1}^2 = (\mathbf{q}_{ij+1}^1 - \mathbf{q}_{ij}^2) - (\mathbf{q}_{ij+1}^2 - \mathbf{q}_{ij}^2) = \mathbf{b}_{ij}^2 - (\mathbf{q}_{ij+1}^2 - \mathbf{q}_{ij}^2).$$

The first term in (7.29) is \mathbf{b}_{ij}^2 . For the second, we have

$$(7.30) \quad \begin{aligned} \mathbf{q}_{ij+1}^2 - \mathbf{q}_{ij}^2 &= (\boldsymbol{\chi}_{ij+1}^2 + \varepsilon\xi(\boldsymbol{\chi}_{ij+1}^2), \varepsilon + \varepsilon\eta(\boldsymbol{\chi}_{ij+1}^2)) - (\boldsymbol{\chi}_{ij}^2 + \varepsilon\xi(\boldsymbol{\chi}_{ij}^2), \varepsilon + \varepsilon\eta(\boldsymbol{\chi}_{ij}^2)) \\ &= \left(\boldsymbol{\chi}_{ij+1}^2 - \boldsymbol{\chi}_{ij}^2 + \varepsilon \left(\nabla\xi \cdot (\boldsymbol{\chi}_{ij+1}^2 - \boldsymbol{\chi}_{ij}^2) + \frac{1}{2} (\boldsymbol{\chi}_{ij+1}^2 - \boldsymbol{\chi}_{ij}^2) H_\xi (\boldsymbol{\chi}_{ij+1}^2 - \boldsymbol{\chi}_{ij}^2) + \text{h.o.t.} \right), \right. \\ &\quad \left. \varepsilon \left(\nabla\eta \cdot (\boldsymbol{\chi}_{ij+1}^2 - \boldsymbol{\chi}_{ij}^2) + \frac{1}{2} (\boldsymbol{\chi}_{ij+1}^2 - \boldsymbol{\chi}_{ij}^2) H_\eta (\boldsymbol{\chi}_{ij+1}^2 - \boldsymbol{\chi}_{ij}^2) + \text{h.o.t.} \right) \right) \\ &= \left(\varepsilon\delta_2\mathbf{a}_2 + \varepsilon^2\delta_2 \left(\nabla\xi \cdot \mathbf{a}_2 + \frac{1}{2}\varepsilon\delta_2\mathbf{a}_1 H_\xi\mathbf{a}_2 + \text{h.o.t.} \right), \right. \\ &\quad \left. \varepsilon^2\delta_2 \left(\nabla\eta \cdot \mathbf{a}_2 + \varepsilon\delta_2\frac{1}{2}\mathbf{a}_2 H_\eta\mathbf{a}_2 + \text{h.o.t.} \right) \right) \end{aligned}$$

Because $\mathbf{v}_2 - \mathbf{a}_2 = \mathbf{v}_1$, we have that

$$(7.31) \quad \begin{aligned} \mathbf{b}_{ij+1}^1 &= \varepsilon\delta_2 \left(v_{11} + \varepsilon\nabla\xi_1 \cdot \mathbf{v}_1 + \varepsilon^2\delta_2\frac{1}{2} (v_2 H_{\xi_1} \mathbf{v}_2 - \mathbf{a}_2 H_{\xi_1} \mathbf{a}_2) + \mathcal{O}(\varepsilon^3), \right. \\ &\quad v_{12} + \varepsilon\nabla\xi_2 \cdot \mathbf{v}_1 + \varepsilon^2\delta_2\frac{1}{2} (v_2 H_{\xi_2} \mathbf{v}_2 - \mathbf{a}_2 H_{\xi_2} \mathbf{a}_2) + \mathcal{O}(\varepsilon^3), \\ &\quad \left. \varepsilon\nabla\eta \cdot \mathbf{v}_1 + \varepsilon^2\delta_2\frac{1}{2} (v_2 H_\eta \mathbf{v}_2 - \mathbf{a}_2 H_\eta \mathbf{a}_2) + \mathcal{O}(\varepsilon^3) \right). \end{aligned}$$

Next, we expand \mathbf{b}_{i+1j}^1

$$(7.32) \quad \mathbf{b}_{i+1j}^1 = \mathbf{q}_{i+1j}^1 - \mathbf{q}_{i+1j}^2 = (\mathbf{q}_{i+1j}^1 - \mathbf{q}_{ij}^2) - (\mathbf{q}_{i+1j}^2 - \mathbf{q}_{ij}^2) = \mathbf{b}_{ij}^3 - (\mathbf{q}_{i+1j}^2 - \mathbf{q}_{ij}^2).$$

For the second, we have

$$(7.33) \quad \begin{aligned} \mathbf{q}_{i+1j}^2 - \mathbf{q}_{ij}^2 &= (\boldsymbol{\chi}_{i+1j}^2 + \varepsilon \boldsymbol{\xi}(\boldsymbol{\chi}_{i+1j}^2), \varepsilon + \varepsilon \eta(\boldsymbol{\chi}_{i+1j}^2)) - (\boldsymbol{\chi}_{ij}^2 + \varepsilon \boldsymbol{\xi}(\boldsymbol{\chi}_{ij}^2), \varepsilon + \varepsilon \eta(\boldsymbol{\chi}_{ij}^2)) \\ &= \left(\boldsymbol{\chi}_{i+1j}^2 - \boldsymbol{\chi}_{ij}^2 + \varepsilon \left(\nabla \boldsymbol{\xi} \cdot (\boldsymbol{\chi}_{i+1j}^2 - \boldsymbol{\chi}_{ij}^2) + \frac{1}{2} (\boldsymbol{\chi}_{i+1j}^2 - \boldsymbol{\chi}_{ij}^2) H_{\boldsymbol{\xi}} (\boldsymbol{\chi}_{i+1j}^2 - \boldsymbol{\chi}_{ij}^2) + \text{h.o.t.} \right), \right. \\ &\quad \left. \varepsilon \left(\nabla \eta \cdot (\boldsymbol{\chi}_{i+1j}^2 - \boldsymbol{\chi}_{ij}^2) + \frac{1}{2} (\boldsymbol{\chi}_{i+1j}^2 - \boldsymbol{\chi}_{ij}^2) H_{\eta} (\boldsymbol{\chi}_{i+1j}^2 - \boldsymbol{\chi}_{ij}^2) + \text{h.o.t.} \right) \right) \\ &= \left(\varepsilon \delta_2 \mathbf{a}_1 + \varepsilon^2 \delta_2 \left(\nabla \boldsymbol{\xi} \cdot \mathbf{a}_1 + \frac{1}{2} \varepsilon \delta_2 \mathbf{a}_1 H_{\boldsymbol{\xi}} \mathbf{a}_1 + \text{h.o.t.} \right), \right. \\ &\quad \left. \varepsilon^2 \delta_2 \left(\nabla \eta \cdot \mathbf{a}_1 + \varepsilon \delta_2 \frac{1}{2} \mathbf{a}_1 H_{\eta} \mathbf{a}_1 + \text{h.o.t.} \right) \right) \end{aligned}$$

Because $\mathbf{v}_3 - \mathbf{a}_1 = \mathbf{v}_1$, we have that

$$(7.34) \quad \begin{aligned} \mathbf{b}_{ij+1}^1 &= \varepsilon \delta_2 \left(v_{11} + \varepsilon \nabla \xi_1 \cdot \mathbf{v}_1 + \varepsilon^2 \delta_2 \frac{1}{2} (\mathbf{v}_3 H_{\xi_1} \mathbf{v}_3 - \mathbf{a}_1 H_{\xi_1} \mathbf{a}_1) + \mathcal{O}(\varepsilon^3), \right. \\ &\quad \left. v_{12} + \varepsilon \nabla \xi_2 \cdot \mathbf{v}_1 + \varepsilon^2 \delta_2 \frac{1}{2} (\mathbf{v}_3 H_{\xi_2} \mathbf{v}_3 - \mathbf{a}_1 H_{\xi_2} \mathbf{a}_1) + \mathcal{O}(\varepsilon^3), \right. \\ &\quad \left. \varepsilon \nabla \eta \cdot \mathbf{v}_1 + \varepsilon^2 \delta_2 \frac{1}{2} (\mathbf{v}_3 H_{\eta} \mathbf{v}_3 - \mathbf{a}_1 H_{\eta} \mathbf{a}_1) + \mathcal{O}(\varepsilon^3) \right). \end{aligned}$$

Lastly, we expand \mathbf{b}_{i+1j-1}^2

$$(7.35) \quad \mathbf{b}_{i+1j-1}^2 = \mathbf{q}_{i+1j-1}^1 - \mathbf{q}_{i+1j-1}^2 = (\mathbf{q}_{i+1j-1}^1 - \mathbf{q}_{ij}^2) - (\mathbf{q}_{i+1j-1}^2 - \mathbf{q}_{ij}^2) = \mathbf{b}_{ij}^3 - (\mathbf{q}_{i+1j-1}^2 - \mathbf{q}_{ij}^2).$$

For the first term, we have

$$(7.36) \quad \begin{aligned} \mathbf{q}_{i+1j-1}^1 - \mathbf{q}_{ij}^2 &= (\boldsymbol{\chi}_{i+1j-1}^1 + \varepsilon \boldsymbol{\xi}(\boldsymbol{\chi}_{i+1j-1}^1), \varepsilon + \varepsilon \eta(\boldsymbol{\chi}_{i+1j-1}^1)) - (\boldsymbol{\chi}_{ij}^2 + \varepsilon \boldsymbol{\xi}(\boldsymbol{\chi}_{ij}^2), \varepsilon + \varepsilon \eta(\boldsymbol{\chi}_{ij}^2)) \\ &= \left(\boldsymbol{\chi}_{i+1j-1}^1 - \boldsymbol{\chi}_{ij}^2 + \varepsilon \left(\nabla \boldsymbol{\xi} \cdot (\boldsymbol{\chi}_{i+1j-1}^1 - \boldsymbol{\chi}_{ij}^2) + \frac{1}{2} (\boldsymbol{\chi}_{i+1j-1}^1 - \boldsymbol{\chi}_{ij}^2) H_{\boldsymbol{\xi}} (\boldsymbol{\chi}_{i+1j-1}^1 - \boldsymbol{\chi}_{ij}^2) + \text{h.o.t.} \right), \right. \\ &\quad \left. \varepsilon \left(\nabla \eta \cdot (\boldsymbol{\chi}_{i+1j-1}^1 - \boldsymbol{\chi}_{ij}^2) + \frac{1}{2} (\boldsymbol{\chi}_{i+1j-1}^1 - \boldsymbol{\chi}_{ij}^2) H_{\eta} (\boldsymbol{\chi}_{i+1j-1}^1 - \boldsymbol{\chi}_{ij}^2) + \text{h.o.t.} \right) \right). \end{aligned}$$

Since

$$(7.37) \quad \begin{aligned} \boldsymbol{\chi}_{i+1j-1}^1 - \boldsymbol{\chi}_{ij}^2 &= \varepsilon \delta_2 \left(i + 1 + \frac{2}{3} \right) \mathbf{a}_1 + \left(j - 1 + \frac{2}{3} \right) \mathbf{a}_2 - \varepsilon \delta_2 \left(\left(i + \frac{2}{3} \right) \mathbf{a}_1 + \left(j + \frac{2}{3} \right) \mathbf{a}_2 \right) \\ &= \varepsilon \delta_2 (\mathbf{a}_1 - \mathbf{a}_2), \end{aligned}$$

then,

$$(7.38) \quad \begin{aligned} \mathbf{q}_{i+1j-1}^2 - \mathbf{q}_{ij}^2 &= \left(\varepsilon \delta_2 (\mathbf{a}_1 - \mathbf{a}_2) + \varepsilon^2 \delta_2 \left(\nabla \boldsymbol{\xi} \cdot (\mathbf{a}_1 - \mathbf{a}_2) + \varepsilon \delta_2 \frac{4}{2} (\mathbf{a}_1 - \mathbf{a}_2) H_{\boldsymbol{\xi}} (\mathbf{a}_1 - \mathbf{a}_2) + \text{h.o.t.} \right), \right. \\ &\quad \left. \varepsilon^2 \delta_2 \left(\nabla \eta \cdot (\mathbf{a}_1 - \mathbf{a}_2) + \varepsilon \delta_2 \frac{4}{2} (\mathbf{a}_1 - \mathbf{a}_2) H_{\eta} (\mathbf{a}_1 - \mathbf{a}_2) + \text{h.o.t.} \right) \right). \end{aligned}$$

Then, using that $\mathbf{v}_3 - (\mathbf{a}_1 - \mathbf{a}_2) = \mathbf{v}_2$ we have that

$$(7.39) \quad \begin{aligned} \mathbf{b}_{i+1j-1}^2 &= \varepsilon \delta_2 \left(v_{21} + \varepsilon \nabla \xi_1 \cdot \mathbf{v}_2 + \varepsilon^2 \delta_2 \frac{1}{2} (\mathbf{v}_3 H_{\xi_1} \mathbf{v}_3 - (\mathbf{a}_1 - \mathbf{a}_2) H_{\xi_1} (\mathbf{a}_1 - \mathbf{a}_2)) + \mathcal{O}(\varepsilon^3), \right. \\ &\quad \left. v_{22} + \varepsilon \nabla \xi_2 \cdot \mathbf{v}_2 + \varepsilon^2 \delta_2 \frac{1}{2} (\mathbf{v}_3 H_{\xi_2} \mathbf{v}_3 - (\mathbf{a}_1 - \mathbf{a}_2) H_{\xi_2} (\mathbf{a}_1 - \mathbf{a}_2)) + \mathcal{O}(\varepsilon^3), \right. \\ &\quad \left. \varepsilon \nabla \eta \cdot \mathbf{v}_2 + \varepsilon^2 \delta_2 \frac{1}{2} (\mathbf{v}_3 H_{\eta} \mathbf{v}_3 - (\mathbf{a}_1 - \mathbf{a}_2) H_{\eta} (\mathbf{a}_1 - \mathbf{a}_2)) + \mathcal{O}(\varepsilon^3) \right). \end{aligned}$$

Returning to (2.9), we now must expand

$$\begin{aligned}
\mathbf{b}_{ij}^1 \times \mathbf{b}_{ij}^2 &= \varepsilon^2 \delta_2^2 \left(\varepsilon (v_{12} \nabla \eta \cdot \mathbf{v}_2 - v_{22} \nabla \eta \cdot \mathbf{v}_1) + \right. \\
&\quad \left. \varepsilon^2 \left[(\nabla \xi_2 \otimes \nabla \eta) \mathbf{v}_2 \cdot \mathbf{v}_1 - (\nabla \xi_2 \otimes \nabla \eta) \mathbf{v}_1 \cdot \mathbf{v}_2 + \delta_2 \frac{1}{2} (v_{12} \mathbf{v}_2 H_\eta \mathbf{v}_2 - v_{22} \mathbf{v}_1 H_\eta \mathbf{v}_1) \right] + \mathcal{O}(\varepsilon^3), \right. \\
&\quad \varepsilon (v_{21} \nabla \eta \cdot \mathbf{v}_1 - v_{11} \nabla \eta \cdot \mathbf{v}_2) + \\
&\quad \left. \varepsilon^2 \left[-(\nabla \xi_1 \otimes \nabla \eta) \mathbf{v}_2 \cdot \mathbf{v}_1 + (\nabla \xi_1 \otimes \nabla \eta) \mathbf{v}_1 \cdot \mathbf{v}_2 + \delta_2 \frac{1}{2} (-v_{11} \mathbf{v}_2 H_\eta \mathbf{v}_2 + v_{21} \mathbf{v}_1 H_\eta \mathbf{v}_1) \right] + \mathcal{O}(\varepsilon^3), \right. \\
&\quad v_{11} v_{22} - v_{12} v_{21} + \varepsilon (v_{11} \nabla \xi_2 \cdot \mathbf{v}_2 + v_{22} \nabla \xi_1 \cdot \mathbf{v}_1 - v_{21} \nabla \xi_2 \cdot \mathbf{v}_1 - v_{12} \nabla \xi_1 \cdot \mathbf{v}_2) + \\
&\quad \left. \varepsilon^2 \left[(\nabla \xi_1 \otimes \nabla \xi_2) \mathbf{v}_2 \cdot \mathbf{v}_1 - (\nabla \xi_1 \otimes \nabla \xi_2) \mathbf{v}_1 \cdot \mathbf{v}_2 \right. \right. \\
(7.40) \quad &\quad \left. \left. + \delta_2 \frac{1}{2} (v_{11} \mathbf{v}_2 H_{\xi_2} \mathbf{v}_2 + v_{22} \mathbf{v}_1 H_{\xi_1} \mathbf{v}_1 - v_{21} \mathbf{v}_1 H_{\xi_2} \mathbf{v}_1 - v_{12} \mathbf{v}_2 H_{\xi_2} \mathbf{v}_2) \right] + \mathcal{O}(\varepsilon^3) \right).
\end{aligned}$$

Next we compute

$$\begin{aligned}
(\mathbf{b}_{ij}^1 \times \mathbf{b}_{ij}^2) \cdot \mathbf{b}_{ij-1}^2 &= \\
&\quad \varepsilon^3 \delta_2^3 \left[\left(\varepsilon (v_{12} \nabla \eta \cdot \mathbf{v}_2 - v_{22} \nabla \eta \cdot \mathbf{v}_1) + \right. \right. \\
&\quad \left. \left. \varepsilon^2 \left[(\nabla \xi_2 \otimes \nabla \eta) \mathbf{v}_2 \cdot \mathbf{v}_1 - (\nabla \xi_2 \otimes \nabla \eta) \mathbf{v}_1 \cdot \mathbf{v}_2 + \delta_2 \frac{1}{2} (v_{12} \mathbf{v}_2 H_\eta \mathbf{v}_2 - v_{22} \mathbf{v}_1 H_\eta \mathbf{v}_1) \right] + \mathcal{O}(\varepsilon^3) \right) \times \right. \\
&\quad \left(v_{21} + \varepsilon \nabla \xi_1 \cdot \mathbf{v}_2 + \varepsilon^2 \delta_2 \frac{1}{2} (\mathbf{v}_1 H_{\xi_1} \mathbf{v}_1 - \mathbf{a}_2 H_{\xi_1} \mathbf{a}_2) + \mathcal{O}(\varepsilon^3) \right) + \\
&\quad \left(\varepsilon (v_{21} \nabla \eta \cdot \mathbf{v}_1 - v_{11} \nabla \eta \cdot \mathbf{v}_2) + \right. \\
&\quad \left. \varepsilon^2 \left[-(\nabla \xi_1 \otimes \nabla \eta) \mathbf{v}_2 \cdot \mathbf{v}_1 + (\nabla \xi_1 \otimes \nabla \eta) \mathbf{v}_1 \cdot \mathbf{v}_2 + \delta_2 \frac{1}{2} (-v_{11} \mathbf{v}_2 H_\eta \mathbf{v}_2 + v_{21} \mathbf{v}_1 H_\eta \mathbf{v}_1) \right] + \mathcal{O}(\varepsilon^3) \right) \times \\
&\quad \left(v_{22} + \varepsilon \nabla \xi_2 \cdot \mathbf{v}_2 + \varepsilon^2 \delta_2 \frac{1}{2} (\mathbf{v}_1 H_{\xi_2} \mathbf{v}_1 - \mathbf{a}_2 H_{\xi_2} \mathbf{a}_2) + \mathcal{O}(\varepsilon^3) \right) + \\
&\quad \left(v_{11} v_{22} - v_{12} v_{21} + \varepsilon (v_{11} \nabla \xi_2 \cdot \mathbf{v}_2 + v_{22} \nabla \xi_1 \cdot \mathbf{v}_1 - v_{21} \nabla \xi_2 \cdot \mathbf{v}_1 - v_{12} \nabla \xi_1 \cdot \mathbf{v}_2) + \right. \\
&\quad \left. \varepsilon^2 \left[(\nabla \xi_1 \otimes \nabla \xi_2) \mathbf{v}_2 \cdot \mathbf{v}_1 - (\nabla \xi_1 \otimes \nabla \xi_2) \mathbf{v}_1 \cdot \mathbf{v}_2 \right. \right. \\
&\quad \left. \left. + \delta_2 \frac{1}{2} (v_{11} \mathbf{v}_2 H_{\xi_2} \mathbf{v}_2 + v_{22} \mathbf{v}_1 H_{\xi_1} \mathbf{v}_1 - v_{21} \mathbf{v}_1 H_{\xi_2} \mathbf{v}_1 - v_{12} \mathbf{v}_2 H_{\xi_2} \mathbf{v}_2) \right] + \mathcal{O}(\varepsilon^3) \right) \times \\
&\quad \left. \left(\varepsilon \nabla \eta \cdot \mathbf{v}_2 + \varepsilon^2 \delta_2 \frac{1}{2} (\mathbf{v}_1 H_\eta \mathbf{v}_1 - \mathbf{a}_2 H_\eta \mathbf{a}_2) + \mathcal{O}(\varepsilon^3) \right) \right] \\
(7.41) \quad &= \varepsilon^3 \delta_2^3 \left[(v_{11} v_{22} - v_{12} v_{21}) \varepsilon^2 \delta_2 \frac{1}{2} (\mathbf{v}_1 H_\eta \mathbf{v}_1 - \mathbf{v}_2 H_\eta \mathbf{v}_2 - \mathbf{a}_2 H_\eta \mathbf{a}_2) + \mathcal{O}(\varepsilon^3) \right].
\end{aligned}$$

Hence

$$(7.42) \quad [(\mathbf{b}_{ij}^1 \times \mathbf{b}_{ij}^2) \cdot \mathbf{b}_{ij-1}^2]^2 = \varepsilon^6 \delta_2^6 \left[\varepsilon^4 \delta_2^2 (v_{11} v_{22} - v_{12} v_{21})^2 \frac{1}{4} (\mathbf{v}_1 H_\eta \mathbf{v}_1 - \mathbf{v}_2 H_\eta \mathbf{v}_2 - \mathbf{a}_2 H_\eta \mathbf{a}_2)^2 + \mathcal{O}(\varepsilon^5) \right].$$

Using (7.7), we have

$$(7.43) \quad \|\mathbf{b}_{ij}^1 \times \mathbf{b}_{ij}^2\|^2 = \varepsilon^4 \delta_2^4 (v_{11} v_{22} - v_{12} v_{21})^2 + \mathcal{O}(\varepsilon) = \varepsilon^4 \delta_2^4 (\det(\mathbf{v}_1, \mathbf{v}_2))^2 + \mathcal{O}(\varepsilon).$$

and

$$(7.44) \quad \|\mathbf{b}_{ij-1}^2\|^2 = \varepsilon^2 \delta_2^2 [\|\mathbf{v}_2\|^2 + 2\varepsilon (\nabla \xi \mathbf{v}_2 \cdot \mathbf{v}_2 + \mathcal{O}(\varepsilon^2))].$$

From (7.43) and (7.44) one checks that

$$(7.45) \quad [\|\mathbf{b}_{ij}^1 \times \mathbf{b}_{ij}^2\|^2 \|\mathbf{b}_{ij-1}^2\|^2]^{-1} = [\varepsilon^6 \delta_2^6 (\det(\mathbf{v}_1, \mathbf{v}_2)^2 \|\mathbf{v}_2\|^2 + \mathcal{O}(\varepsilon))]^{-1} = \varepsilon^{-6} \delta_2^{-6} (\det(\mathbf{v}_1, \mathbf{v}_2)^2 \|\mathbf{v}_2\|^2)^{-1} (1 + \mathcal{O}(\varepsilon)).$$

Finally, combining (7.9) and (7.17), we get the expansion

$$(7.46) \quad \frac{((\mathbf{b}_{ij}^1 \times \mathbf{b}_{ij}^2) \cdot \mathbf{b}_{ij-1}^2)^2}{\|\mathbf{b}_{ij}^1 \times \mathbf{b}_{ij}^2\|^2 \|\mathbf{b}_{ij-1}^2\|^2} = \frac{\delta_2^2 \varepsilon^4}{4 \|\mathbf{v}_2\|^2} (\mathbf{v}_1 H_\eta \mathbf{v}_1 - \mathbf{v}_2 H_\eta \mathbf{v}_2 - \mathbf{a}_2 H_\eta \mathbf{a}_2)^2 + \mathcal{O}(\varepsilon^5).$$

So similar computations gives us the following equalities.

$$(7.47) \quad \frac{((\mathbf{b}_{ij}^1 \times \mathbf{b}_{ij}^2) \cdot \mathbf{b}_{i-1j}^3)^2}{\|\mathbf{b}_{ij}^1 \times \mathbf{b}_{ij}^2\|^2 \|\mathbf{b}_{i-1j}^3\|^2} = \frac{\delta_2^2 \varepsilon^4}{4 \|\mathbf{v}_3\|^2} (\mathbf{v}_2 H_\eta \mathbf{v}_2 + 2\mathbf{v}_1 H_\eta \mathbf{v}_1 - \mathbf{a}_1 H_\eta \mathbf{a}_1)^2 + \mathcal{O}(\varepsilon^5).$$

$$(7.48) \quad \frac{((\mathbf{b}_{ij}^1 \times \mathbf{b}_{ij}^3) \cdot \mathbf{b}_{ij-1}^2)^2}{\|\mathbf{b}_{ij}^1 \times \mathbf{b}_{ij}^3\|^2 \|\mathbf{b}_{ij-1}^2\|^2} = \frac{\delta_2^2 \varepsilon^4}{4 \|\mathbf{v}_2\|^2} (\mathbf{v}_3 H_\eta \mathbf{v}_3 + 2\mathbf{v}_1 H_\eta \mathbf{v}_1 - \mathbf{a}_2 H_\eta \mathbf{a}_2)^2 + \mathcal{O}(\varepsilon^5).$$

$$(7.49) \quad \frac{((\mathbf{b}_{ij}^1 \times \mathbf{b}_{ij}^3) \cdot \mathbf{b}_{i-1j}^3)^2}{\|\mathbf{b}_{ij}^1 \times \mathbf{b}_{ij}^3\|^2 \|\mathbf{b}_{i-1j}^3\|^2} = \frac{\delta_2^2 \varepsilon^4}{4 \|\mathbf{v}_3\|^2} (\mathbf{v}_1 H_\eta \mathbf{v}_1 - \mathbf{v}_3 H_\eta \mathbf{v}_3 - \mathbf{a}_1 H_\eta \mathbf{a}_1)^2 + \mathcal{O}(\varepsilon^5).$$

$$(7.50) \quad \frac{((\mathbf{b}_{ij}^2 \times \mathbf{b}_{i-1j+1}^3) \cdot \mathbf{b}_{ij}^1)^2}{\|\mathbf{b}_{ij}^2 \times \mathbf{b}_{i-1j+1}^3\|^2 \|\mathbf{b}_{ij}^1\|^2} = \frac{\delta_2^2 \varepsilon^4}{4 \|\mathbf{v}_1\|^2} (\mathbf{v}_1 H_\eta \mathbf{v}_1 + 2\mathbf{v}_2 H_\eta \mathbf{v}_2 - (\mathbf{a}_2 - \mathbf{a}_1) H_\eta (\mathbf{a}_2 - \mathbf{a}_1))^2 + \mathcal{O}(\varepsilon^5).$$

$$(7.51) \quad \frac{((\mathbf{b}_{ij}^2 \times \mathbf{b}_{i-1j+1}^3) \cdot \mathbf{b}_{ij}^3)^2}{\|\mathbf{b}_{ij}^2 \times \mathbf{b}_{i-1j+1}^3\|^2 \|\mathbf{b}_{ij}^3\|^2} = \frac{\delta_2^2 \varepsilon^4}{4 \|\mathbf{v}_3\|^2} (\mathbf{v}_3 H_\eta \mathbf{v}_3 - \mathbf{v}_2 H_\eta \mathbf{v}_2 + (\mathbf{a}_2 - \mathbf{a}_1) H_\eta (\mathbf{a}_2 - \mathbf{a}_1))^2 + \mathcal{O}(\varepsilon^5).$$

$$(7.52) \quad \frac{((\mathbf{b}_{ij}^2 \times \mathbf{b}_{ij+1}^1) \cdot \mathbf{b}_{ij}^1)^2}{\|\mathbf{b}_{ij}^2 \times \mathbf{b}_{ij+1}^1\|^2 \|\mathbf{b}_{ij}^1\|^2} = \frac{\delta_2^2 \varepsilon^4}{4 \|\mathbf{v}_1\|^2} (\mathbf{v}_2 H_\eta \mathbf{v}_2 - \mathbf{v}_1 H_\eta \mathbf{v}_1 - \mathbf{a}_2 H_\eta \mathbf{a}_2)^2 + \mathcal{O}(\varepsilon^5).$$

$$(7.53) \quad \frac{((\mathbf{b}_{ij}^2 \times \mathbf{b}_{ij+1}^1) \cdot \mathbf{b}_{ij}^3)^2}{\|\mathbf{b}_{ij}^2 \times \mathbf{b}_{ij+1}^1\|^2 \|\mathbf{b}_{ij}^3\|^2} = \frac{\delta_2^2 \varepsilon^4}{4 \|\mathbf{v}_3\|^2} (\mathbf{v}_3 H_\eta \mathbf{v}_3 + 2\mathbf{v}_2 H_\eta \mathbf{v}_2 - \mathbf{a}_2 H_\eta \mathbf{a}_2)^2 + \mathcal{O}(\varepsilon^5).$$

$$(7.54) \quad \frac{((\mathbf{b}_{ij}^3 \times \mathbf{b}_{ij}^2) \cdot \mathbf{b}_{i+1j}^1)^2}{\|\mathbf{b}_{ij}^3 \times \mathbf{b}_{ij}^2\|^2 \|\mathbf{b}_{i+1j}^1\|^2} = \frac{\delta_2^2 \varepsilon^4}{4 \|\mathbf{v}_1\|^2} (\mathbf{v}_2 H_\eta \mathbf{v}_2 + 2\mathbf{v}_3 H_\eta \mathbf{v}_3 - \mathbf{a}_1 H_\eta \mathbf{a}_1)^2 + \mathcal{O}(\varepsilon^5).$$

$$(7.55) \quad \frac{((\mathbf{b}_{ij}^3 \times \mathbf{b}_{ij}^2) \cdot \mathbf{b}_{i+1j-1}^2)^2}{\|\mathbf{b}_{ij}^3 \times \mathbf{b}_{ij}^2\|^2 \|\mathbf{b}_{i+1j-1}^2\|^2} = \frac{\delta_2^2 \varepsilon^4}{4 \|\mathbf{v}_2\|^2} (-\mathbf{v}_2 H_\eta \mathbf{v}_2 + \mathbf{v}_3 H_\eta \mathbf{v}_3 - (\mathbf{a}_1 - \mathbf{a}_2) H_\eta (\mathbf{a}_1 - \mathbf{a}_2))^2 + \mathcal{O}(\varepsilon^5).$$

$$(7.56) \quad \frac{((\mathbf{b}_{ij}^3 \times \mathbf{b}_{ij}^1) \cdot \mathbf{b}_{i+1j}^1)^2}{\|\mathbf{b}_{ij}^3 \times \mathbf{b}_{ij}^1\|^2 \|\mathbf{b}_{i+1j}^1\|^2} = \frac{\delta_2^2 \varepsilon^4}{4 \|\mathbf{v}_1\|^2} (-\mathbf{v}_1 H_\eta \mathbf{v}_1 + \mathbf{v}_3 H_\eta \mathbf{v}_3 - \mathbf{a}_1 H_\eta \mathbf{a}_1)^2 + \mathcal{O}(\varepsilon^5).$$

$$(7.57) \quad \frac{((\mathbf{b}_{ij}^3 \times \mathbf{b}_{ij}^1) \cdot \mathbf{b}_{i+1j-1}^2)^2}{\|\mathbf{b}_{ij}^3 \times \mathbf{b}_{ij}^1\|^2 \|\mathbf{b}_{i+1j-1}^2\|^2} = \frac{\delta_2^2 \varepsilon^4}{4 \|\mathbf{v}_2\|^2} (\mathbf{v}_1 H_\eta \mathbf{v}_1 + 2\mathbf{v}_3 H_\eta \mathbf{v}_3 - (\mathbf{a}_1 - \mathbf{a}_2) H_\eta (\mathbf{a}_1 - \mathbf{a}_2))^2 + \mathcal{O}(\varepsilon^5).$$

By combining (7.45)–(7.57), we get

$$\begin{aligned}
\mathcal{E}_d[\boldsymbol{\xi}, \eta] &:= \sum_{i,j=1}^{N_2} \frac{3k_d}{4\omega} [7((\mathbf{v}_1 H_\eta \mathbf{v}_1)^2 + (\mathbf{v}_2 H_\eta \mathbf{v}_2)^2 + (\mathbf{v}_3 H_\eta \mathbf{v}_3)^2) \\
&\quad + 2((\mathbf{v}_1 H_\eta \mathbf{v}_2)^2 + (\mathbf{v}_1 H_\eta \mathbf{v}_3)^2 + (\mathbf{v}_2 H_\eta \mathbf{v}_1)^2 + (\mathbf{v}_2 H_\eta \mathbf{v}_3)^2 + (\mathbf{v}_3 H_\eta \mathbf{v}_1)^2 + (\mathbf{v}_3 H_\eta \mathbf{v}_2)^2) \\
&\quad + 2(\mathbf{v}_1 H_\eta \mathbf{v}_3)(\mathbf{v}_2 H_\eta \mathbf{v}_2) - 2(\mathbf{v}_2 H_\eta \mathbf{v}_1)(\mathbf{v}_2 H_\eta \mathbf{v}_2) - 2(\mathbf{v}_2 H_\eta \mathbf{v}_2)(\mathbf{v}_2 H_\eta \mathbf{v}_3) \\
&\quad + 4(\mathbf{v}_1 H_\eta \mathbf{v}_3)(\mathbf{v}_3 H_\eta \mathbf{v}_1) + 2(\mathbf{v}_2 H_\eta \mathbf{v}_2)(\mathbf{v}_3 H_\eta \mathbf{v}_1) - 2(\mathbf{v}_2 H_\eta \mathbf{v}_2)(\mathbf{v}_3 H_\eta \mathbf{v}_2) \\
&\quad + 4(\mathbf{v}_2 H_\eta \mathbf{v}_3)(\mathbf{v}_3 H_\eta \mathbf{v}_2) - 2(\mathbf{v}_1 H_\eta \mathbf{v}_3)(\mathbf{v}_3 H_\eta \mathbf{v}_3) + 2(\mathbf{v}_2 H_\eta \mathbf{v}_1)(\mathbf{v}_3 H_\eta \mathbf{v}_3) \\
&\quad - 2(\mathbf{v}_2 H_\eta \mathbf{v}_2)(\mathbf{v}_3 H_\eta \mathbf{v}_3) - 2(\mathbf{v}_2 H_\eta \mathbf{v}_3)(\mathbf{v}_3 H_\eta \mathbf{v}_3) - 2(\mathbf{v}_3 H_\eta \mathbf{v}_1)(\mathbf{v}_3 H_\eta \mathbf{v}_3) \\
&\quad - 2(\mathbf{v}_3 H_\eta \mathbf{v}_2)(\mathbf{v}_3 H_\eta \mathbf{v}_3) + 2(\mathbf{v}_1 H_\eta \mathbf{v}_2)(2(\mathbf{v}_2 H_\eta \mathbf{v}_1) - \mathbf{v}_2 H_\eta \mathbf{v}_2 + \mathbf{v}_3 H_\eta \mathbf{v}_3) \\
&\quad - 2\mathbf{v}_1 H_\eta \mathbf{v}_1(\mathbf{v}_1 H_\eta \mathbf{v}_2 + \mathbf{v}_1 H_\eta \mathbf{v}_3 + \mathbf{v}_2 H_\eta \mathbf{v}_1 + \mathbf{v}_2 H_\eta \mathbf{v}_2 - \mathbf{v}_2 H_\eta \mathbf{v}_3 + \mathbf{v}_3 H_\eta \mathbf{v}_1 - \mathbf{v}_3 H_\eta \mathbf{v}_2 + \mathbf{v}_3 H_\eta \mathbf{v}_3)] \delta_2^2 \varepsilon^5 \\
&\quad + \mathcal{O}(\varepsilon^6) \\
(7.58) \quad &= \sum_{i,j=1}^{N_2} \frac{3k_d}{8\omega} \delta_2^2 \varepsilon^5 [7\eta_{,11}^2 + 4\eta_{,12}^2 + 4\eta_{,21}^2 + 8\eta_{,12}\eta_{,21} - 2\eta_{,11}\eta_{,22} + 7\eta_{,22}^2] + \mathcal{O}(\varepsilon^6).
\end{aligned}$$

Assuming the symmetry of H_η , we get

$$\begin{aligned}
\mathcal{E}_d[\boldsymbol{\xi}, \eta] &:= \sum_{i,j=1}^{N_2} \frac{3k_d}{4\omega} [7((\mathbf{v}_1 H_\eta \mathbf{v}_1)^2 + (\mathbf{v}_2 H_\eta \mathbf{v}_2)^2 + (\mathbf{v}_3 H_\eta \mathbf{v}_3)^2) \\
&\quad + 8((\mathbf{v}_1 H_\eta \mathbf{v}_2)^2 + (\mathbf{v}_1 H_\eta \mathbf{v}_3)^2 + (\mathbf{v}_2 H_\eta \mathbf{v}_3)^2) \\
&\quad + 4(\mathbf{v}_1 H_\eta \mathbf{v}_1)(-\mathbf{v}_1 H_\eta \mathbf{v}_2 - \mathbf{v}_1 H_\eta \mathbf{v}_3 + \mathbf{v}_2 H_\eta \mathbf{v}_3 - \mathbf{v}_2 H_\eta \mathbf{v}_2 - \mathbf{v}_3 H_\eta \mathbf{v}_3) \\
&\quad + 4(\mathbf{v}_2 H_\eta \mathbf{v}_2)(-\mathbf{v}_1 H_\eta \mathbf{v}_2 + \mathbf{v}_1 H_\eta \mathbf{v}_3 - \mathbf{v}_2 H_\eta \mathbf{v}_3) \\
&\quad + 4(\mathbf{v}_3 H_\eta \mathbf{v}_3)(\mathbf{v}_1 H_\eta \mathbf{v}_2 - \mathbf{v}_1 H_\eta \mathbf{v}_3 - \mathbf{v}_2 H_\eta \mathbf{v}_3) \\
&\quad - 2(\mathbf{v}_2 H_\eta \mathbf{v}_2)(\mathbf{v}_3 H_\eta \mathbf{v}_3)] \delta_2^2 \varepsilon^5 + \mathcal{O}(\varepsilon^6) \\
(7.59) \quad &= \sum_{i,j=1}^{N_2} \frac{3k_d}{8\omega} \delta_2^2 \varepsilon^5 [7\eta_{,11}^2 + 16\eta_{,12}^2 - 2\eta_{,11}\eta_{,22} + 7\eta_{,22}^2] + \mathcal{O}(\varepsilon^6).
\end{aligned}$$

Here, we define $\gamma_d = \frac{\sqrt{3k_d}}{2\omega}$.

7.2. Energies in Matrix Forms. We define the matrix

$$V = \begin{pmatrix} \mathbf{v}_1 \\ \mathbf{v}_2 \\ \mathbf{v}_3 \end{pmatrix} = \begin{pmatrix} v_{11} & v_{12} \\ v_{21} & v_{22} \\ v_{31} & v_{32} \end{pmatrix}.$$

Then,

$$(7.60) \quad V \nabla \boldsymbol{\xi} V^T = \begin{pmatrix} \mathbf{v}_1 \\ \mathbf{v}_2 \\ \mathbf{v}_3 \end{pmatrix} \nabla \boldsymbol{\xi} \begin{pmatrix} \mathbf{v}_1^T & \mathbf{v}_2^T & \mathbf{v}_3^T \end{pmatrix}$$

$$(7.61) \quad = \begin{pmatrix} \mathbf{v}_1 \\ \mathbf{v}_2 \\ \mathbf{v}_3 \end{pmatrix} \begin{pmatrix} \nabla \boldsymbol{\xi} \cdot \mathbf{v}_1 & \nabla \boldsymbol{\xi} \cdot \mathbf{v}_2 & \nabla \boldsymbol{\xi} \cdot \mathbf{v}_3 \end{pmatrix}$$

$$(7.62) \quad = \begin{pmatrix} \mathbf{v}_1 \cdot \nabla \boldsymbol{\xi} \cdot \mathbf{v}_1 & \mathbf{v}_1 \cdot \nabla \boldsymbol{\xi} \cdot \mathbf{v}_2 & \mathbf{v}_1 \cdot \nabla \boldsymbol{\xi} \cdot \mathbf{v}_3 \\ \mathbf{v}_2 \cdot \nabla \boldsymbol{\xi} \cdot \mathbf{v}_1 & \mathbf{v}_2 \cdot \nabla \boldsymbol{\xi} \cdot \mathbf{v}_2 & \mathbf{v}_2 \cdot \nabla \boldsymbol{\xi} \cdot \mathbf{v}_3 \\ \mathbf{v}_3 \cdot \nabla \boldsymbol{\xi} \cdot \mathbf{v}_1 & \mathbf{v}_3 \cdot \nabla \boldsymbol{\xi} \cdot \mathbf{v}_2 & \mathbf{v}_3 \cdot \nabla \boldsymbol{\xi} \cdot \mathbf{v}_3 \end{pmatrix}.$$

If $A = V \nabla \boldsymbol{\xi} V^T$, then

$$\frac{A + A^T}{2} = \begin{pmatrix} \frac{\mathbf{v}_1 \cdot \nabla \boldsymbol{\xi} \cdot \mathbf{v}_1}{\mathbf{v}_1 \cdot \nabla \boldsymbol{\xi} \cdot \mathbf{v}_2 + \mathbf{v}_2 \cdot \nabla \boldsymbol{\xi} \cdot \mathbf{v}_1} & \frac{\mathbf{v}_1 \cdot \nabla \boldsymbol{\xi} \cdot \mathbf{v}_2 + \mathbf{v}_2 \cdot \nabla \boldsymbol{\xi} \cdot \mathbf{v}_1}{2} & \frac{\mathbf{v}_1 \cdot \nabla \boldsymbol{\xi} \cdot \mathbf{v}_3 + \mathbf{v}_3 \cdot \nabla \boldsymbol{\xi} \cdot \mathbf{v}_1}{2} \\ \frac{\mathbf{v}_1 \cdot \nabla \boldsymbol{\xi} \cdot \mathbf{v}_2 + \mathbf{v}_2 \cdot \nabla \boldsymbol{\xi} \cdot \mathbf{v}_1}{2} & \frac{\mathbf{v}_2 \cdot \nabla \boldsymbol{\xi} \cdot \mathbf{v}_2}{\mathbf{v}_2 \cdot \nabla \boldsymbol{\xi} \cdot \mathbf{v}_3 + \mathbf{v}_3 \cdot \nabla \boldsymbol{\xi} \cdot \mathbf{v}_2} & \frac{\mathbf{v}_2 \cdot \nabla \boldsymbol{\xi} \cdot \mathbf{v}_3 + \mathbf{v}_3 \cdot \nabla \boldsymbol{\xi} \cdot \mathbf{v}_1}{2} \\ \frac{\mathbf{v}_1 \cdot \nabla \boldsymbol{\xi} \cdot \mathbf{v}_3 + \mathbf{v}_3 \cdot \nabla \boldsymbol{\xi} \cdot \mathbf{v}_1}{2} & \frac{\mathbf{v}_2 \cdot \nabla \boldsymbol{\xi} \cdot \mathbf{v}_3 + \mathbf{v}_3 \cdot \nabla \boldsymbol{\xi} \cdot \mathbf{v}_2}{2} & \mathbf{v}_3 \cdot \nabla \boldsymbol{\xi} \cdot \mathbf{v}_3 \end{pmatrix}.$$

$$(7.63) \quad V(\nabla\eta \otimes \nabla\eta)V^T = \begin{pmatrix} \mathbf{v}_1 \cdot (\nabla\eta \otimes \nabla\eta) \cdot \mathbf{v}_1 & \mathbf{v}_1 \cdot (\nabla\eta \otimes \nabla\eta) \cdot \mathbf{v}_2 & \mathbf{v}_1 \cdot (\nabla\eta \otimes \nabla\eta) \cdot \mathbf{v}_3 \\ \mathbf{v}_2 \cdot (\nabla\eta \otimes \nabla\eta) \cdot \mathbf{v}_1 & \mathbf{v}_2 \cdot (\nabla\eta \otimes \nabla\eta) \cdot \mathbf{v}_2 & \mathbf{v}_2 \cdot (\nabla\eta \otimes \nabla\eta) \cdot \mathbf{v}_3 \\ \mathbf{v}_3 \cdot (\nabla\eta \otimes \nabla\eta) \cdot \mathbf{v}_1 & \mathbf{v}_3 \cdot (\nabla\eta \otimes \nabla\eta) \cdot \mathbf{v}_2 & \mathbf{v}_3 \cdot (\nabla\eta \otimes \nabla\eta) \cdot \mathbf{v}_3 \end{pmatrix}.$$

7.3. Euler-Lagrange Equations. In here we want to deduce the Euler-Lagrange equations corresponding to our continuum energy

$$(7.64) \quad \mathcal{F}^\varepsilon[\boldsymbol{\xi}, \eta] := \frac{\varepsilon}{2} \int_{D_1} f \left(D(V\nabla\boldsymbol{\xi}V^T) + \frac{\varepsilon}{2} V(\nabla\eta \otimes \nabla\eta)V^T \right) d\boldsymbol{\chi}$$

$$(7.65) \quad + \gamma_d \varepsilon^3 \int_{D_1} [7\eta_{,11}^2 + 16\eta_{,12}^2 - 2\eta_{,11}\eta_{,22} + 7\eta_{,22}^2] d\boldsymbol{\chi} + \frac{1}{\varepsilon} \int_{D_1} G(\boldsymbol{\chi}, \boldsymbol{\xi}, \eta) d\boldsymbol{\chi}.$$

Recall that $D(A) = (A + A^T)/2$ for any $A \in M^{3 \times 3}$ and $f: M^{3 \times 3} \rightarrow \mathbb{R}$ is defined by

$$f(M) = \gamma_s (m_{11}^2 + m_{22}^2 + m_{33}^2) + \gamma_t (m_{12}^2 + m_{21}^2 + m_{13}^2 + m_{31}^2 + m_{23}^2 + m_{32}^2),$$

for any $M = \begin{pmatrix} m_{11} & m_{12} & m_{13} \\ m_{21} & m_{22} & m_{23} \\ m_{31} & m_{32} & m_{33} \end{pmatrix}.$

Then, we have that for any $\nabla f(M) = 2 \begin{pmatrix} \gamma_s m_{11} & \gamma_t m_{12} & \gamma_t m_{13} \\ \gamma_t m_{21} & \gamma_s m_{22} & \gamma_t m_{23} \\ \gamma_t m_{31} & \gamma_t m_{32} & \gamma_s m_{33} \end{pmatrix}.$

Let $(\bar{\boldsymbol{\xi}}, \bar{\eta})$ be the minimizer of the energy $\mathcal{F}^\varepsilon[\boldsymbol{\xi}, \eta]$. Let $\boldsymbol{\xi}^1 = \begin{pmatrix} \xi_1 \\ 0 \end{pmatrix}$. We define

$$(7.66) \quad A(\gamma) = D(V\nabla(\bar{\boldsymbol{\xi}} + \gamma\boldsymbol{\xi}^1)V^T) + \frac{\varepsilon}{2} V(\nabla\bar{\eta} \otimes \nabla\bar{\eta})V^T,$$

Then, at $\gamma = 0$ we have that $A(0) = D(V\nabla\bar{\boldsymbol{\xi}}V^T) + \frac{\varepsilon}{2} V(\nabla\bar{\eta} \otimes \nabla\bar{\eta})V^T$ and because of linearity of D and ∇ , we have that $A'(0) = D(V\nabla\boldsymbol{\xi}^1V^T)$. So, we can write that

$$(7.67) \quad \frac{\partial}{\partial\gamma} \left\{ \frac{\varepsilon}{2} \int_{D_1} f(A(\gamma)), dx \right\} \Big|_{\gamma=0} = \frac{\varepsilon}{2} \int_{D_1} \nabla f(A(0)) : \frac{\partial A(0)}{\partial\gamma} dx,$$

where $A : B = \sum_i \sum_j A_{ij} B_{ij}$.

Let us rewrite the term inside the integral

$$\begin{aligned} \nabla f(A(0)) : \frac{\partial A(0)}{\partial\gamma} &= \nabla f(A(0)) : D(V\nabla\boldsymbol{\xi}^1V^T) \\ &= \nabla f(A(0)) : \frac{V\nabla\boldsymbol{\xi}^1V^T + V\nabla\boldsymbol{\xi}^1V^T}{2} \\ &= \frac{1}{2} \left(\nabla f(A(0)) : V\nabla\boldsymbol{\xi}^1V^T + \nabla f(A(0)) : V(\nabla\boldsymbol{\xi}^1)^T V^T \right) \\ &= \frac{1}{2} \left(\nabla f(A(0)) : V\nabla\boldsymbol{\xi}^1V^T + (\nabla f(A(0)))^T : V\nabla\boldsymbol{\xi}^1V^T \right) \\ &= \frac{1}{2} (\nabla f(A(0)) : V\nabla\boldsymbol{\xi}^1V^T + \nabla f(A(0)) : V\nabla\boldsymbol{\xi}^1V^T) \\ &= \nabla f(A(0)) : V\nabla\boldsymbol{\xi}^1V^T \\ &= V^T \nabla f(A(0)) : \nabla\boldsymbol{\xi}^1V^T \\ &= \nabla f(A(0))V : V(\nabla\boldsymbol{\xi}^1)^T \\ &= V^T \nabla f(A(0))V : (\nabla\boldsymbol{\xi}^1)^T \\ &= V^T \nabla f(A(0))V : \nabla\boldsymbol{\xi}^1 \\ &= V^T \nabla f(A(0))V : \begin{pmatrix} \nabla\xi_1 \\ 0 \end{pmatrix} \\ (7.68) \quad &= R_1(V^T \nabla f(A(0))V) \cdot \nabla\xi_1 \end{aligned}$$

Returning to the integral and integrating by parts and assuming Dirichlet boundary conditions, we have that

$$(7.69) \quad \frac{\varepsilon}{2} \int_{D_1} R_1(V^T \nabla f(A(0))V) \cdot \nabla \xi_1 dx, = - \int_{D_1} \frac{\varepsilon}{2} \operatorname{div} (R_1(V^T \nabla f(A(0))V)) \cdot \nabla \xi_1 dx.$$